NASA Technical Memorandum 103933

An Experimental Investigation of a Supercritical Airfoil at Transonic Speeds

G. G. Mateer, H. L. Seegmiller, L. A. Hand and J. Szodruch

July1992

National Aeronautics and Space Administration

NASA Technical Memorandum 103933

An Experimental Investigation of a Supercritical Airfoil at Transonic Speeds

G. G. Mateer, H. L. Seegmiller, L. A. Hand and J. Szodruch

July1992

National Aeronautics and
Space Administration

Ames Research Center
Moffett Field, California 94035-1000

AN EXPERIMENTAL INVESTIGATION OF A SUPERCRITICAL AIRFOIL AT TRANSONIC SPEEDS

George G. Mateer, H. Lee Seegmiller, Lawrence A. Hand and Joachim Szodruch*
NASA Ames Research Center, Moffett Field, California

Summary

Detailed experimental data have been obtained on a supercritical airfoil and in the surrounding flowfield. Surface pressures were measured on both the model and wind-tunnel walls. The velocity field above the airfoil and the field in its wake was documented using a laser Doppler velocimeter. The data illustrate the effect of Mach number and angle of attack on the flow over the airfoil. Angles of attack ranged from 0.5 to 1.5 degrees and the Mach number was varied from 0.73 to 0.8. These variations were sufficient to provide separated and attached flows on the airfoil that were not time dependent. The profile drag was determined via non-intrusive measurements. The data are also on a 3.5-inch diskette included with this document, and are available through E-mail.

Nomenclature

a	speed of sound
c	airfoil chord
C_p	pressure coefficient
C_D'	point drag coefficient
C_D	drag coefficient
M	freestream Mach number
p	pressure
q	dynamic pressure
Re	free-stream Reynolds number based on airfoil chord
s	airfoil span
u	axial velocity
v	vertical velocity
x	axial coordinate from the wing leading edge
y	spanwise coordinate from the tunnel wall
z	vertical coordinate from the tunnel centerline
α	angle of attack
γ	ratio of specific heats
ρ	density
σ	standard deviation
$< >$	ensemble average

Superscripts

'	fluctuating component

Subscripts

CL	centerline
int	integral
sd	statistically dependent
si	statistically independent
t	value based on total temperature
∞	free stream value

Introduction

The purpose of this investigation is to provide a compre-

*MBB, Bremen, Germany.

hensive data base for the validation of numerical simulations. The initial results of the study (single angle of attack) were presented in ref.1, where the effects of various parameters and the adequacies of selected turbulence models were discussed. The objective of the present paper is to provide a tabulation of the experimental data and to present additional data for other angles of attack. The data were obtained in the two-dimensional, transonic flowfield surrounding a supercritical airfoil. A variety of flows were studied in which the boundary layer at the trailing edge of the model was either attached or separated. Unsteady flows were avoided by controlling the Mach number and angle of attack. Surface pressures were measured on both the model and wind tunnel walls, and the flowfield surrounding the model was documented using a laser Doppler velocimeter (LDV). Although wall interference could not be completely eliminated, its effect was minimized by employing the following techniques: Sidewall boundary layers were reduced by aspiration, and upper and lower walls were contoured to accommodate the flow around the model and the boundary-layer growth on the tunnel walls. A data base with minimal interference from a tunnel with solid walls provides an ideal basis for evaluating the development of codes for the transonic speed range because the codes can include the wall boundary conditions more precisely than interference corrections can be made to the data sets.

Apparatus and Test Techniques

Facility

The investigation was conducted in the NASA Ames High Reynolds Channel No. 2 (fig. 1), which is described in detail in ref. 2. This blowdown facility uses unheated dry air at ambient temperature. The high Reynolds number capability is achieved by testing at elevated total pressures (up to 5 atm.). The test section is located inside a pressure shell that is maintained at essentially free-stream static pressure by sidewall vent panels located just upstream from the throat. This technique alleviates many of the structural problems associated with high-pressure testing by reducing the pressure difference across the test section walls. The influence of the wind tunnel walls on the flow is attenuated by: 1) suction to reduce the sidewall boundary layers and 2) contouring the upper and lower walls to allow for flow expansion. Contouring accounts for wall boundary-layer growth, sidewall suction, and the model itself. The details of these procedures are described in refs. 1 and 3. For all of the data presented herein the walls were fixed at a single shape corresponding to $M_\infty = 0.78$, and $\alpha = 1°$. As was shown in ref. 1, this shape was sufficient to preserve the major features of the flow field (e.g., shock-wave position and separation) with only a slight alteration in the pressure distributions at the "off-contour" conditions.

LDV System

The flowfield velocity data were obtained with a laser Doppler velocimeter developed exclusively for this facility (ref. 4). This two-component system employs a 4-watt argon laser utilizing the blue 488 nm and green 514.5 nm lines in forward scatter. One of each pair of beams is frequency-shifted 40 mhz to prevent directional ambiguity in the measurement plane. The two, fringe systems are orientated approximately 45 to the x-direction. The beams are transmitted through a window in the pressure shell to an optical assembly that straddles the test section. This unit consists of a three-dimensional, computer-controlled scanning mechanism with mirrors, focusing lens, and receiving optics. Doppler signal is transmitted from the receiving optics through a 10 m optical fiber to photomultiplier tubes outside the tunnel. Because of large excursions in the traversing mechanism, provision was made to easily change the beam path lengths to place the beam waist at the fringe volume, thereby minimizing variations in fringe spacing. Because both the inner and outer optical assemblies were mounted directly to the pressure vessel, special consideration was given to reducing the transmission of vibration and thermal or pressure strain to the optical components. In order to provide light-scattering particles of known aerodynamic response, the flow was seeded with polystyrene spheres 0.35 to 0.55 microns in diameter. A special atomizer was developed to insure a uniform distribution of seed in the core flow and to prevent deposition on the windows and side-wall suction panels. For this investigation, 1792 simultaneous measurements of the blue and green velocities were made at each point in the flow. The nominal data rate was 500 samples per second, although it varied somewhat from run to run and with location in the flowfield.

Model and Test Conditions

The model (designated VA-2) used in this study was developed by Messerschmitt-Bolkow-Blohm Transport- und Verkehrsflugzeuge of West Germany. It is a supercritical airfoil that combines high lift and low drag with moderate rear loading. A sketch and coordinates of the model are shown in fig. 2. Pressure taps were located primarily on the 50% span line with a lesser number at 25 and 75% span. Boundary layer trips (230K) were applied at 7% chord to both the upper and lower surfaces of the wing. Oilflow data were used to determine the size of grit necessary to cause transition at the trip location. This was accomplished in preliminary tests by placing patches of various grit sizes at different span locations and finding the minimum grit size that caused transition to occur at the patch. The data were obtained at nominal freestream Mach

numbers of 0.73, 0.75, 0.78, and 0.80 and angles of attack of 0.5, 0.9 (denoted as 1° in ref. 1), and 1.5 degrees. The nominal angle of attack of the model was set relative to the wind tunnel wall centerline to an accuracy of $\pm 0.02^\circ$ by rotating the model about its midchord. No stream angle measurements were made, consequently uncertainty exists as to the actual value of angle of attack. The tests were carried out at a Reynolds number of 6 million based on model chord. The corresponding total pressure was 2 atm. A limited amount of data were also obtained at 2 million Reynolds number. For this blowdown facility, the total temperature is a function of the runtime. This variation was measured for each run with eight thermocouples located in the stagnation chamber. These data were then used to correct all temperature-dependent quantities (velocities, Reynolds numbers, etc.) to a constant total temperature of 475 R.

Computational Prologue

Because these data were taken to validate numerical simulations, it is appropriate to address issues pertinent to the computational perspective. These include boundary definitions, correction techniques, Reynolds number effects, flowfield uniformity, and error analysis. The purpose of this section is to expand on these issues with the intent of providing background information for the computational fluid dynamicist.

Wall Contouring

The influence of the wind tunnel walls on the flow is attenuated by 1) suction to reduce the sidewall boundary layers and 2) contouring the upper and lower walls to allow for flow expansion. The sidewall suction panels are shown in fig. 1. The upstream panel removed 4.5% of the total mass flow in the tunnel and the downstream panel removed an additional 1%. Contouring accounts for wall boundary layers, suction, and the model. The magnitude of each of these corrections is shown in table 1. Boundary layer growth corrections were determined by running the tunnel empty and diverging the top and bottom walls until the Mach number was constant along the tunnel axis. The area-ruling technique described in ref. 2 was used to correct for sidewall mass removal. Airfoil code validation computations that specify upper and lower solid wall shape boundaries with no slip velocity conditions should subtract the boundary layer and suction corrections from the final settings listed in table 1. Finally, the flow expansion around the model was accounted for by adding the displacement of the computed (ref. 1, 5), free-air streamlines (upper and lower). These streamlines were selected by specifying that they must contain the flex-points of the upper and lower walls. The flex-point is defined as the first position on the wall that is no longer rigid. It was determined experimentally from the wall pressures during the boundary layer growth correction study and was the same for both walls.

Free-stream Mach Number Correction

Free-stream Mach number was determined from a sidewall pressure tap located on centerline at x/c=-2.389 and a total pressure probe located at z/c=-0.889 below the static pressure tap. The Mach numbers calculated from these measurements were corrected in two ways to arrive at the free-stream value. First, the tunnel centerline Mach number was determined by correcting the sidewall value by -0.003 to account for spanwise nonuniformities in the flow (ref. 2). Second, the centerline value was corrected for the presence of the model by using the previous calculations of ref. 1, 5. This correction was a linear function of the measured Mach number over the range of 0.73 to 0.80 and is given by the equation:

$$\text{correction}=-0.028507+0.044776*M$$

where M is the Mach number determined from the pressure measurements at x/c=-2.389.

Effect of Reynolds Number

Fig. 3 illustrates Reynolds number effects on wing pressures for Mach numbers of 0.73 and 0.78. These two untripped cases were chosen because of their differences in trailing edge flows. At 0.73 the flow is attached, and at 0.78 it is separated. The departure of the trailing edge pressure coefficient from a value of 0.1 was used to define the onset of separation on the upper surface. For the lower Mach number (attached flow) the effects of Reynolds number are confined to the area of the shockwave; whereas, for the separated case, Reynolds number affects the flow from the shock to the trailing edge. The degree of separation is coupled to the position of the shockwave and both effects are a function of the Reynolds number. These changes in the flowfield are due to a combination of boundary layer transition movement and unit Reynolds number variations. In order to avoid the need to predict transition location the boundary layer was tripped near the leading edge (x/c=0.07). Fixing transition also eliminates the possibility that flow-induced roughness would cause transition movement on an otherwise smooth model. The consequences of fixing transition are shown on fig.4. The effect of trips on the low Reynolds number flow of fig.4a is significant. The amount of separation is reduced and the pressure distribution is very similar to the higher Reynolds number flow of fig.4b. The influence of trips is minimal at the higher Reynolds number, indicating that natural transition occurs very close to the trip location (x/c=0.07). Therefore, further changes in the flowfield above 6 million

Reynolds number are due to variations in unit Reynolds number; whereas, below 6 million the changes are due to the movement of transition.

Flowfield Uniformity

The spanwise uniformity of the flow over the airfoil was assessed by the use of surface oilflow patterns, an example of which is shown on fig. 5. It is from the upper surface between the shockwave (x/c=0.5) and the trailing edge. The Mach number and angle of attack are sufficient to produce separated flow at the trailing edge. At this angle of attack these data represent a "worst case" condition for developing flowfield nonuniformities. Although the shockwave is slightly curved, the streaklines downstream are parallel to the free-stream, indicating small spanwise gradients. The parallel streaklines also indicate that sidewall end-effects are slight. Estimates of spanwise pressure gradients can be obtained from surface pressure data that will be presented in subsequent figures.

Error Analysis

The static and total pressures used to determine the freestream Mach numbers were measured with Datametrics, Inc., model 570D transducers and model 1015 signal conditioners. These systems were calibrated at intervals during the test with a Consolidated Electrodynamics Corp., type 6-201-001 primary pressure standard. Calibrations were done over three separate ranges (0-10 psia, 0-45 psia, and 0-100 psia) for improved system accuracy. Based on these procedures and the specifications of the manufacturer, the overall system accuracy was estimated to be ±0.06% of reading. This translates to an uncertainty in Mach number of ±0.001. The remaining wall and wing pressures were measured with Pressure Systems, Inc., ESP-32 modules having ranges of ±45 psig. These units were mounted on constant temperature heaters to minimize temperature sensitivity of the calibrations. All modules were calibrated before each run over reduced ranges to minimize the uncertainty in the measurement. As a result of these measures, the static error band was reduced to approximately ±0.08% of full-scale reading and the corresponding uncertainty in pressure coefficient was ±0.006.

It is convenient to separate the factors that affect the accuracy of the LDV measurements into three groups. The first group consists of those fixed geometric uncertainties, which are invariant during a test run or series of runs. The second group contains the random variations, generally introduced by sample size statistics. In the third group are placed the more difficult to quantify effects of tunnel flow unsteadiness, particle tracking fidelity, velocity bias, and noise. The fixed, geometric uncertainties were evaluated from extensive experience with many tests in which the laser beam geometry was measured in a variety of ways. These uncertainties can be as large as ±2% for u, $\langle u'v' \rangle$, and $\langle u'^2+v'^2 \rangle$. When $v << u$ the geometric uncertainty in v is expressed as $0.027u$. Uncertainties due to sample-size statistics for these measurements vary between ±0.2% and ±0.6% for the mean velocities and ±3% for the turbulent quantities. Tunnel-flow variations (spatial and temporal) are more difficult to quantify. All data are normalized using measured total temperatures to correct for temperature change during each run and for run-to-run variations. Small, unexplained spatial/temporal variations in the mean axial velocity were noted for some conditions in the flow downstream of the airfoil. Although small (1-2%), they present difficulties in evaluating the drag. Estimates of the response of the sub-micron polystyrene seed spheres indicate that a 99% velocity adjustment occurs within 0.9 mm of passage through a normal shock. The measurements taken in axial sweeps through the airfoil shock support this estimate of excellent tracking fidelity. Velocity bias corrections were deemed to be inappropriate for these data and were not made. The influence of noise is difficult to evaluate. Care was taken to maintain clean, well-aligned optics. The special seeding injector prevented seed deposition on the test-section windows, and laser flare was largely avoided in the study, because near-surface measurements were not attempted in the thin airfoil boundary layer. The small fraction (<<1%) of the data that exceeded three standard deviations was discarded in forming the velocity histograms. The uncertainties (95% confidence limits) assigned to the measured quantities for the three groups are shown in table 2. Also shown are the root-sum-square and worst case combinations.

Experimental Results

The experimental data were obtained in three regions of the flow. Surface pressure measurements were made on the wing and tunnel walls, and LDV data were obtained in the flowfield over the wing and in the wake. The results include both separated and attached flows at the trailing edge.

Pressure Measurements

The surface pressure data for both the wing and tunnel walls are shown in fig. 6 for all Mach numbers and angles of attack. Each figure includes a plot of wing pressures as an aid in identifying the flowfield (e.g. separated/unseparated), and a tabulation of all the data at a particular Mach number and angle of attack. The pressure distributions on the tunnel walls indicate that neither the shockwave nor the region of supersonic flow extends to the upper wall. Comparisons between wing and sidewall data indicate a fairly two-dimensional, normal shockwave.

LDV Measurements

The wake profile data are shown in fig. 7 and were obtained during the same tunnel runs as the pressure data of the previous figure. The majority of the data were obtained at x/c=2.5; however, a few sets are included for x/c=1.04 to illustrate wake development. The format is the same as the pressure data; i.e., tabulation plus plot. The velocity field above the wing is presented in fig. 8. The primary focus of this data set was to provide a description of the shockwave (strength and shape) in this region of the flow. The steadiness of the shock could also be determined by examining the individual LDV measurements as a function of time. These data indicated that the movement of the shock was very limited: ±1.5% of chord about its mean position.

Drag Determination

The profile drag of the airfoil was determined from wake velocity and static pressure profiles using the momentum integral method of Jones (ref. 6) extended to high-speed flow (ref. 7 - 9). (This method is summarized by Schlichting, ref. 10) The technique was modified to calculate the drag using the nonintrusive LDV and sidewall pressure measurements rather than the traditional pitot and static pressure traverse data. The resulting data reduction formulas are presented in the appendix. The experimental drag data in ref. 1 are superseded by those presented here. The former were calculated using a less accurate technique without detailed measurements of the wake static pressure profile.

The static pressure profile at x/c=2.5 was measured in a separate test for which the downstream LDV window (labeled "sidewall hatch" in fig. 1) on each side of the tunnel was replaced with a solid metal plate. Each plate incorporated a vertical array of 33 static pressure taps uniformly spaced over the interval -203.2mm ≤z≤ 203.2mm. The pressures were measured with two Pressure Systems Model 3201B 32-port scanning transducers having a full-scale range of ±1 psid. Prior to each run, these transducers were calibrated with a Datametrics Type 511-11 pressure transducer having a range of approximately ±2 psi. The manufacturer's specifications indicate that the measurements should be accurate to ±0.0030 psi (C_p uncertainty ±0.00036).

Pressures were measured differentially, relative to the value at z=0 on each sidewall. They were approximated on the vertical center plane (y=0) by averaging the data on both sides (fig. 9). This procedure helped to attenuate the effects of slight spanwise nonuniformities in the flow. The error bars indicate a 95% confidence interval based on the Student t-distribution with 11 degrees of freedom (approximately 2.2 standard deviations). The uncertainty is consistent with the precision of the instrumentation.

At each vertical position a point drag coefficient, C_D', was calculated from the velocity and static pressure (fig. 10). The absolute static pressure on the tunnel centerline was determined from the velocity measurements. The value of C_p (z=0) was adjusted iteratively until the mean value of C_D' was equal to zero outside the region of viscous and/or shock losses. This procedure virtually eliminates the effects of systematic errors (Group 1 LDV uncertainty, spanwise nonuniformity of the flow, etc.) and minimizes the effects of random errors on the baseline position. The resulting values of C_p (z=0) are listed in table 3.

The drag coefficient, C_D (table 3), was obtained by numerical integration of C_D' with respect to z/c between the limits denoted by the horizontal lines in fig. 10. The lower limit marks the edge of the viscous wake and is characterized by a sharp rise in the turbulent kinetic energy. When shocks are present on the lower surface the point drag data indicate that they do not produce significant losses beyond the viscous wake. This criterion was used to determine the lower limit in all cases except one (α=1.5, M_∞=0.749). In that case, the limit was moved from z/c=-0.312 to -0.184 to eliminate an anomalous fluctuation. This action caused an increase in the computed drag of approximately 2.5% and an increase in its uncertainty of about 17%.

The upper limit of integration was determined in the same way as the lower limit when significant shock losses were not observed above the viscous wake. Otherwise, this limit was defined by examination of the point drag coefficient profile (e.g., ref. 11). Differences in the drag resulting from various apparently reasonable choices of the upper limit were generally much less than the overall uncertainty.

Outside the limits of integration, the scatter of C_D' around zero provides a direct measure of the uncertainty in the data. Table 3 includes the standard deviation, σ, of these points. It is assumed that the data within the limits contains errors that are statistically equivalent to those beyond the limits. This assumption is permissible because the turbulence levels at x/c=2.5 are low enough to make the Group 2 LDV uncertainty unimportant. Theoretical error sensitivity analyses indicate that only a small fraction of the observed uncertainty in C_D' is due to the observed uncertainty in C_p. The uncertainty in the velocity data is the dominant cause.

Each set of baseline data was tested for normality (Gaussian distribution) with six Chi-square goodness-of-fit tests using 4, 5, 6, 7, 8, and 9 equiprobable cells (see ref. 12-15)

and a Kolmogorov-Smirnov test (see ref. 13-16). These analyses indicate that it is highly likely that the errors in the C_D' data are normally distributed. However, this does not necessarily imply that the errors are randomly ordered. Dependence may exist between errors at neighboring points. Long runs of either positive or negative C_D' values in the baseline data of several of the test cases (most notably α=0.5, M_∞=0.750 and α=0.9, M_∞=0.781) indicate that such dependence is likely in these cases.

The drag coefficient comprises a weighted sum of C_D' values with weights equal to the increments in z/c. Similarly, σ of each term in the sum is equal to the product of the weight and the standard deviation of C_D'. If the errors in the terms are statistically independent, σ of the sum (table 3) is equal to the root-sum-square of the standard deviations of the terms.

The effect of statistical dependence on the uncertainty of the numerical integral was estimated by computing a moving weighted sum (using the same weights and number of terms as the integral) on continuous segments of baseline data having more data points than the integral (i.e., the C_D' values of contiguous baseline data points were used in order of occurrence and their spacing was disregarded). The standard deviation of the sums in this series provides an estimate of the uncertainty of the numerical integral. Although this procedure lacks statistical rigor, comparing the two values of σ (table 3) provides an indication of the magnitude of the effect of nonindependence. (In cases where neither the number of data points above the upper limit of integration nor the number below the lower limit exceed the number within the limits, the procedure is inapplicable and the result is given as zero.) The larger of these two estimates was taken as the standard deviation of the numerical integral.

Although the drag tare is nominally zero, there is uncertainty associated with it. Its standard deviation (table 3) is equal to the product of σ of the mean of the baseline data (σ of C_D' divided by the square root of the number of baseline data points) and the normalized distance between the integration limits ($\Delta z/c$). The standard deviation of the drag coefficient, shown in table 3, is equal to the root-sum-square of the σ's for the numerical integral and the drag tare (table 3). The half-width of a 95% confidence interval (approximately 1.96 σ) ranges from 4% to 11% of the drag coefficient in the twelve test cases.

Conclusions

Detailed experimental data have been obtained on a supercritical airfoil and in the surrounding flowfield. Surface pressures were measured on both the model and wind tunnel walls. The velocity field above the airfoil and in its wake was documented using a laser Doppler velocimeter. The data illustrate the effect of Mach number and angle of attack on the flow over the airfoil. Angles of attack ranged from 0.5 to 1.5° and the Mach number was varied from 0.73 to 0.8. These variations were sufficient to provide separated and attached flows on the airfoil that were not time dependent. Although the drag data are less precise than those typically used in aircraft design, they are based entirely on nonintrusive measurements, they are virtually free of systematic errors, and their uncertainties are quantified.

References

1. Mateer, G. G.; Seegmiller, H. L.; Coakley, T. J.; Hand, L. A.; and Szodruch, J.: An Experimental Investigation of a Supercritical Airfoil at Transonic Speeds. AIAA Paper 87-1241, June 1987.

2. McDevitt, J. B.; Polek, T. E.; and Hand, L. A.: A New Facility and Technique for Two-Dimensional Aerodynamic Testing. AIAA J. Aircraft, vol. 20, no. 6, June 1983, pp. 543-551.

3. McDevitt, J. B.; and Okuno, A. F.: Static and Dynamic Pressure Measurements on a NACA 0012 Airfoil in the Ames High Reynolds Number Facility. NASA Technical Paper 2485, June 1985.

4. Seegmiller, H. L.; Bader, J. B.; Cooney, J. P.; De Young, A.; Donaldson, R. W., Jr.; Gunter, W. D., Jr.; and Harrison, D. R.: Development of a New Laser Doppler Velocimeter for the Ames High Reynolds Channel No. II. NASA TM-86772, July 1985.

5. Coakley, T. J.: Implicit Upwind Methods for the Compressible Navier-Stokes Equations. AIAA Journal, vol. 23, no. 3, March 1985, p. 374.

6. The Cambridge University Aerodynamics Laboratory (Jones, B.M.): The Measurement of Profile Drag by the Pitot-Traverse Method. Reports and Memoranda No. 1688, (British) Aeronautical Research Committee, January 1936.

7. Young, A.D.: Note on the Effect of Compressibility on Jones' Momentum Method of Measuring Profile Drag. Reports and Memoranda No. 1881, (British) Aeronautical Research Committee, February 1939.

8. Young, A.D.: Note on Momentum Methods of Mea-

suring Profile Drags at High Speeds. Reports and Memoranda No. 1963, (British) Aeronautical Research Committee, February 1940.

9. Lock, C.N.H.; Hilton, W.F.; and Goldstein, S.: Determination of Profile Drag at High Speeds by a Pitot Traverse Method. Reports and Memoranda No. 1971, (British) Aeronautical Research Committee, September 1940.

10. Schlichting, H.: Boundary-Layer Theory, Seventh Edition. McGraw-Hill Book Company, New York, 1979, pp. 761-764.

11. Jenkins, R.V.: Tabulation of Data From Tests of an NPL 9510 Airfoil in the Langley 0.3-Meter Transonic Cryogenic Tunnel. NASA TM-84579, November 1983.

12. Meyer, P.L.: Introductory Probability and Statistical Applications, Second Edition. Addison-Wesley Publishing Company, Reading, Massachusetts, 1970, pp. 328-335.

13. Ostle, B.: Statistics in Research, Second Edition. The Iowa State University Press, Ames, Iowa, 1963, pp.126-127,471-472.

14. Lindgren, B.W.: Statistical Theory. The Macmillan Company, New York, 1962, pp. 294-304.

15. Kendall, M.G.; and Stuart, A.: The Advanced Theory of Statistics, Volume 2, Second Edition. Charles Griffin & Company, London, 1967, pp. 419-464.

16. Birnbaum, Z.W.: Numerical Tabulation of the Distribution of Kolmogorov's Test Statistic for Finite Sample Size. Journal of the American Statistical Association, vol. 47, 1952, pp. 425-441.

Appendix

Drag Calculation Equations

The drag coefficient can be expressed:

$$C_D = \int_{-\infty}^{\infty} C_D' d\left(\frac{z}{c}\right) \tag{1}$$

where the integrand, C_D', is called the "point drag coefficient". According to the theory of the Jones wake momentum integral method for high-speed flow (ref. 7 - 10),

$$C_D' = 2\left(1 - \frac{u_1}{u_\infty}\right)\frac{\rho}{\rho_\infty}\frac{u}{u_\infty} \tag{2}$$

ρ and u represent the density and axial velocity at the wake traverse station. u_1 is the axial velocity that would occur at a point infinitely far downstream (where the static pressure is equal to its freestream value, p_∞) on a *hypothetical isentropic streamline* extending rearward from the wake traverse station. Notice that $C_D'=0$ when $u_1=u_\infty$. Therefore, it is unnecessary for the integration to include streamlines along which the flow upstream of the wake traverse station is isentropic. Hence, the infinite limits of integration in Equation 1 can be replaced by finite values.

The ratios appearing in Equation 2 can be expressed as functions of the freestream Mach number, M_∞, a local Mach number based on the stagnation sound speed,

$$M_t = \left[\left(\frac{u}{a_t}\right)^2 + \left(\frac{v}{a_t}\right)^2\right]^{1/2} \tag{3}$$

and the local static pressure ratio,

$$\frac{p}{p_\infty} = 1 + \frac{\gamma}{2}M_\infty^2 C_P \tag{4}$$

where C_p is the local static pressure coefficient and γ is the specific-heat ratio (γ=1.4 for air). The resulting formulas are:

$$\frac{u_1}{u_\infty} = \left[\frac{2}{(\gamma-1)M_\infty^2} \cdot (1+\frac{\gamma-1}{2}M_\infty^2)\right]^{1/2} X$$

$$\left[1-(\frac{p}{p_\infty})^{-\frac{\gamma-1}{\gamma}}(1-\frac{\gamma-1}{2}M_t^2)\right]^{1/2} \qquad (5)$$

$$\frac{\rho}{\rho_\infty} = \frac{p}{p_\infty}\left[(1+\frac{\gamma-1}{2}M_\infty^2)\,(1-\frac{\gamma-1}{2}M_t^2)\right]^{-1} \qquad (6)$$

and

$$\frac{u}{u_\infty} = (\frac{u}{a_t})\frac{1}{M_\infty}(1+\frac{\gamma-1}{2}M_\infty^2)^{1/2} \qquad (7)$$

Table 1: Wall Coordinates

Jack Station	x/c	Straight wall setting (z/c)	Boundary layer correction ($\Delta z/c$)	Suction correction ($\Delta z/c$)	Streamline curvature ($\Delta z/c$)	Final setting (sum cols. 3-6) (z/c)
	Upper Wall					
1	-0.770	1.524	0.0081	-0.0229	0.0271	1.5363
2	-0.008	1.524	0.0114	-0.0229	0.0530	1.5655
3	0.500	1.524	0.0137	-0.0229	0.0630	1.5778
4	1.008	1.524	0.0160	-0.0229	0.0540	1.5711
5	1.770	1.524	0.0193	-0.0229	0.0320	1.5524
6	4.104	1.524	0.0295	-0.0229	-0.0060	1.5246
7	5.739	1.524	0.0340	-0.0229	-0.0170	1.5181
	Lower Wall					
1	-0.770	-1.524	-0.0081	0.0229	0.0100	-1.4992
2	-0.008	-1.524	-0.0114	0.0229	0.0090	-1.5035
3	0.500	-1.524	-0.0137	0.0229	0.0080	-1.5068
4	1.008	-1.524	-0.0160	0.0229	0.0070	-1.5101
5	1.770	-1.524	-0.0193	0.0229	0.0010	-1.5194
6	4.104	-1.524	-0.0295	0.0229	-0.0240	-1.5546
7	5.739	-1.524	-0.0340	0.0229	-0.0340	-1.5691

Note: $dz/dx=0$ for $x/c= -3.516$

Table 2: LDV Uncertainties

quantity	group 1	group 2	group 3	worst case	root-sum-square
u	±1-2%	±0.2-0.6%	±1-2%	±4.6%	±1.4-2.9%
v	±0.027u	±0.2-0.6%	±1-2%	±0.027u±0.026v	±0.027u±0.012-0.026v
$\langle u'v' \rangle$	±2%	±3%	±2-4%	±9%	±4.1-5.4%
$\langle u'^2+v'^2 \rangle$	±2%	±3%	±2-4%	±9%	±4.1-5.4%

Table 3: Drag Data

			standard deviation				
M_∞	$(C_p)_{z=0}$	C_D	C_D'	$((C_D)_{int})_{si}$	$((C_D)_{int})_{sd}$	$(C_D)_{tare}$	C_D
α=0.5°							
0.728	0.0043	0.01009	0.00518	0.00024	0.00011	0.00013	0.00027
0.750	0.0148	0.01010	0.00695	0.00032	0.00057	0.00015	0.00059
0.784	0.0100	0.01537	0.00560	0.00045	0.00045	0.00030	0.00054
0.802	-0.0245	0.03321	0.00549	0.00058	0	0.00045	0.00074
α=0.9°							
0.729	-0.0003	0.01078	0.00402	0.00024	0.00023	0.00011	0.00026
0.750	-0.0026	0.01198	0.00505	0.00032	0.00033	0.00017	0.00037
0.781	-0.0253	-0.02684	0.00664	0.00070	0.00136	0.00043	0.00142
0.803	-0.0510	0.04585	0.00555	0.00068	0	0.00050	0.00085
α=1.5°							
0.730	-0.0083	0.01556	0.00382	0.00044	0	0.000032	0.00054
0.749	-0.0061	0.02075	0.00531	0.00052	0.00067	0.00030	0.00073
0.781	-0.0195	0.04031	0.00637	0.00070	0	0.00065	0.00095
0.803	-0.0406	0.05337	0.00668	0.00086	0	0.00099	0.00131

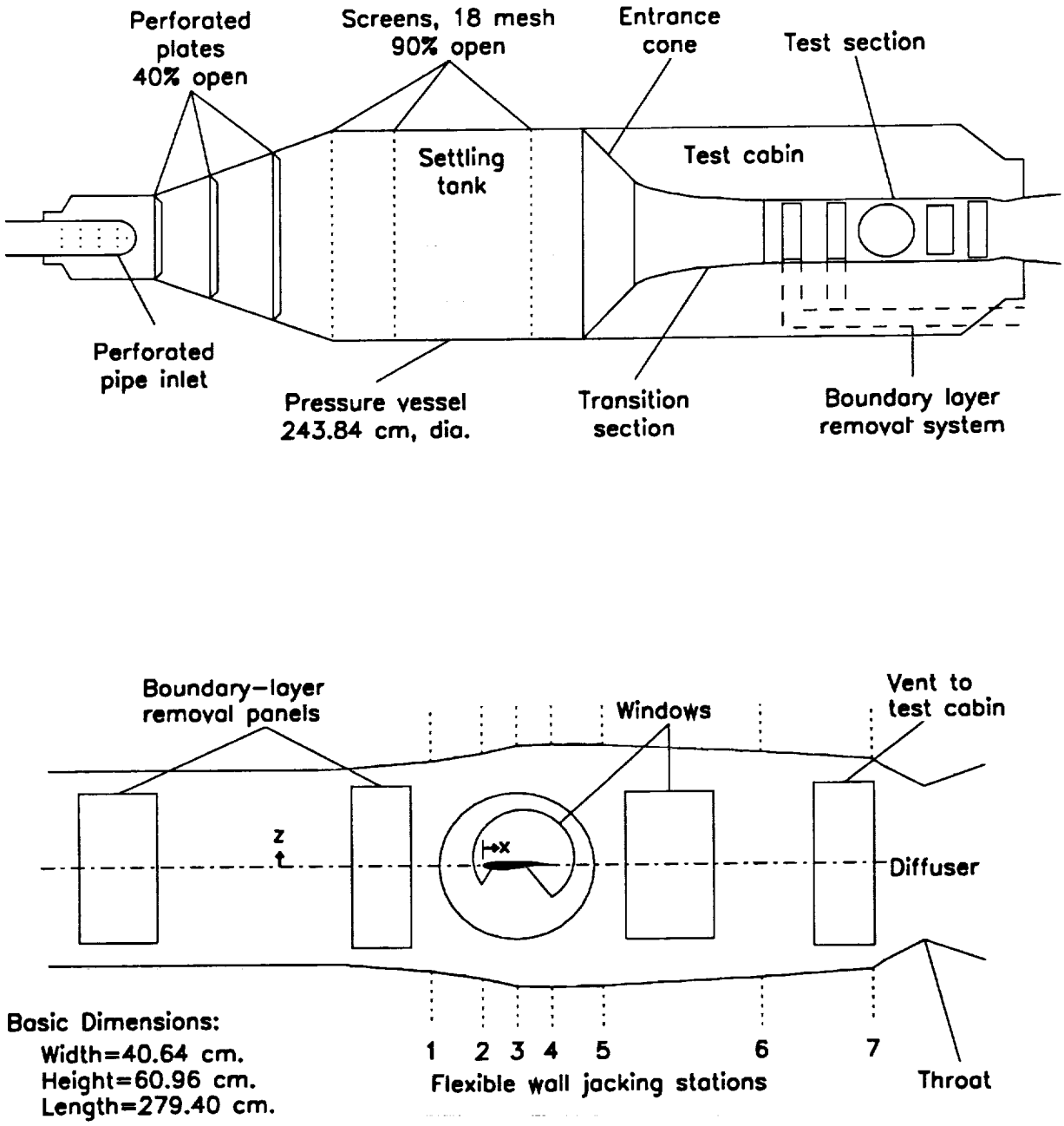

Figure 1. NASA Ames High Reynolds Channel No. 2.

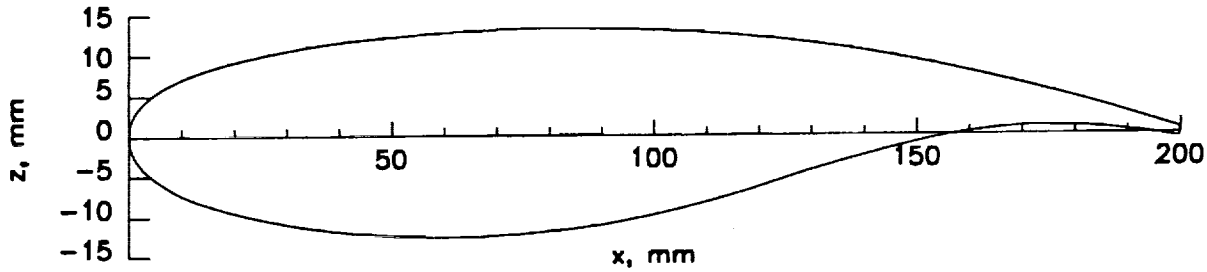

x, upper	z, upper	x, lower	z, lower	x, upper	z, upper	x, lower	z, lower
0.00000	0.00000	0.00000	0.00000	8.00000	6.44000	8.00000	-6.67200
0.08000	0.87009	0.08000	-0.75555	8.40000	6.56779	8.40000	-6.81966
0.16000	1.17772	0.16000	-1.08605	8.80000	6.69186	8.80000	-6.96244
0.24000	1.41029	0.24000	-1.33602	9.20000	6.81223	9.20000	-7.10038
0.32000	1.60310	0.32000	-1.54358	9.60000	6.92894	9.60000	-7.23355
0.40000	1.77000	0.40000	-1.72360	10.0000	7.04200	10.0000	-7.36200
0.48000	1.91408	0.48000	-1.88197	10.7200	7.23471	10.7230	-7.57275
0.56000	2.04638	0.56000	-2.02626	11.4400	7.41899	11.4461	-7.77138
0.64000	2.16889	0.64000	-2.15908	12.1600	7.59492	12.1691	-7.95806
0.72000	2.28307	0.72000	-2.28227	12.8800	7.76257	12.8922	-8.13296
0.80000	2.39000	0.80000	-2.39720	13.6000	7.92200	13.6152	-8.29620
0.96000	2.58858	0.96000	-2.60115	14.4000	8.09435	14.4150	-8.47042
1.12000	2.77168	1.12000	-2.78830	15.2000	8.25989	15.2147	-8.63765
1.28000	2.94131	1.28000	-2.96109	16.0000	8.41865	16.0145	-8.79793
1.44000	3.09900	1.44000	-3.12133	16.8000	8.57068	16.8142	-8.95130
1.60000	3.24600	1.60000	-3.27040	17.6000	8.71600	17.6140	-9.09780
1.84000	3.45051	1.84000	-3.49566	18.3200	8.84103	18.3325	-9.23085
2.08000	3.64157	2.08000	-3.68670	19.0400	8.96253	19.0504	-9.35908
2.32000	3.82027	2.32000	-3.87468	19.7600	9.08052	19.7694	-9.48491
2.56000	3.98749	2.56000	-4.05057	20.4800	9.19501	20.4879	-9.60755
2.80000	4.14400	2.80000	-4.21520	21.2000	9.30600	21.2064	-9.72700
3.04000	4.29639	3.04000	-4.36845	22.3616	9.48374	22.3664	-9.91364
3.28000	4.44195	3.28000	-4.51532	23.5232	9.65551	23.5265	-10.0929
3.52000	4.58092	3.52000	-4.65605	24.6848	9.82134	24.6865	-10.2649
3.76000	4.71353	3.76000	-4.79088	25.8464	9.98123	25.8466	-10.4295
4.00000	4.84000	4.00000	-4.92000	27.0080	10.1352	27.0065	-10.5868
4.24000	4.96082	4.24000	-5.05172	28.6081	10.3353	28.6064	-10.7913
4.48000	5.07734	4.48000	-5.17917	30.2082	10.5257	30.2065	-10.9837
4.72000	5.18965	4.72000	-5.30244	31.8084	10.7065	31.8065	-11.1638
4.96000	5.29785	4.96000	-5.42162	33.4085	10.8777	33.4064	-11.3319
5.20000	5.40200	5.20000	-5.53680	35.0085	11.0394	35.0064	-11.4878
5.44000	5.50381	5.44000	-5.64227	36.4086	11.1753	36.4062	-11.6160
5.68000	5.60288	5.68000	-5.74503	37.8085	11.3056	37.8061	-11.7361
5.92000	5.69925	5.92000	-5.84515	39.2085	11.4302	39.2059	-11.8482
6.16000	5.79295	6.16000	-5.94266	40.6084	11.5491	40.6058	-11.9521
6.40000	5.88400	6.40000	-6.03760	42.0084	11.6624	42.0056	-12.0480
6.72000	6.00180	6.72000	-6.16901	43.6083	11.7860	43.6053	-12.1483
7.04000	6.11627	7.04000	-6.29814	45.2082	11.9036	45.2050	-12.2389
7.36000	6.22743	7.36000	-6.42501	46.8082	12.0151	46.8045	-12.3200
7.68000	6.33534	7.68000	-6.54962	48.4081	12.1207	48.4043	-12.3914

Figure 2. Supercritical airfoil; MBB VA-2.

x, upper	z, upper	x, lower	z, lower	x, upper	z, upper	x, lower	z, lower
50.0080	12.2202	50.0040	-12.4532	151.925	8.92425	151.856	-0.68844
52.0078	12.3371	52.0033	-12.5177	153.922	8.65410	153.864	-0.42349
54.0075	12.4462	54.0026	-12.5682	155.918	8.37656	155.872	-0.17965
56.0073	12.5473	56.0018	-12.6046	157.915	8.09159	157.880	0.04316
58.0070	12.6406	58.0011	-12.6270	159.911	7.79920	159.888	0.24500
60.0068	12.7260	60.0004	-12.6354	161.508	7.56023	161.499	0.38730
62.0064	12.8048	61.9993	-12.6307	163.105	7.31725	163.110	0.51391
64.0059	12.8766	63.9982	-12.6124	164.701	7.07026	164.721	0.62488
66.0055	12.9413	65.9972	-12.5804	166.298	6.81924	166.333	0.72024
68.0050	12.9992	67.9961	-12.5348	167.895	6.56420	167.944	0.80000
70.0046	13.0500	69.9950	-12.4756	169.092	6.37091	169.154	0.84722
72.0040	13.0945	71.9933	-12.4062	170.289	6.17581	170.364	0.88583
74.0034	13.1324	73.9916	-12.3171	171.486	5.97889	171.574	0.91582
76.0028	13.1636	75.9894	-12.2171	172.683	5.78015	172.784	0.93721
78.0022	13.1883	77.9883	-12.1033	173.880	5.57960	173.994	0.95000
80.0015	13.2064	79.9865	-11.9756	175.475	5.31383	175.605	0.95545
82.0009	13.2185	81.9846	-11.8337	177.071	5.04343	177.216	0.94678
84.0002	13.2239	83.9825	-11.6776	178.666	4.76840	178.828	0.92399
85.9994	13.2227	85.9805	-11.5074	180.262	4.48873	180.439	0.88706
87.9987	13.2149	87.9784	-11.3229	181.857	4.20440	182.050	0.83600
89.9980	13.2004	89.9764	-11.1242	183.086	3.97722	183.240	0.78904
91.9968	13.1793	91.9738	-10.9101	184.314	3.74679	184.430	0.73477
93.9956	13.1513	93.9713	-10.6820	185.543	3.51312	185.620	0.67318
95.9945	13.1162	95.9687	-10.4401	186.771	3.27619	186.810	0.60426
97.9934	13.0742	97.9662	-10.1841	188.000	3.03600	188.000	0.52800
99.9922	13.0252	99.9635	-9.91420	189.200	2.79988	189.200	0.44277
101.991	12.9692	101.960	-9.62900	190.400	2.56122	190.400	0.35127
103.989	12.9057	103.956	-9.33168	191.600	2.32002	191.600	0.25347
105.988	12.8346	105.952	-9.02219	192.800	2.07629	192.800	0.14939
107.986	12.7561	107.949	-8.70051	194.000	1.83000	194.000	0.03900
109.985	12.6700	109.945	-8.36660	194.400	1.74740	194.400	0.00180
111.983	12.5760	111.939	-8.02541	194.800	1.66450	194.800	-0.03610
113.981	12.4739	113.934	-7.67326	195.200	1.58130	195.200	-0.07470
115.979	12.3638	115.928	-7.31014	195.600	1.49780	195.600	-0.11400
117.978	12.2453	117.922	-6.93599	196.000	1.41400	196.000	-0.15400
119.976	12.1189	119.917	-6.55080	196.400	1.32912	196.400	-0.19580
121.973	11.9835	121.790	-6.15913	196.800	1.24428	196.800	-0.23800
123.970	11.8397	123.664	-5.76716	197.200	1.15948	197.200	-0.28060
125.968	11.6873	125.537	-5.37487	197.600	1.07472	197.600	-0.32360
127.966	11.5263	127.412	-4.98223	198.000	0.99000	198.000	-0.36700
129.963	11.3568	129.285	-4.58920	198.400	0.90640	198.400	-0.40960
131.960	11.1783	131.399	-4.18368	198.800	0.82320	198.800	-0.45220
133.957	10.9911	133.513	-3.78734	199.200	0.74040	199.200	-0.49480
135.954	10.7954	135.627	-3.40016	199.600	0.65800	199.600	-0.53740
137.951	10.5911	137.741	-3.02212	200.000	0.00000	200.000	0.00000
139.948	10.3782	139.855	-2.65320				
141.944	10.1563	141.853	-2.29282				
143.940	9.92627	143.852	-1.94482				
145.937	9.68805	145.851	-1.60915				
147.933	9.44163	147.849	-1.28576				
149.929	9.18700	149.848	-0.97460				

Figure 2. Concluded.

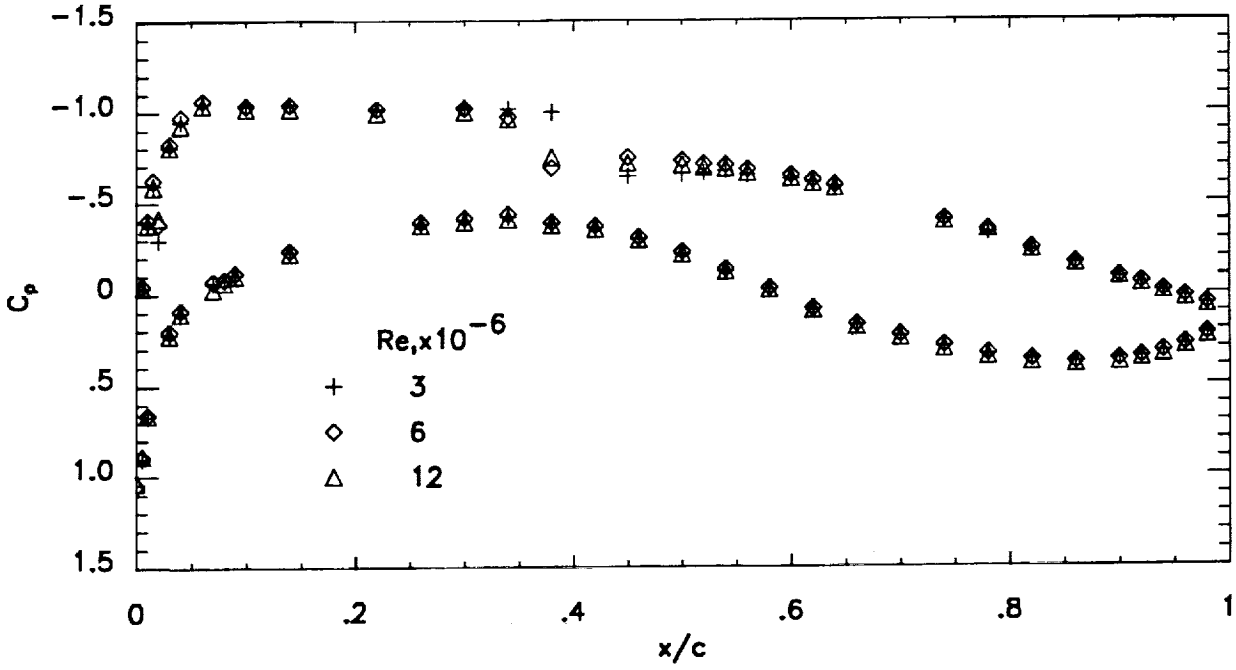

(a) M_∞=0.734, α=1.1°

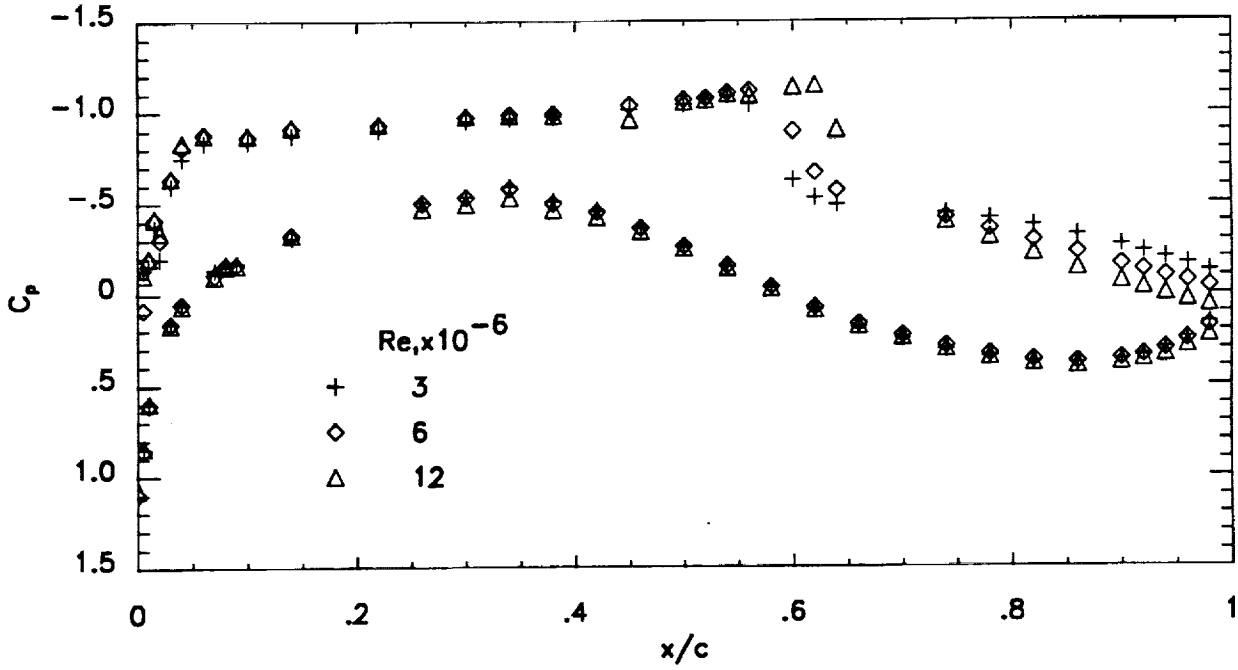

(b) M_∞=0.780, α=1.0°

Figure 3. Effect of Reynolds number on wing surface pressures.

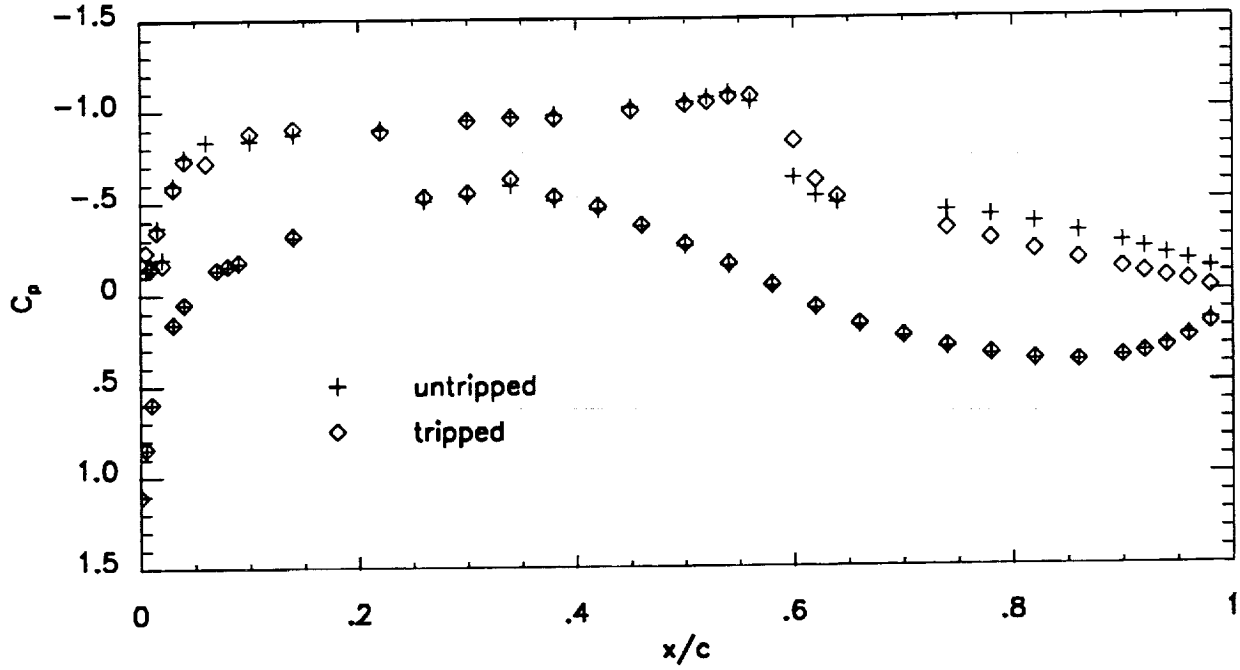

(a) Re=3x10^6, α=1.05°, M_∞=0.784

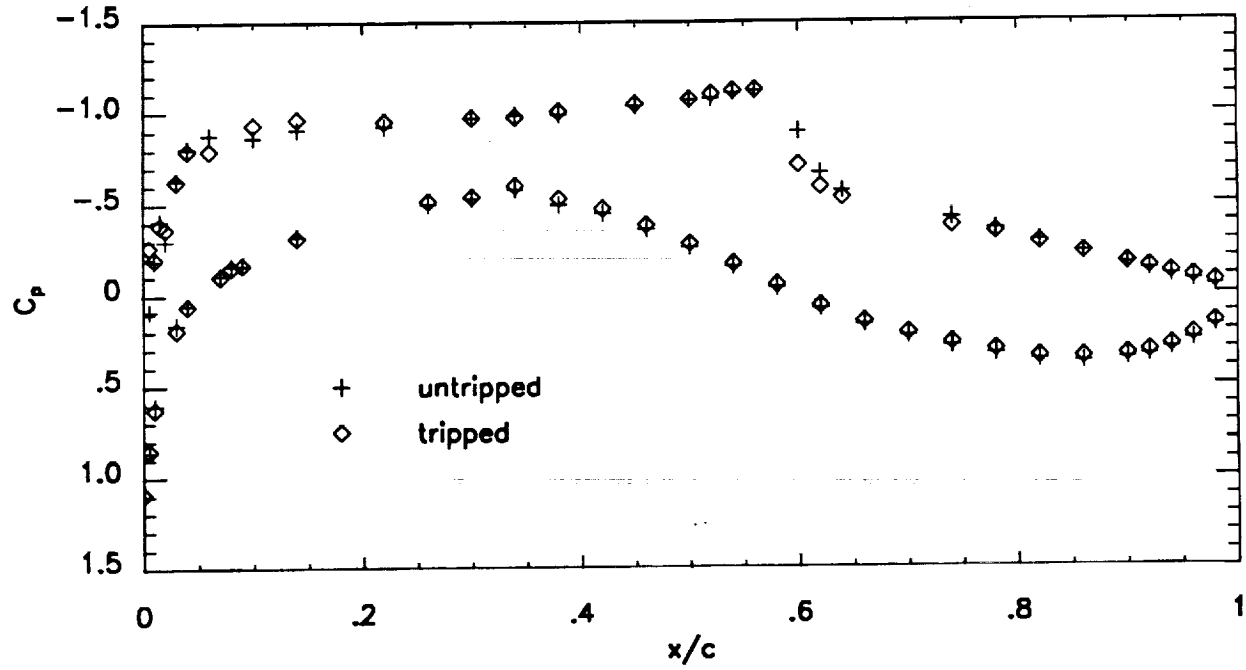

(b) Re=6x10^6, α=1.0°, M_∞=0.778

Figure 4. Effect of boundary layer trips on wing surface pressures.

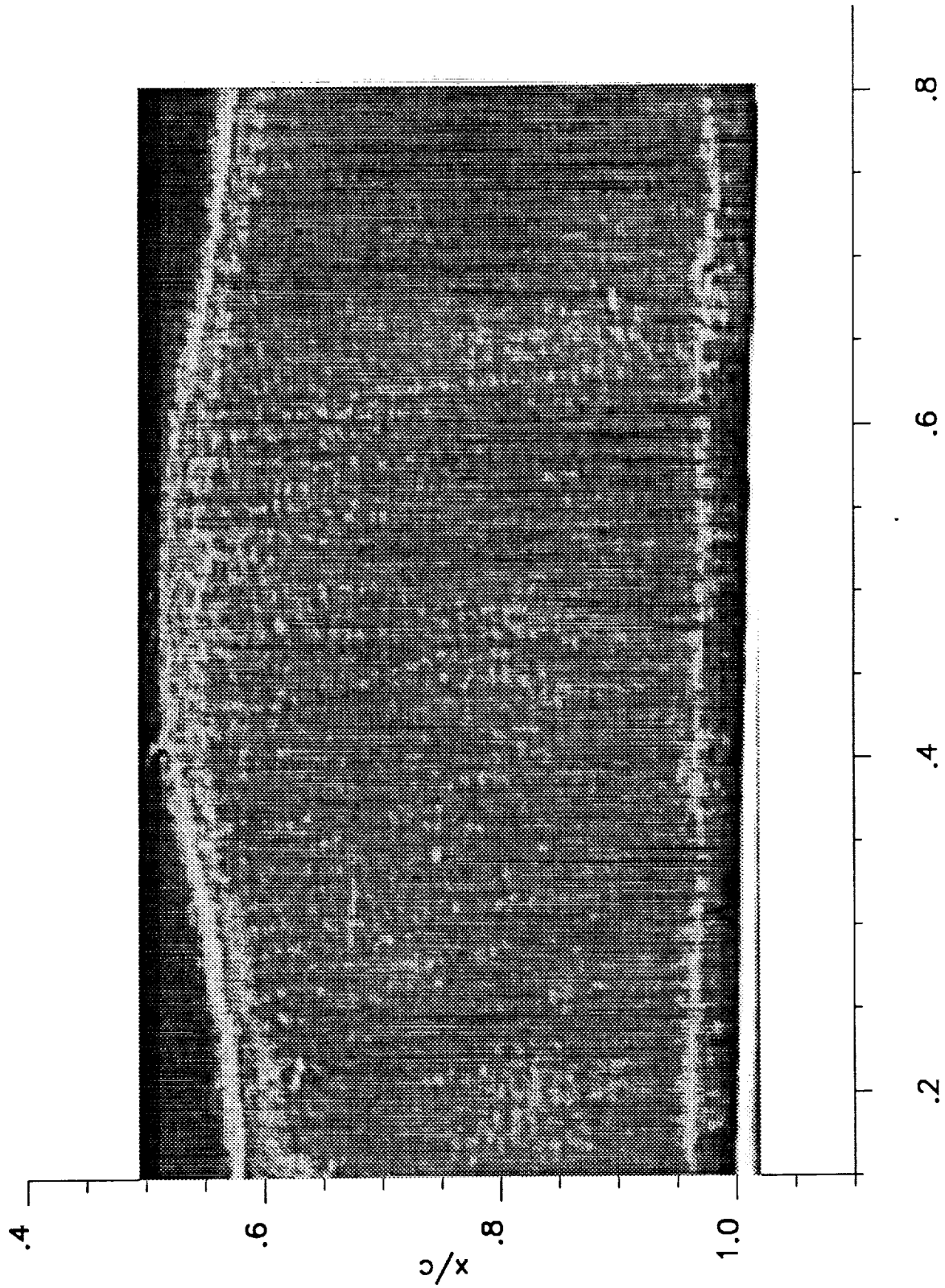

Figure 5. Oilflow at α=2.0°, M_∞=0.782.

MBB VA-2

y/s=	.25	.50		.75
	UPPER	UPPER	LOWER	UPPER
x/c				
0.000		1.093		
0.005		−0.512	0.806	
0.010		−0.354	0.578	
0.015		−0.439		
0.020		−0.538		
0.030		−0.697	0.120	
0.040		−0.846	0.005	
0.060		−0.905		
0.070			−0.151	
0.080			−0.186	
0.090			−0.195	
0.100		−0.807		
0.140		−0.767	−0.318	
0.180	−0.754			−0.755
0.220		−0.743		
0.260			−0.448	
0.300		−0.716	−0.456	
0.340		−0.688	−0.467	
0.380	−0.669	−0.655	−0.426	
0.420			−0.396	
0.450	−0.635	−0.675		−0.651
0.460			−0.328	
0.500	−0.626	−0.639	−0.237	−0.628
0.520	−0.619	−0.628		−0.620
0.540	−0.606	−0.616	−0.136	−0.602
0.560	−0.597	−0.604		
0.580	−0.584		−0.036	−0.580
0.600	−0.563	−0.571		−0.557
0.620	−0.545	−0.549	0.078	−0.539
0.640		−0.526		
0.660			0.167	
0.700			0.228	
0.740		−0.360	0.284	
0.780		−0.297	0.325	
0.820		−0.217	0.359	
0.860		−0.144	0.373	
0.900		−0.073	0.365	
0.920		−0.039	0.348	
0.940		0.003	0.327	
0.960		0.036	0.285	
0.980		0.078	0.232	
1.000	0.107			0.111

WALL

y/s=	0			.50		1		
z/c=	1.397	0	−1.397	1.524	−1.524	1.397	0	−1.397
x/c								
−6.136	0.007							
−4.548	0.029							
−3.309	0.007	0.017	0.025			0.015	0.019	0.033
−3.055				0.007	0.027			
−2.293				−0.021	0.016			
−2.039	−0.034					−0.024		
−1.531	−0.027			−0.017	0.033	−0.029		
−1.023	−0.032					−0.025		
−0.769		0.054		−0.056	0.007		0.067	
−0.515	−0.054		0.016			−0.056		0.005
−0.007	−0.071		0.013	−0.059	0.035	−0.075		0.038
0.501	−0.070		0.031	−0.039	0.034	−0.065		0.033
1.009	−0.066		0.048	−0.046	0.033	−0.053		0.026
1.515	−0.043		0.040			−0.038		0.030
1.771		0.039		−0.020	0.038		0.054	
2.025	−0.021		0.037			−0.010		0.042
2.533	−0.012		0.036	−0.004	0.033	−0.005		0.035
3.041	−0.007		0.038			−0.002		0.025
3.295				−0.003	0.028			
4.088				0.012	0.024			
4.311	0.012	0.013	0.023			0.012	0.000	0.029
4.850				0.009	0.034			

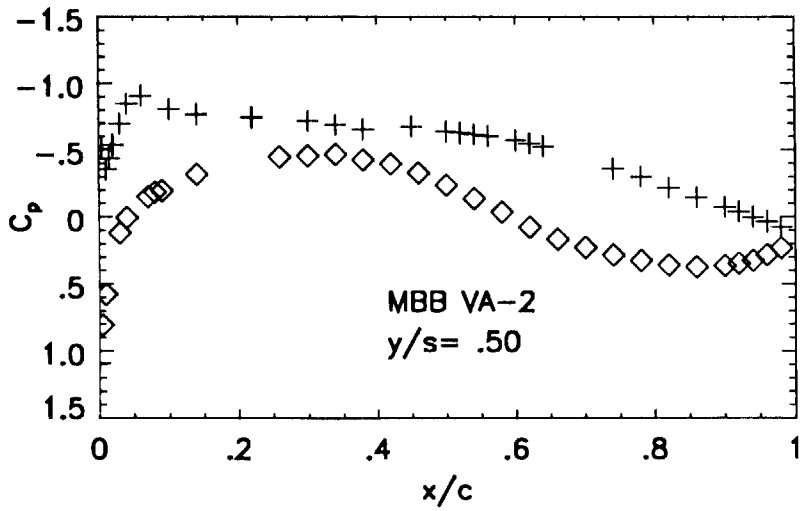

Figure 6. Surface pressure coefficient. (a) M_∞=0.728, α=0.5°, Re=6x10^6.

MBB VA-2

y/s=	.25	.50		.75
	UPPER	UPPER	LOWER	UPPER
x/c				
0.000		1.029		
0.005		−0.357	0.871	
0.010		−0.405	0.644	
0.015		−0.571		
0.020		−0.650		
0.030		−0.802	0.203	
0.040		−1.006	0.089	
0.060		−0.954		
0.070			−0.056	
0.080			−0.097	
0.090			−0.108	
0.100		−1.047		
0.140		−1.042	−0.236	
0.180	−1.008			−1.019
0.220		−0.958		
0.260			−0.373	
0.300		−0.709	−0.392	
0.340		−0.717	−0.401	
0.380	−0.716	−0.685	−0.371	
0.420			−0.348	
0.450	−0.666	−0.717		−0.679
0.460			−0.292	
0.500	−0.650	−0.666	−0.209	−0.652
0.520	−0.643	−0.650		−0.641
0.540	−0.627	−0.634	−0.120	−0.621
0.560	−0.616	−0.620		
0.580	−0.602		−0.023	−0.594
0.600	−0.577	−0.584		−0.568
0.620	−0.556	−0.563	0.089	−0.546
0.640		−0.546		
0.660			0.176	
0.700			0.235	
0.740		−0.373	0.291	
0.780		−0.301	0.330	
0.820		−0.216	0.363	
0.860		−0.145	0.375	
0.900		−0.075	0.363	
0.920		−0.042	0.345	
0.940		0.001	0.324	
0.960		0.032	0.280	
0.980		0.072	0.228	
1.000	0.099			0.104

WALL

y/s=	0			.50		1		
z/c=	1.397	0	−1.397	1.524	−1.524	1.397	0	−1.397
x/c								
−6.136	0.009							
−4.548	0.030							
−3.309	0.007	0.017	0.025			0.016	0.020	0.034
−3.055				0.008	0.025			
−2.293				−0.018	0.022			
−2.039	−0.033					−0.026		
−1.531	−0.029			−0.018	0.035	−0.030		
−1.023	−0.038					−0.030		
−0.769		0.057		−0.067	0.022		0.069	
−0.515	−0.070		0.028			−0.069		0.019
−0.007	−0.094		0.029	−0.084	0.055	−0.098		0.054
0.501	−0.092		0.052	−0.068	0.049	−0.091		0.051
1.009	−0.084		0.062	−0.057	0.044	−0.072		0.038
1.515	−0.052		0.049			−0.047		0.039
1.771		0.039		−0.025	0.042		0.052	
2.025	−0.025		0.040			−0.013		0.048
2.533	−0.015		0.038	−0.005	0.035	−0.006		0.037
3.041	−0.009		0.039			−0.001		0.027
3.295				−0.005	0.026			
4.088				0.013	0.023			
4.311	0.013	0.012	0.024			0.011	0.000	0.030
4.850				0.011	0.035			

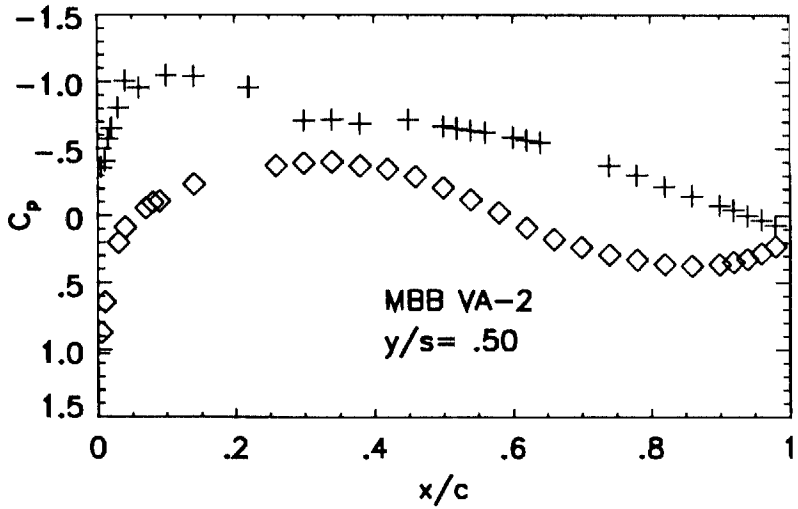

Figure 6. Continued. (b) M_∞=0.729, α=0.9°, Re=6x10^6.

MBB VA-2

y/s=	.25	.50		.75
	UPPER	UPPER	LOWER	UPPER
x/c				
0.000		0.994		
0.005		−0.580	0.962	
0.010		−0.520	0.745	
0.015		−0.743		
0.020		−0.828		
0.030		−0.934	0.314	
0.040		−1.117	0.196	
0.060		−1.143		
0.070			0.045	
0.080			−0.003	
0.090			−0.018	
0.100		−1.140		
0.140		−1.212	−0.157	
0.180	−1.207			−1.214
0.220		−1.184		
0.260			−0.311	
0.300		−1.186	−0.328	
0.340		−1.187	−0.349	
0.380	−1.112	−1.172	−0.327	
0.420			−0.311	
0.450	−0.616	−0.659		−0.626
0.460			−0.260	
0.500	−0.605	−0.595	−0.188	−0.590
0.520	−0.607	−0.590		−0.588
0.540	−0.605	−0.588	−0.098	−0.584
0.560	−0.601	−0.584		
0.580	−0.597		−0.004	−0.576
0.600	−0.577	−0.567		−0.557
0.620	−0.562	−0.552	0.109	−0.543
0.640		−0.530		
0.660			0.196	
0.700			0.255	
0.740		−0.375	0.313	
0.780		−0.306	0.349	
0.820		−0.222	0.383	
0.860		−0.149	0.393	
0.900		−0.075	0.380	
0.920		−0.042	0.361	
0.940		−0.003	0.338	
0.960		0.033	0.292	
0.980		0.073	0.236	
1.000	0.099			0.104

WALL

y/s=	0			.50		1		
z/c=	1.397	0	−1.397	1.524	−1.524	1.397	0	−1.397
x/c								
−6.136	0.007							
−4.548	0.030							
−3.309	0.009	0.016	0.026			0.016	0.021	0.035
−3.055				0.009	0.025			
−2.293				−0.021	0.024			
−2.039	−0.036					−0.025		
−1.531	−0.032			−0.021	0.042	−0.034		
−1.023	−0.048					−0.039		
−0.769		0.057		−0.083	0.032		0.068	
−0.515	−0.091		0.039			−0.093		0.033
−0.007	−0.136		0.050	−0.131	0.074	−0.145		0.075
0.501	−0.151		0.072	−0.115	0.071	−0.143		0.069
1.009	−0.120		0.072	−0.086	0.056	−0.101		0.051
1.515	−0.068		0.054			−0.062		0.046
1.771		0.035		−0.036	0.045		0.050	
2.025	−0.032		0.043			−0.021		0.047
2.533	−0.018		0.039	−0.012	0.036	−0.012		0.036
3.041	−0.011		0.039			−0.006		0.026
3.295				−0.009	0.025			
4.088				0.010	0.022			
4.311	0.010	0.010	0.022			0.008	−0.003	0.028
4.850				0.008	0.033			

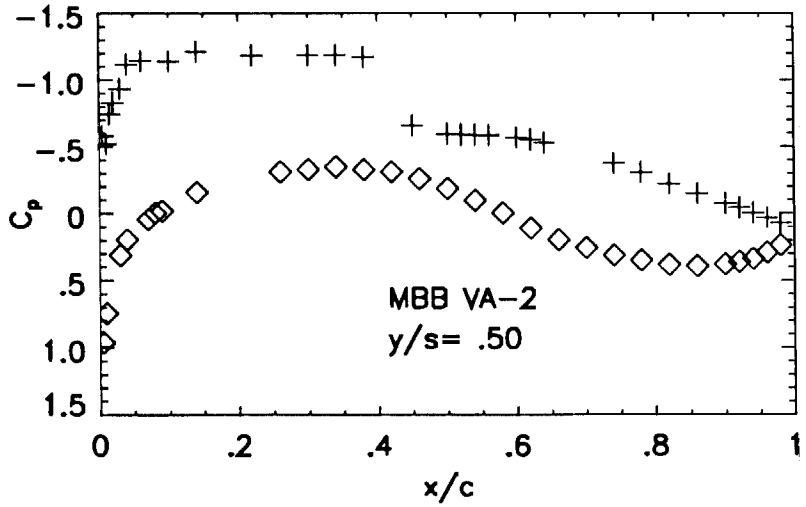

Figure 6. Continued. (c) M_∞=0.730, α=1.5°, Re=6x10^6.

MBB VA−2

y/s=	.25	.50		.75
	UPPER	UPPER	LOWER	UPPER
x/c				
0.000		1.105		
0.005		−0.476	0.808	
0.010		−0.181	0.574	
0.015		−0.366		
0.020		−0.484		
0.030		−0.665	0.108	
0.040		−0.793	−0.003	
0.060		−0.836		
0.070			−0.157	
0.080			−0.191	
0.090			−0.200	
0.100		−0.909		
0.140		−0.861	−0.332	
0.180	−0.670			−0.844
0.220		−0.777		
0.260			−0.482	
0.300		−0.802	−0.492	
0.340		−0.811	−0.505	
0.380	−0.798	−0.779	−0.457	
0.420			−0.418	
0.450	−0.653	−0.707		−0.680
0.460			−0.341	
0.500	−0.665	−0.675	−0.248	−0.665
0.520	−0.660	−0.665		−0.658
0.540	−0.647	−0.650	−0.136	−0.638
0.560	−0.632	−0.634		
0.580	−0.614		−0.033	−0.605
0.600	−0.588	−0.593		−0.576
0.620	−0.565	−0.567	0.081	−0.555
0.640		−0.541		
0.660			0.168	
0.700			0.230	
0.740		−0.362	0.285	
0.780		−0.292	0.325	
0.820		−0.210	0.362	
0.860		−0.137	0.377	
0.900		−0.066	0.368	
0.920		−0.031	0.352	
0.940		0.009	0.328	
0.960		0.043	0.289	
0.980		0.082	0.237	
1.000	0.110			0.114

WALL

y/s=	0			.50		1		
z/c=	1.397	0	−1.397	1.524	−1.524	1.397	0	−1.397
x/c								
−6.136	0.015							
−4.548	0.036							
−3.309	0.014	0.021	0.030			0.021	0.024	0.037
−3.055				0.012	0.028			
−2.293				−0.015	0.022			
−2.039	−0.030					−0.020		
−1.531	−0.022			−0.013	0.037	−0.026		
−1.023	−0.029					−0.022		
−0.769		0.058		−0.056	0.010		0.067	
−0.515	−0.056		0.020			−0.057		0.008
−0.007	−0.077		0.012	−0.069	0.035	−0.084		0.039
0.501	−0.086		0.029	−0.059	0.031	−0.082		0.032
1.009	−0.077		0.045	−0.053	0.035	−0.064		0.027
1.515	−0.046		0.041			−0.040		0.031
1.771		0.042		−0.019	0.039		0.053	
2.025	−0.021		0.037			−0.010		0.044
2.533	−0.011		0.036	−0.003	0.034	−0.003		0.034
3.041	−0.006		0.039			−0.001		0.027
3.295				−0.005	0.027			
4.088				0.013	0.024			
4.311	0.014	0.015	0.024			0.012	0.000	0.030
4.850				0.012	0.035			

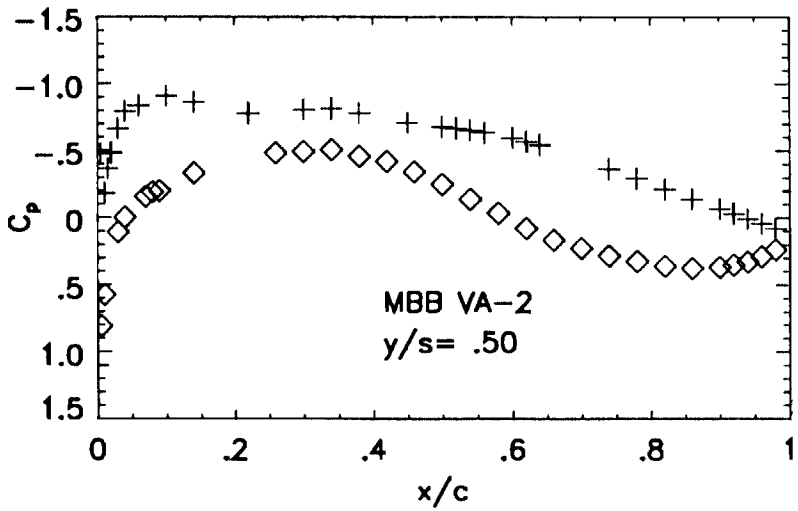

Figure 6. Continued. (d) M_∞=0.750, α=0.5°, Re=6x10^6.

MBB VA-2

y/s=	.25	.50		.75
	UPPER	UPPER	LOWER	UPPER
x/c				
0.000		1.066		
0.005		−0.415	0.892	
0.010		−0.305	0.645	
0.015		−0.501		
0.020		−0.581		
0.030		−0.746	0.203	
0.040		−0.937	0.088	
0.060		−0.902		
0.070			−0.068	
0.080			−0.103	
0.090			−0.117	
0.100		−0.992		
0.140		−1.034	−0.249	
0.180	−1.025			−1.013
0.220		−1.012		
0.260			−0.404	
0.300		−1.026	−0.422	
0.340		−1.034	−0.435	
0.380	−0.972	−1.021	−0.402	
0.420			−0.374	
0.450	−0.949	−1.018		−1.029
0.460			−0.309	
0.500	−0.641	−0.681	−0.224	−0.655
0.520	−0.590	−0.595		−0.572
0.540	−0.580	−0.570	−0.123	−0.547
0.560	−0.581	−0.562		
0.580	−0.580		−0.020	−0.545
0.600	−0.563	−0.549		−0.535
0.620	−0.550	−0.539	0.095	−0.524
0.640		−0.520		
0.660			0.182	
0.700			0.243	
0.740		−0.365	0.300	
0.780		−0.293	0.342	
0.820		−0.213	0.373	
0.860		−0.140	0.386	
0.900		−0.071	0.376	
0.920		−0.034	0.359	
0.940		0.005	0.335	
0.960		0.039	0.292	
0.980		0.078	0.238	
1.000	0.103			0.110

WALL

y/s=	0			.50		1		
z/c=	1.397	0	−1.397	1.524	−1.524	1.397	0	−1.397
x/c								
−6.136	0.011							
−4.548	0.034							
−3.309	0.012	0.021	0.029			0.019	0.023	0.037
−3.055				0.010	0.027			
−2.293				−0.018	0.025			
−2.039	−0.030					−0.021		
−1.531	−0.027			−0.017	0.040	−0.030		
−1.023	−0.039					−0.030		
−0.769		0.058		−0.070	0.021		0.069	
−0.515	−0.075		0.029			−0.076		0.020
−0.007	−0.114		0.030	−0.112	0.055	−0.125		0.055
0.501	−0.126		0.049	−0.104	0.050	−0.127		0.048
1.009	−0.109		0.062	−0.082	0.042	−0.092		0.038
1.515	−0.061		0.046			−0.056		0.037
1.771		0.039		−0.029	0.042		0.053	
2.025	−0.028		0.040			−0.016		0.044
2.533	−0.015		0.037	−0.007	0.034	−0.008		0.033
3.041	−0.009		0.038			−0.005		0.027
3.295				−0.007	0.026			
4.088				0.011	0.021			
4.311	0.012	0.012	0.022			0.010	−0.003	0.027
4.850				0.008	0.031			

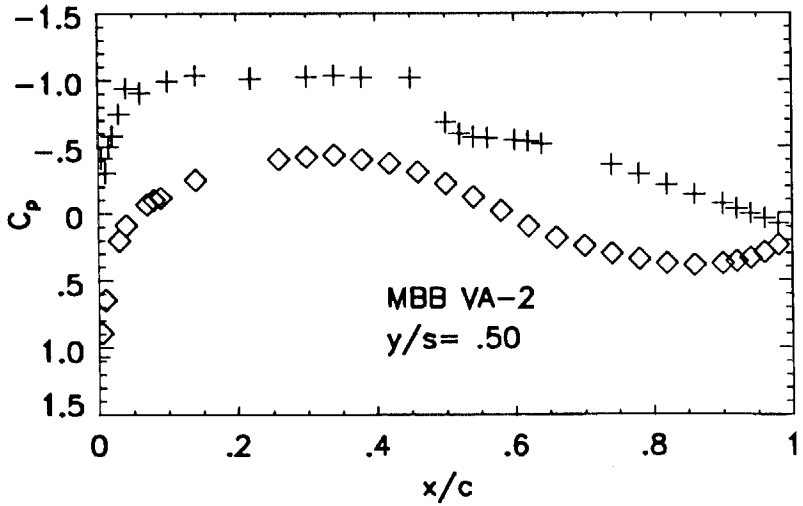

Figure 6. Continued. (e) M_∞=0.750, α=0.9°, Re=6x10^6.

MBB VA-2

y/s=	.25	.50		.75
	UPPER	UPPER	LOWER	UPPER
x/c				
0.000		1.027		
0.005		−0.446	0.945	
0.010		−0.409	0.740	
0.015		−0.627		
0.020		−0.717		
0.030		−0.855	0.288	
0.040		−1.011	0.165	
0.060		−1.044		
0.070			0.017	
0.080			−0.027	
0.090			−0.042	
0.100		−1.058		
0.140		−1.134	−0.185	
0.180	−1.144			−1.149
0.220		−1.135		
0.260			−0.354	
0.300		−1.154	−0.373	
0.340		−1.156	−0.396	
0.380	−1.145	−1.165	−0.370	
0.420			−0.349	
0.450	−1.143	−1.195		−1.157
0.460			−0.291	
0.500	−1.184	−1.219	−0.209	−1.203
0.520	−1.184	−1.235		−1.226
0.540	−1.181	−1.241	−0.115	−1.211
0.560	−1.037	−0.997		
0.580	−0.756		−0.015	−0.735
0.600	−0.620	−0.649		−0.622
0.620	−0.550	−0.587	0.099	−0.557
0.640		−0.540		
0.660			0.188	
0.700			0.248	
0.740		−0.348	0.306	
0.780		−0.276	0.345	
0.820		−0.203	0.377	
0.860		−0.133	0.389	
0.900		−0.068	0.377	
0.920		−0.037	0.356	
0.940		−0.003	0.332	
0.960		0.027	0.285	
0.980		0.063	0.226	
1.000	0.085			0.085

WALL

y/s=	0			.50		1		
z/c=	1.397	0	−1.397	1.524	−1.524	1.397	0	−1.397
x/c								
−6.136	0.013							
−4.548	0.035							
−3.309	0.011	0.021	0.029			0.018	0.024	0.038
−3.055				0.011	0.027			
−2.293				−0.020	0.023			
−2.039	−0.034					−0.023		
−1.531	−0.028			−0.021	0.042	−0.032		
−1.023	−0.045					−0.038		
−0.769		0.059		−0.083	0.028		0.068	
−0.515	−0.092		0.035			−0.095		0.029
−0.007	−0.158		0.042	−0.160	0.067	−0.169		0.067
0.501	−0.202		0.059	−0.174	0.060	−0.195		0.058
1.009	−0.160		0.068	−0.119	0.046	−0.136		0.042
1.515	−0.087		0.045			−0.079		0.034
1.771		0.031		−0.049	0.035		0.046	
2.025	−0.042		0.035			−0.032		0.039
2.533	−0.024		0.030	−0.022	0.027	−0.021		0.027
3.041	−0.020		0.030			−0.016		0.017
3.295				−0.017	0.018			
4.088				0.002	0.013			
4.311	0.001	0.003	0.011			0.000	−0.012	0.017
4.850				0.000	0.023			

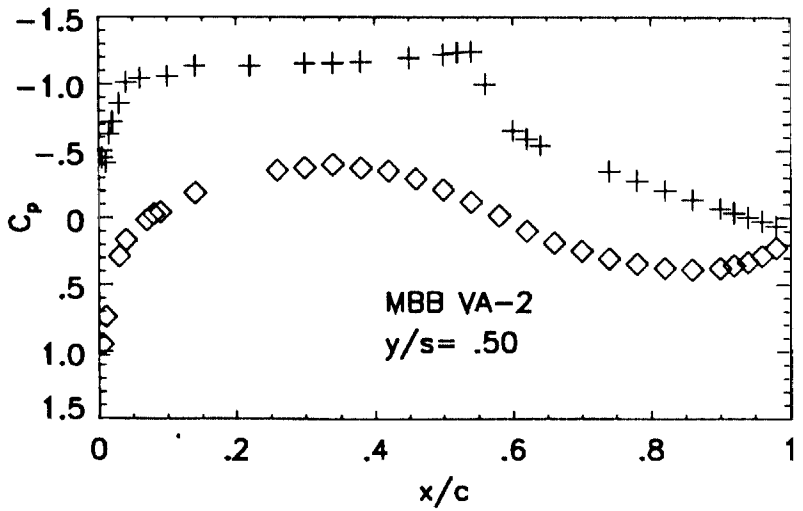

Figure 6. Continued. (f) M_∞=0.749, α=1.5°, Re=6x10^6.

MBB VA-2

y/s=	.25	.50		.75
	UPPER	UPPER	LOWER	UPPER
x/c				
0.000		1.133		
0.005		−0.339	0.800	
0.010		−0.004	0.552	
0.015		−0.231		
0.020		−0.343		
0.030		−0.499	0.090	
0.040		−0.664	−0.024	
0.060		−0.710		
0.070			−0.188	
0.080			−0.225	
0.090			−0.231	
0.100		−0.795		
0.140		−0.778	−0.375	
0.180	−0.801			−0.811
0.220		−0.798		
0.260			−0.603	
0.300		−0.859	−0.606	
0.340		−0.869	−0.672	
0.380	−0.877	−0.881	−0.650	
0.420			−0.465	
0.450	−0.903	−0.914		−0.929
0.460			−0.374	
0.500	−0.932	−0.945	−0.269	−0.960
0.520	−0.945	−0.968		−0.975
0.540	−0.959	−0.986	−0.149	−0.971
0.560	−0.982	−0.997		
0.580	−1.001		−0.041	−1.014
0.600	−1.015	−1.024		−1.025
0.620	−1.025	−1.035	0.071	−1.040
0.640		−0.973		
0.660			0.156	
0.700			0.218	
0.740		−0.350	0.275	
0.780		−0.273	0.316	
0.820		−0.198	0.354	
0.860		−0.131	0.370	
0.900		−0.066	0.363	
0.920		−0.033	0.344	
0.940		−0.001	0.323	
0.960		0.028	0.277	
0.980		0.061	0.221	
1.000	0.085			0.090

WALL

y/s=	0			.50		1		
z/c=	1.397	0	−1.397	1.524	−1.524	1.397	0	−1.397
x/c								
−6.136	0.016							
−4.548	0.040							
−3.309	0.017	0.025	0.033			0.025	0.028	0.041
−3.055				0.015	0.030			
−2.293				−0.013	0.024			
−2.039	−0.028					−0.018		
−1.531	−0.016			−0.007	0.038	−0.021		
−1.023	−0.021					−0.017		
−0.769		0.061		−0.050	0.006		0.073	
−0.515	−0.052		0.013			−0.054		0.001
−0.007	−0.094		0.000	−0.097	0.019	−0.108		0.027
0.501	−0.142		0.008	−0.124	0.007	−0.141		0.009
1.009	−0.123		0.031	−0.085	0.022	−0.102		0.012
1.515	−0.065		0.032			−0.057		0.021
1.771		0.031		−0.031	0.029		0.049	
2.025	−0.029		0.028			−0.019		0.034
2.533	−0.018		0.027	−0.012	0.025	−0.010		0.026
3.041	−0.013		0.028			−0.009		0.017
3.295				−0.014	0.019			
4.088				0.005	0.014			
4.311	0.006	0.006	0.013			0.005	−0.011	0.020
4.850				0.004	0.024			

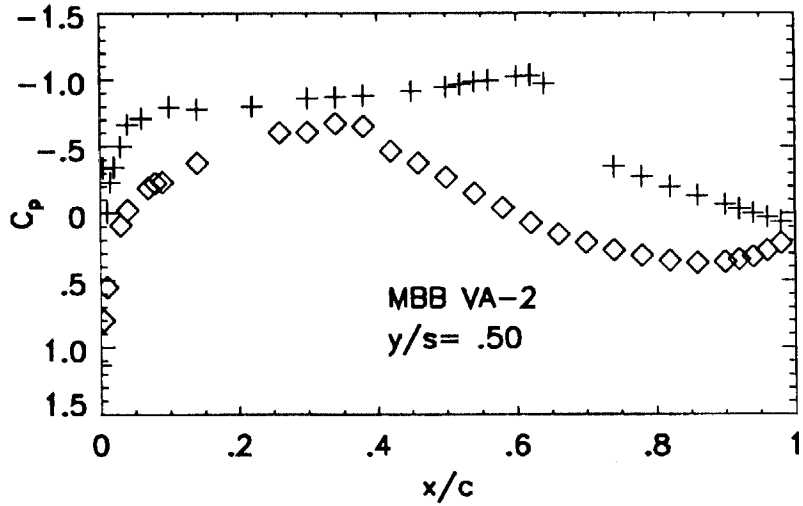

Figure 6. Continued. (g) M_∞=0.784, α=0.5°, Re=6x10^6.

MBB VA-2

y/s=	.25	.50		.75
	UPPER	UPPER	LOWER	UPPER
x/c				
0.000		1.123		
0.005		−0.367	0.837	
0.010		−0.113	0.602	
0.015		−0.324		
0.020		−0.416		
0.030		−0.570	0.143	
0.040		−0.767	0.041	
0.060		−0.764		
0.070			−0.132	
0.080			−0.174	
0.090			−0.183	
0.100		−0.865		
0.140		−0.898	−0.327	
0.180	−0.891			−0.900
0.220		−0.902		
0.260			−0.543	
0.300		−0.942	−0.561	
0.340		−0.965	−0.651	
0.380	−0.944	−0.972	−0.550	
0.420			−0.476	
0.450	−0.980	−0.997		−1.003
0.460			−0.384	
0.500	−1.003	−1.032	−0.278	−1.043
0.520	−1.014	−1.056		−1.052
0.540	−1.027	−1.077	−0.166	−1.059
0.560	−1.047	−1.090		
0.580	−1.072		−0.051	−1.094
0.600	−1.083	−1.048		−1.107
0.620	−1.090	−0.762	0.064	−0.949
0.640		−0.586		
0.660			0.150	
0.700			0.212	
0.740		−0.382	0.269	
0.780		−0.321	0.311	
0.820		−0.258	0.346	
0.860		−0.198	0.360	
0.900		−0.137	0.346	
0.920		−0.110	0.325	
0.940		−0.080	0.297	
0.960		−0.056	0.243	
0.980		−0.027	0.174	
1.000	0.035			0.031

WALL

y/s=	0			.50		1		
z/c=	1.397	0	−1.397	1.524	−1.524	1.397	0	−1.397
x/c								
−6.136	0.015							
−4.548	0.037							
−3.309	0.015	0.023	0.031			0.020	0.030	0.040
−3.055				0.013	0.030			
−2.293				−0.018	0.024			
−2.039	−0.030					−0.018		
−1.531	−0.019			−0.010	0.039	−0.024		
−1.023	−0.025					−0.019		
−0.769		0.061		−0.057	0.012		0.072	
−0.515	−0.061		0.015			−0.064		0.006
−0.007	−0.114		0.005	−0.121	0.029	−0.131		0.030
0.501	−0.177		0.015	−0.162	0.017	−0.176		0.015
1.009	−0.150		0.035	−0.097	0.018	−0.127		0.012
1.515	−0.080		0.028			−0.071		0.018
1.771		0.028		−0.042	0.023		0.043	
2.025	−0.039		0.026			−0.028		0.028
2.533	−0.026		0.024	−0.019	0.020	−0.021		0.021
3.041	−0.021		0.024			−0.017		0.011
3.295				−0.018	0.014			
4.088				−0.002	0.006			
4.311	−0.002	0.000	0.008			−0.002	−0.015	0.012
4.850				−0.004	0.016			

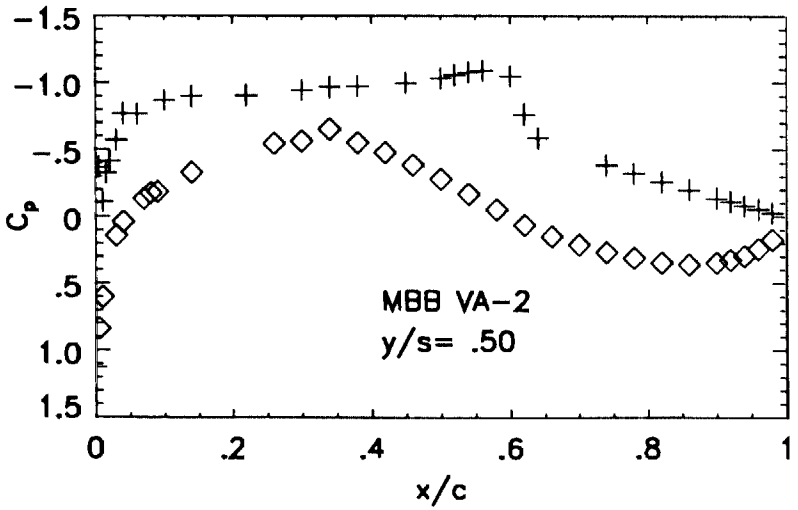

Figure 6. Continued. (h) M_∞=0.781, α=0.9°, Re=6x10^6.

MBB VA-2

y/s=	.25	.50		.75
	UPPER	UPPER	LOWER	UPPER
x/c				
0.000		1.103		
0.005		−0.392	0.875	
0.010		−0.183	0.656	
0.015		−0.393		
0.020		−0.487		
0.030		−0.633	0.206	
0.040		−0.807	0.082	
0.060		−0.829		
0.070			−0.083	
0.080			−0.121	
0.090			−0.141	
0.100		−0.883		
0.140		−0.950	−0.289	
0.180	−0.978			−0.962
0.220		−0.971		
0.260			−0.513	
0.300		−1.007	−0.541	
0.340		−1.012	−0.633	
0.380	−1.013	−1.035	−0.577	
0.420			−0.492	
0.450	−1.032	−1.064		−1.049
0.460			−0.401	
0.500	−1.071	−1.097	−0.296	−1.095
0.520	−1.077	−1.083		−1.117
0.540	−1.091	−0.920	−0.179	−1.117
0.560	−1.105	−0.657		
0.580	−1.130		−0.072	−1.085
0.600	−1.052	−0.519		−0.719
0.620	−0.741	−0.499	0.046	−0.604
0.640		−0.479		
0.660			0.136	
0.700			0.199	
0.740		−0.408	0.257	
0.780		−0.373	0.298	
0.820		−0.335	0.332	
0.860		−0.293	0.340	
0.900		−0.254	0.319	
0.920		−0.234	0.290	
0.940		−0.213	0.255	
0.960		−0.195	0.189	
0.980		−0.175	0.099	
1.000	−0.023			−0.051

WALL

y/s=	0			.50		1		
z/c=	1.397	0	−1.397	1.524	−1.524	1.397	0	−1.397
x/c								
−6.136	0.018							
−4.548	0.040							
−3.309	0.017	0.027	0.034			0.025	0.030	0.044
−3.055				0.016	0.031			
−2.293				−0.014	0.024			
−2.039	−0.029					−0.016		
−1.531	−0.016			−0.008	0.043	−0.021		
−1.023	−0.024					−0.018		
−0.769		0.064		−0.058	0.012		0.075	
−0.515	−0.062		0.019			−0.065		0.010
−0.007	−0.123		0.007	−0.132	0.030	−0.142		0.034
0.501	−0.197		0.014	−0.180	0.011	−0.198		0.014
1.009	−0.167		0.032	−0.118	0.014	−0.140		0.006
1.515	−0.089		0.022			−0.082		0.011
1.771		0.021		−0.050	0.018		0.036	
2.025	−0.045		0.019			−0.036		0.024
2.533	−0.032		0.016	−0.026	0.012	−0.026		0.014
3.041	−0.028		0.019			−0.024		0.005
3.295				−0.026	0.005			
4.088				−0.007	0.000			
4.311	−0.008	−0.006	0.000			−0.009	−0.022	0.007
4.850				−0.009	0.010			

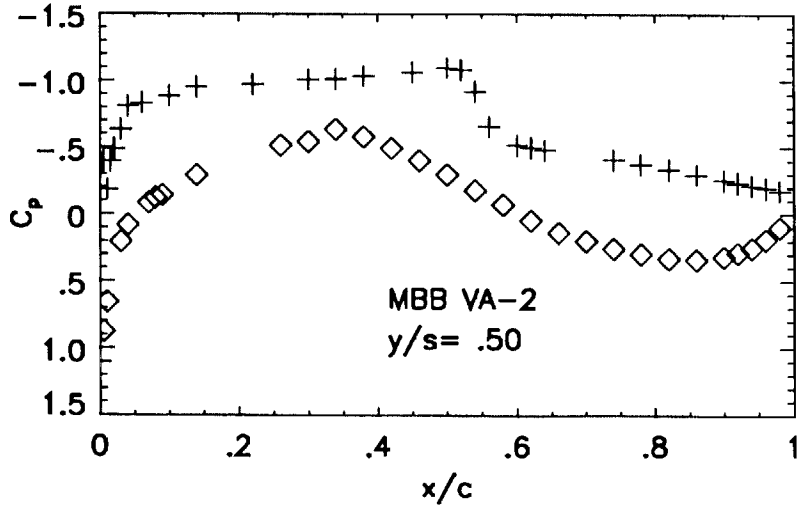

Figure 6. Continued. (i) M_∞=0.781, α=1.5°, Re=6x10^6.

MBB VA-2

y/s=	.25	.50		.75
	UPPER	UPPER	LOWER	UPPER
x/c				
0.000		1.153		
0.005		−0.346	0.753	
0.010		0.053	0.518	
0.015		−0.140		
0.020		−0.262		
0.030		−0.404	0.040	
0.040		−0.571	−0.062	
0.060		−0.620		
0.070			−0.238	
0.080			−0.272	
0.090			−0.275	
0.100		−0.708		
0.140		−0.697	−0.419	
0.180	−0.710			−0.721
0.220		−0.727		
0.260			−0.677	
0.300		−0.789	−0.729	
0.340		−0.806	−0.804	
0.380	−0.824	−0.824	−0.884	
0.420			−0.946	
0.450	−0.850	−0.874		−0.872
0.460			−0.545	
0.500	−0.891	−0.902	−0.330	−0.914
0.520	−0.902	−0.925		−0.930
0.540	−0.923	−0.951	−0.230	−0.927
0.560	−0.943	−0.953		
0.580	−0.965		−0.134	−0.977
0.600	−0.981	−0.989		−0.992
0.620	−0.997	−0.992	−0.060	−1.008
0.640		−0.791		
0.660			0.015	
0.700			0.089	
0.740		−0.351	0.159	
0.780		−0.300	0.215	
0.820		−0.249	0.264	
0.860		−0.204	0.290	
0.900		−0.155	0.290	
0.920		−0.134	0.271	
0.940		−0.109	0.252	
0.960		−0.089	0.204	
0.980		−0.065	0.142	
1.000	−0.004			−0.001

WALL

y/s=	0			.50		1		
z/c=	1.397	0	−1.397	1.524	−1.524	1.397	0	−1.397
x/c								
−6.136	0.020							
−4.548	0.043							
−3.309	0.018	0.028	0.036			0.027	0.030	0.044
−3.055				0.017	0.033			
−2.293				−0.011	0.023			
−2.039	−0.029					−0.014		
−1.531	−0.013			−0.005	0.038	−0.017		
−1.023	−0.014					−0.009		
−0.769		0.062		−0.041	−0.007		0.070	
−0.515	−0.038		−0.002			−0.043		−0.018
−0.007	−0.076		−0.033	−0.083	−0.023	−0.094		−0.015
0.501	−0.135		−0.056	−0.128	−0.056	−0.141		−0.050
1.009	−0.126		−0.029	−0.096	−0.024	−0.108		−0.034
1.515	−0.074		−0.002			−0.067		−0.010
1.771		0.017		−0.041	0.004		0.032	
2.025	−0.042		0.003			−0.031		0.013
2.533	−0.032		0.007	−0.025	0.005	−0.025		0.007
3.041	−0.029		0.008			−0.026		0.000
3.295				−0.030	0.000			
4.088				−0.012	−0.005			
4.311	−0.011	−0.010	−0.005			−0.012	−0.024	0.000
4.850				−0.013	0.004			

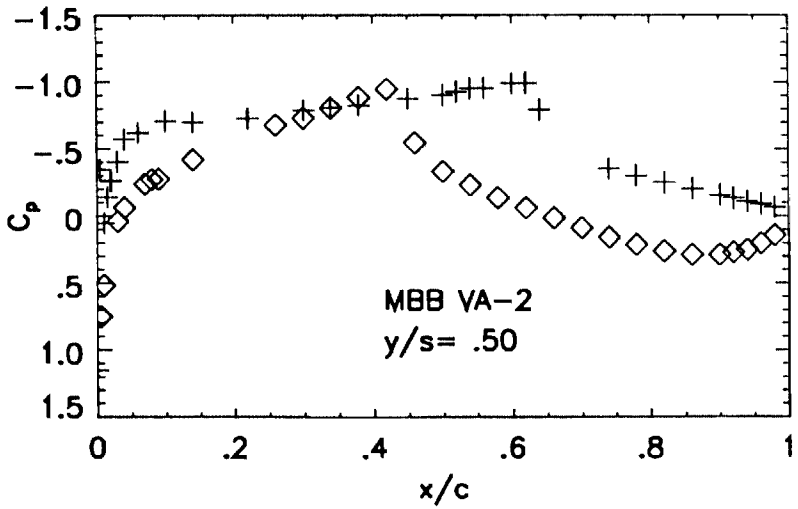

Figure 6. Continued. (j) M_∞=0.802, α=0.5°, Re=6x10^6.

MBB VA-2

y/s=	.25	.50		.75
	UPPER	UPPER	LOWER	UPPER
x/c				
0.000		1.148		
0.005		−0.178	0.801	
0.010		0.004	0.528	
0.015		−0.192		
0.020		−0.296		
0.030		−0.445	0.098	
0.040		−0.618	−0.010	
0.060		−0.666		
0.070			−0.192	
0.080			−0.231	
0.090			−0.238	
0.100		−0.761		
0.140		−0.768	−0.385	
0.180	−0.781			−0.793
0.220		−0.785		
0.260			−0.649	
0.300		−0.856	−0.705	
0.340		−0.876	−0.787	
0.380	−0.858	−0.881	−0.859	
0.420			−0.918	
0.450	−0.889	−0.914		−0.929
0.460			−0.765	
0.500	−0.929	−0.961	−0.365	−0.963
0.520	−0.943	−0.979		−0.980
0.540	−0.959	−1.001	−0.260	−0.986
0.560	−0.983	−1.015		
0.580	−1.009		−0.165	−1.026
0.600	−1.023	−0.762		−1.030
0.620	−1.015	−0.555	−0.097	−0.846
0.640		−0.468		
0.660			−0.022	
0.700			0.053	
0.740		−0.363	0.126	
0.780		−0.329	0.186	
0.820		−0.298	0.239	
0.860		−0.264	0.267	
0.900		−0.230	0.260	
0.920		−0.214	0.242	
0.940		−0.199	0.215	
0.960		−0.183	0.160	
0.980		−0.167	0.087	
1.000	−0.073			−0.080

WALL

y/s=	0			.50		1		
z/c=	1.397	0	−1.397	1.524	−1.524	1.397	0	−1.397
x/c								
−6.136	0.016							
−4.548	0.041							
−3.309	0.018	0.026	0.035			0.026	0.029	0.044
−3.055				0.015	0.031			
−2.293				−0.014	0.024			
−2.039	−0.026					−0.015		
−1.531	−0.013			−0.005	0.036	−0.018		
−1.023	−0.018					−0.011		
−0.769		0.059		−0.045	−0.005		0.069	
−0.515	−0.043		−0.005			−0.047		−0.019
−0.007	−0.090		−0.036	−0.098	−0.021	−0.108		−0.015
0.501	−0.163		−0.058	−0.159	−0.061	−0.171		−0.059
1.009	−0.146		−0.039	−0.114	−0.039	−0.129		−0.049
1.515	−0.089		−0.018			−0.079		−0.022
1.771		0.006		−0.055	−0.009		0.020	
2.025	−0.053		−0.012			−0.042		0.000
2.533	−0.044		−0.005	−0.031	−0.007	−0.037		−0.005
3.041	−0.042		−0.003			−0.037		−0.012
3.295				−0.041	−0.011			
4.088				−0.022	−0.016			
4.311	−0.023	−0.023	−0.016			−0.023	−0.037	−0.010
4.850				−0.025	−0.007			

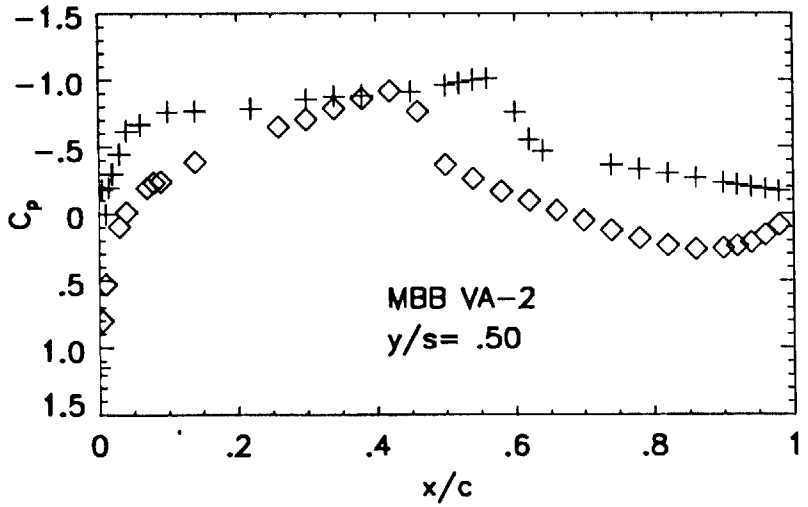

Figure 6. Continued. (k) M_∞=0.803, α=0.9°, Re=6x10^6.

MBB VA-2

y/s=	.25	.50		.75
	UPPER	UPPER	LOWER	UPPER
x/c				
0.000		1.130		
0.005		−0.264	0.831	
0.010		−0.153	0.617	
0.015		−0.257		
0.020		−0.370		
0.030		−0.511	0.146	
0.040		−0.690	0.018	
0.060		−0.689		
0.070			−0.143	
0.080			−0.181	
0.090			−0.195	
0.100		−0.797		
0.140		−0.845	−0.350	
0.180	−0.868			−0.843
0.220		−0.868		
0.260			−0.621	
0.300		−0.909	−0.675	
0.340		−0.937	−0.753	
0.380	−0.933	−0.953	−0.832	
0.420			−0.902	
0.450	−0.962	−0.986		−0.971
0.460			−0.969	
0.500	−0.989	−1.020	−0.400	−1.019
0.520	−1.005	−1.029		−1.041
0.540	−1.020	−0.942	−0.278	−1.047
0.560	−1.032	−0.658		
0.580	−1.061		−0.177	−1.069
0.600	−0.965	−0.480		−0.740
0.620	−0.676	−0.460	−0.103	−0.582
0.640		−0.442		
0.660			−0.028	
0.700			0.052	
0.740		−0.401	0.129	
0.780		−0.379	0.189	
0.820		−0.358	0.240	
0.860		−0.335	0.261	
0.900		−0.313	0.247	
0.920		−0.302	0.221	
0.940		−0.291	0.188	
0.960		−0.281	0.122	
0.980		−0.265	0.035	
1.000	−0.153			−0.161

WALL

y/s=	0			.50		1		
z/c=	1.397	0	−1.397	1.524	−1.524	1.397	0	−1.397
x/c								
−6.136	0.019							
−4.548	0.042							
−3.309	0.018	0.029	0.034			0.029	0.030	0.043
−3.055				0.017	0.032			
−2.293				−0.012	0.023			
−2.039	−0.028					−0.015		
−1.531	−0.015			−0.006	0.036	−0.021		
−1.023	−0.021					−0.016		
−0.769		0.058		−0.050	−0.009		0.069	
−0.515	−0.049		−0.005			−0.053		−0.018
−0.007	−0.105		−0.037	−0.114	−0.025	−0.125		−0.015
0.501	−0.195		−0.057	−0.197	−0.071	−0.206		−0.064
1.009	−0.174		−0.045	−0.135	−0.048	−0.153		−0.057
1.515	−0.107		−0.026			−0.097		−0.033
1.771		−0.004		−0.066	−0.018		0.012	
2.025	−0.066		−0.020			−0.055		−0.010
2.533	−0.055		−0.016	−0.046	−0.016	−0.048		−0.015
3.041	−0.052		−0.013			−0.048		−0.023
3.295				−0.050	−0.020			
4.088				−0.032	−0.026			
4.311	−0.032	−0.032	−0.029			−0.033	−0.046	−0.020
4.850				−0.034	−0.017			

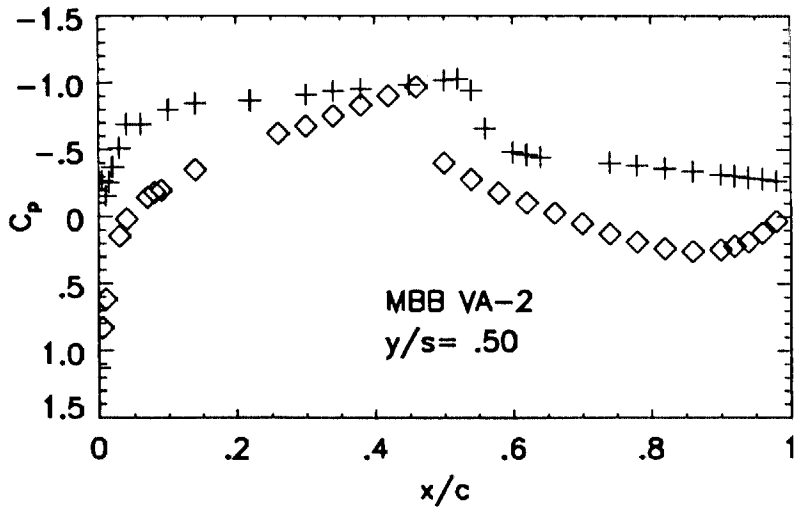

Figure 6. Concluded. (l) M_∞=0.803, α=1.5°, Re=6x10^6.

$\frac{z}{c}$	$\frac{u}{a_t}$	$\frac{v}{a_t}$	$\frac{\langle u'^2+v'^2\rangle}{2a_t^2}$	$\frac{\langle u'v'\rangle}{a_t^2}$
−0.648	0.687	-6.699^{-3}	1.002^{-4}	-1.818^{-7}
−0.616	0.688	-5.916^{-3}	9.713^{-5}	-7.056^{-6}
−0.584	0.686	-7.774^{-3}	8.650^{-5}	-4.342^{-6}
−0.552	0.690	-8.191^{-3}	9.150^{-5}	-6.960^{-6}
−0.520	0.688	-7.697^{-3}	8.565^{-5}	-3.860^{-6}
−0.488	0.693	-7.801^{-3}	1.153^{-4}	-1.212^{-5}
−0.456	0.689	-8.111^{-3}	1.141^{-4}	1.731^{-6}
−0.424	0.689	-9.444^{-3}	1.058^{-4}	-7.465^{-6}
−0.392	0.690	-1.006^{-2}	1.121^{-4}	-4.737^{-6}
−0.360	0.689	-9.050^{-3}	1.148^{-4}	-6.432^{-6}
−0.328	0.687	-8.905^{-3}	1.229^{-4}	-1.415^{-5}
−0.296	0.690	-1.106^{-2}	9.786^{-5}	-1.641^{-6}
−0.264	0.687	-8.601^{-3}	1.138^{-4}	3.868^{-6}
−0.232	0.690	-1.231^{-2}	1.056^{-4}	-5.613^{-6}
−0.200	0.690	-1.200^{-2}	1.102^{-4}	-4.101^{-7}
−0.174	0.690	-1.030^{-2}	1.072^{-4}	1.359^{-6}
−0.161	0.688	-8.666^{-3}	1.093^{-4}	6.659^{-6}
−0.148	0.693	-1.238^{-2}	1.211^{-4}	3.960^{-6}
−0.136	0.688	-1.030^{-2}	1.511^{-4}	1.483^{-5}
−0.123	0.684	-8.848^{-3}	1.604^{-4}	1.070^{-5}
−0.110	0.684	-1.124^{-2}	3.253^{-4}	9.309^{-5}
−0.097	0.673	-9.567^{-3}	4.658^{-4}	1.716^{-4}
−0.084	0.660	-1.010^{-2}	6.248^{-4}	2.288^{-4}
−0.072	0.644	-1.247^{-2}	7.414^{-4}	2.080^{-4}
−0.059	0.634	-1.308^{-2}	7.805^{-4}	4.289^{-5}
−0.046	0.638	-1.249^{-2}	7.709^{-4}	-5.677^{-5}
−0.033	0.648	-1.268^{-2}	7.954^{-4}	-1.956^{-4}
−0.020	0.666	-1.229^{-2}	6.685^{-4}	-1.622^{-4}
−0.008	0.676	-1.116^{-2}	4.586^{-4}	-1.235^{-4}
0.005	0.689	-1.347^{-2}	2.870^{-4}	-5.520^{-5}
0.018	0.693	-1.371^{-2}	1.825^{-4}	-2.090^{-6}
0.031	0.691	-1.391^{-2}	1.675^{-4}	4.035^{-6}
0.044	0.694	-1.597^{-2}	1.531^{-4}	1.500^{-5}
0.056	0.694	-1.295^{-2}	1.577^{-4}	1.405^{-5}
0.088	0.692	-1.342^{-2}	1.364^{-4}	1.008^{-5}
0.120	0.692	-1.338^{-2}	1.377^{-4}	6.912^{-6}
0.152	0.695	-1.450^{-2}	1.446^{-4}	1.974^{-5}
0.184	0.693	-9.712^{-3}	1.589^{-4}	8.671^{-6}
0.216	0.693	-1.404^{-2}	1.555^{-4}	3.587^{-6}
0.248	0.691	-1.328^{-2}	1.495^{-4}	3.579^{-6}
0.280	0.694	-1.414^{-2}	1.415^{-4}	1.014^{-5}
0.312	0.693	-1.378^{-2}	1.365^{-4}	5.388^{-6}
0.344	0.694	-1.285^{-2}	1.328^{-4}	5.061^{-6}
0.376	0.696	-1.375^{-2}	1.323^{-4}	4.142^{-6}
0.408	0.693	-1.289^{-2}	1.308^{-4}	1.233^{-5}
0.440	0.699	-1.353^{-2}	1.428^{-4}	-6.404^{-6}
0.472	0.692	-1.441^{-2}	1.262^{-4}	9.038^{-6}
0.504	0.695	-1.430^{-2}	1.288^{-4}	1.400^{-5}
0.536	0.692	-1.377^{-2}	1.249^{-4}	1.123^{-5}
0.568	0.695	-1.387^{-2}	1.170^{-4}	5.660^{-6}
0.600	0.695	-1.521^{-2}	1.243^{-4}	1.133^{-5}

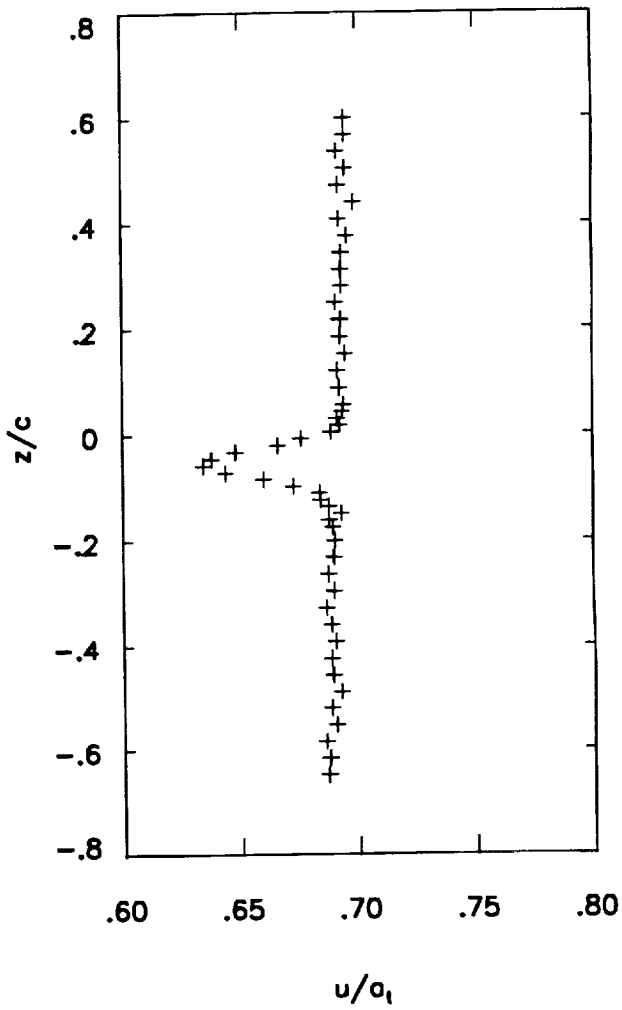

Figure 7. LDV wake data. (a) M_∞=0.728, α=0.5°, Re=6x10^6, x/c=2.5.

$\frac{z}{c}$	$\frac{u}{a_t}$	$\frac{v}{a_t}$	$\frac{\langle u'^2+v'^2\rangle}{2a_t^2}$	$\frac{\langle u'v'\rangle}{a_t^2}$
−0.648	0.690	-5.504^{-3}	9.998^{-5}	1.167^{-5}
−0.616	0.691	-4.889^{-3}	8.757^{-5}	1.525^{-5}
−0.584	0.690	-6.833^{-3}	8.935^{-5}	5.897^{-6}
−0.552	0.692	-6.888^{-3}	8.749^{-5}	2.053^{-7}
−0.520	0.689	-6.354^{-3}	7.050^{-5}	-5.227^{-7}
−0.488	0.689	-6.213^{-3}	8.172^{-5}	-1.561^{-6}
−0.456	0.692	-7.122^{-3}	9.501^{-5}	1.308^{-5}
−0.424	0.693	-8.678^{-3}	7.355^{-5}	-4.751^{-7}
−0.392	0.691	-1.031^{-2}	9.084^{-5}	4.093^{-6}
−0.360	0.692	-9.050^{-3}	7.809^{-5}	-3.925^{-6}
−0.328	0.688	-8.215^{-3}	9.647^{-5}	-1.821^{-6}
−0.296	0.687	-1.013^{-2}	9.512^{-5}	-3.119^{-6}
−0.264	0.690	-1.382^{-2}	9.686^{-5}	5.553^{-6}
−0.232	0.693	-1.242^{-2}	9.222^{-5}	2.468^{-6}
−0.200	0.692	-7.311^{-3}	9.414^{-5}	5.610^{-6}
−0.168	0.692	-8.961^{-3}	8.563^{-5}	1.293^{-5}
−0.136	0.692	-9.360^{-3}	1.523^{-4}	2.427^{-5}
−0.110	0.681	-6.567^{-3}	3.376^{-4}	1.090^{-4}
−0.097	0.669	-6.305^{-3}	5.341^{-4}	2.009^{-4}
−0.091	0.662	-6.466^{-3}	5.587^{-4}	2.065^{-4}
−0.084	0.651	-9.676^{-3}	7.417^{-4}	2.847^{-4}
−0.078	0.644	-1.122^{-2}	7.542^{-4}	2.618^{-4}
−0.074	0.642	-1.214^{-2}	7.484^{-4}	2.015^{-4}
−0.072	0.639	-1.130^{-2}	7.111^{-4}	1.506^{-4}
−0.070	0.636	-1.222^{-2}	7.418^{-4}	1.709^{-4}
−0.069	0.636	-1.032^{-2}	7.653^{-4}	1.288^{-4}
−0.067	0.637	-1.180^{-2}	7.404^{-4}	7.785^{-5}
−0.061	0.637	-1.330^{-2}	7.596^{-4}	2.513^{-5}
−0.059	0.635	-1.254^{-2}	7.066^{-4}	-8.861^{-6}
−0.046	0.645	-1.248^{-2}	8.354^{-4}	-1.569^{-4}
−0.033	0.660	-1.266^{-2}	6.909^{-4}	-1.625^{-4}
−0.020	0.675	-9.419^{-3}	5.387^{-4}	-1.429^{-4}
−0.008	0.684	-1.086^{-2}	3.433^{-4}	-6.838^{-5}
0.024	0.694	-1.115^{-2}	1.384^{-4}	1.172^{-5}
0.056	0.695	-1.288^{-2}	1.122^{-4}	2.483^{-5}
0.088	0.694	-1.189^{-2}	1.116^{-4}	3.232^{-5}
0.120	0.698	-1.263^{-2}	1.218^{-4}	3.300^{-5}
0.152	0.696	-1.216^{-2}	1.114^{-4}	3.151^{-5}
0.184	0.696	-1.246^{-2}	1.090^{-4}	2.800^{-5}
0.216	0.695	-1.319^{-2}	1.135^{-4}	2.702^{-5}
0.248	0.698	-1.498^{-2}	1.227^{-4}	2.861^{-5}
0.280	0.696	-1.256^{-2}	1.162^{-4}	2.963^{-5}
0.312	0.696	-1.310^{-2}	1.265^{-4}	3.629^{-5}
0.344	0.696	-1.392^{-2}	1.335^{-4}	4.026^{-5}
0.376	0.697	-1.341^{-2}	1.107^{-4}	2.210^{-5}
0.408	0.696	-1.369^{-2}	8.895^{-5}	1.352^{-5}
0.440	0.696	-1.434^{-2}	7.172^{-5}	3.990^{-6}
0.472	0.698	-1.457^{-2}	7.160^{-5}	9.786^{-6}
0.504	0.697	-1.547^{-2}	6.799^{-5}	5.872^{-6}
0.536	0.698	-1.567^{-2}	8.144^{-5}	1.256^{-5}
0.568	0.697	-1.493^{-2}	7.850^{-5}	9.262^{-6}

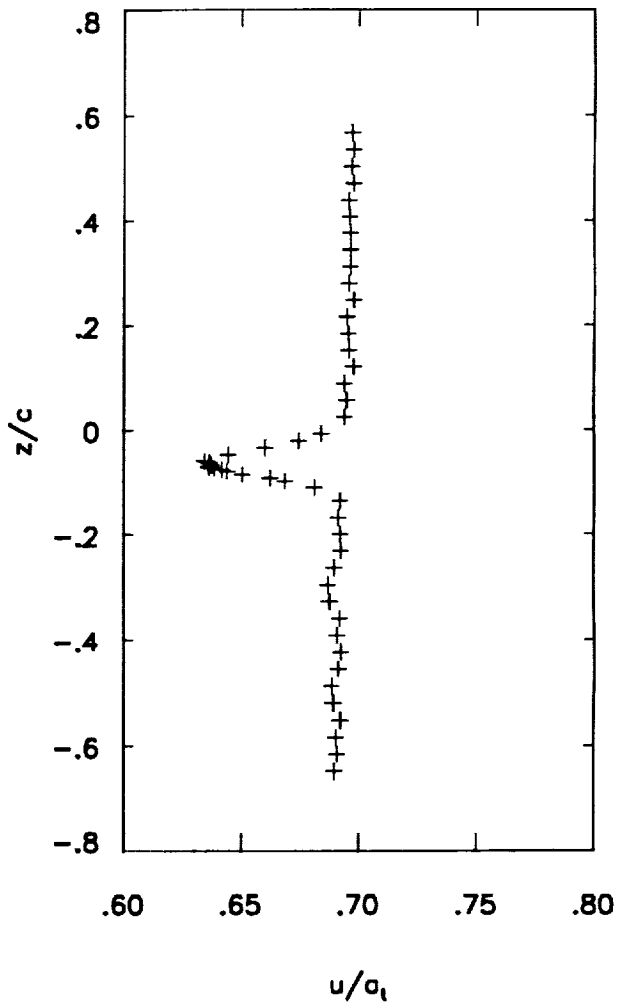

Figure 7. Continued. (b) M_∞=0.729, α=0.9°, Re=6x10^6, x/c=2.5.

$\frac{z}{c}$	$\frac{u}{a_t}$	$\frac{v}{a_t}$	$\frac{\langle u'^2+v'^2\rangle}{2a_t^2}$	$\frac{\langle u'v'\rangle}{a_t^2}$
−0.648	0.694	-3.656^{-3}	1.490^{-4}	1.238^{-6}
−0.616	0.694	-4.233^{-3}	1.397^{-4}	8.731^{-6}
−0.584	0.693	-6.698^{-3}	1.360^{-4}	7.555^{-6}
−0.552	0.696	-5.537^{-3}	1.349^{-4}	1.862^{-5}
−0.520	0.695	-5.284^{-3}	1.435^{-4}	1.679^{-5}
−0.488	0.694	-6.235^{-3}	1.305^{-4}	1.940^{-5}
−0.456	0.695	-6.122^{-3}	1.579^{-4}	3.777^{-5}
−0.424	0.696	-7.218^{-3}	1.350^{-4}	1.642^{-5}
−0.392	0.695	-8.684^{-3}	1.370^{-4}	1.790^{-5}
−0.360	0.696	-8.597^{-3}	1.436^{-4}	2.372^{-5}
−0.328	0.696	-5.532^{-3}	1.427^{-4}	2.141^{-5}
−0.296	0.691	-9.636^{-3}	1.411^{-4}	2.442^{-5}
−0.264	0.695	-1.180^{-2}	1.393^{-4}	2.187^{-5}
−0.232	0.697	-9.077^{-3}	1.415^{-4}	2.011^{-5}
−0.200	0.695	-8.376^{-3}	1.477^{-4}	3.052^{-5}
−0.168	0.694	-8.035^{-3}	1.586^{-4}	2.909^{-5}
−0.136	0.692	-8.180^{-3}	3.175^{-4}	1.163^{-4}
−0.104	0.665	-8.211^{-3}	7.027^{-4}	3.211^{-4}
−0.097	0.659	-1.262^{-2}	7.755^{-4}	3.303^{-4}
−0.091	0.649	-1.183^{-2}	8.488^{-4}	2.933^{-4}
−0.084	0.646	-1.333^{-2}	8.481^{-4}	2.259^{-4}
−0.078	0.638	-1.440^{-2}	8.462^{-4}	1.596^{-4}
−0.072	0.634	-1.002^{-2}	8.415^{-4}	4.921^{-5}
−0.065	0.636	-1.411^{-2}	8.386^{-4}	-2.753^{-5}
−0.059	0.638	-1.276^{-2}	8.520^{-4}	-8.111^{-5}
−0.052	0.645	-1.554^{-2}	8.309^{-4}	-1.345^{-4}
−0.046	0.649	-1.284^{-2}	8.545^{-4}	-1.733^{-4}
−0.040	0.658	-1.557^{-2}	7.805^{-4}	-1.783^{-4}
−0.033	0.663	-1.555^{-2}	7.020^{-4}	-1.809^{-4}
−0.020	0.680	-1.277^{-2}	5.081^{-4}	-1.229^{-4}
−0.008	0.684	-1.306^{-2}	3.261^{-4}	-3.149^{-5}
0.005	0.688	-1.240^{-2}	2.372^{-4}	1.212^{-5}
0.024	0.691	-1.360^{-2}	1.778^{-4}	2.340^{-5}
0.056	0.693	-1.240^{-2}	1.567^{-4}	2.340^{-5}
0.088	0.694	-1.320^{-2}	1.581^{-4}	3.333^{-5}
0.120	0.697	-1.389^{-2}	1.569^{-4}	2.648^{-5}
0.152	0.697	-1.242^{-2}	1.610^{-4}	2.695^{-5}
0.184	0.700	-1.253^{-2}	1.578^{-4}	2.629^{-5}
0.216	0.700	-1.463^{-2}	1.639^{-4}	3.175^{-5}
0.248	0.698	-1.345^{-2}	1.579^{-4}	2.289^{-5}
0.280	0.699	-1.044^{-2}	1.847^{-4}	3.977^{-5}
0.312	0.701	-1.215^{-2}	2.127^{-4}	5.012^{-5}
0.344	0.702	-1.081^{-2}	1.837^{-4}	5.046^{-5}
0.376	0.702	-1.395^{-2}	1.861^{-4}	3.249^{-5}
0.408	0.704	-1.396^{-2}	1.880^{-4}	3.708^{-5}
0.440	0.702	-1.288^{-2}	1.758^{-4}	4.152^{-5}
0.472	0.703	-1.387^{-2}	1.743^{-4}	4.713^{-5}
0.504	0.703	-1.449^{-2}	1.686^{-4}	3.685^{-5}
0.536	0.703	-1.538^{-2}	1.768^{-4}	2.352^{-5}

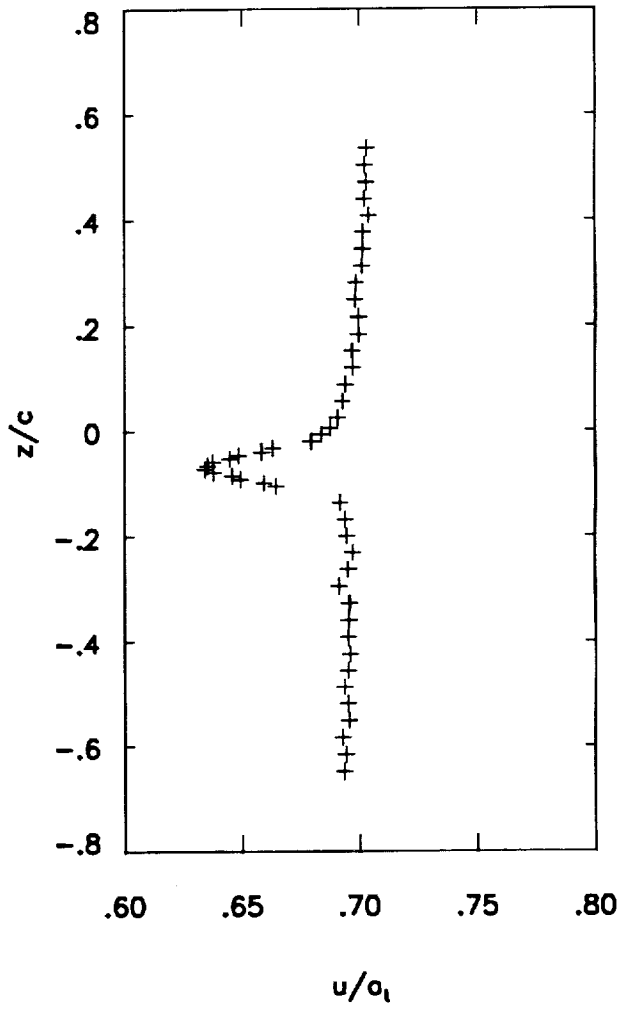

Figure 7. Continued. (c) M_∞=0.730, α=1.5°, Re=6x10^6, x/c=2.5.

$\frac{z}{c}$	$\frac{u}{a_t}$	$\frac{v}{a_t}$	$\frac{\langle u'^2+v'^2\rangle}{2a_t^2}$	$\frac{\langle u'v'\rangle}{a_t^2}$
−0.648	0.700	-5.550^{-3}	1.151^{-4}	8.647^{-7}
−0.616	0.701	-4.757^{-3}	1.149^{-4}	5.345^{-7}
−0.584	0.702	-7.728^{-3}	1.143^{-4}	3.620^{-6}
−0.577	0.700	-3.399^{-3}	1.076^{-4}	3.343^{-6}
−0.571	0.702	-7.943^{-3}	1.089^{-4}	4.703^{-6}
−0.558	0.701	-4.723^{-3}	9.899^{-5}	9.178^{-6}
−0.552	0.697	-1.104^{-2}	1.608^{-4}	-7.240^{-6}
−0.545	0.699	-4.529^{-3}	1.116^{-4}	9.705^{-6}
−0.532	0.702	-6.374^{-3}	1.015^{-4}	9.151^{-7}
−0.520	0.700	-8.249^{-3}	1.349^{-4}	2.388^{-6}
−0.488	0.704	-7.761^{-3}	1.386^{-4}	2.469^{-7}
−0.456	0.704	-8.367^{-3}	1.190^{-4}	5.567^{-6}
−0.424	0.708	-9.869^{-3}	1.238^{-4}	-2.314^{-6}
−0.392	0.708	-1.151^{-2}	1.266^{-4}	-5.772^{-6}
−0.360	0.704	-1.091^{-2}	1.271^{-4}	-5.406^{-7}
−0.328	0.706	-1.008^{-2}	1.219^{-4}	2.610^{-6}
−0.296	0.705	-9.131^{-3}	1.243^{-4}	4.066^{-6}
−0.264	0.708	-1.358^{-2}	1.260^{-4}	-2.529^{-6}
−0.232	0.707	-1.020^{-2}	1.373^{-4}	5.008^{-6}
−0.200	0.707	-1.331^{-2}	1.289^{-4}	2.851^{-6}
−0.174	0.705	-1.286^{-2}	1.206^{-4}	3.998^{-6}
−0.161	0.705	-1.274^{-2}	1.250^{-4}	4.793^{-6}
−0.148	0.709	-1.221^{-2}	1.279^{-4}	-3.368^{-6}
−0.136	0.706	-1.354^{-2}	1.664^{-4}	7.246^{-6}
−0.123	0.704	-1.225^{-2}	2.059^{-4}	1.956^{-5}
−0.110	0.701	-8.997^{-3}	2.815^{-4}	4.993^{-5}
−0.097	0.689	-1.015^{-2}	5.450^{-4}	1.901^{-4}
−0.084	0.673	-9.233^{-3}	7.030^{-4}	2.671^{-4}
−0.072	0.657	-6.989^{-3}	7.898^{-4}	2.662^{-4}
−0.059	0.647	-1.151^{-2}	8.073^{-4}	1.176^{-4}
−0.046	0.648	-9.036^{-3}	8.136^{-4}	-8.112^{-5}
−0.033	0.660	-1.168^{-2}	8.232^{-4}	-1.661^{-4}
−0.020	0.676	-1.128^{-2}	6.850^{-4}	-1.897^{-4}
−0.008	0.690	-9.122^{-3}	5.748^{-4}	-1.471^{-4}
0.005	0.701	-1.162^{-2}	3.730^{-4}	-6.662^{-5}
0.018	0.705	-1.170^{-2}	2.567^{-4}	-2.736^{-5}
0.031	0.709	-1.138^{-2}	1.797^{-4}	5.661^{-6}
0.044	0.707	-1.351^{-2}	1.328^{-4}	1.368^{-5}
0.056	0.706	-1.130^{-2}	1.234^{-4}	2.029^{-5}
0.069	0.707	-1.313^{-2}	1.211^{-4}	9.712^{-6}
0.082	0.707	-1.086^{-2}	1.183^{-4}	1.836^{-5}
0.095	0.705	-1.149^{-2}	1.195^{-4}	1.194^{-5}
0.108	0.704	-1.135^{-2}	1.186^{-4}	1.492^{-5}
0.120	0.707	-1.291^{-2}	1.161^{-4}	1.134^{-5}
0.152	0.706	-1.199^{-2}	1.162^{-4}	1.781^{-5}
0.184	0.709	-1.422^{-2}	1.257^{-4}	7.897^{-6}
0.216	0.709	-1.220^{-2}	1.292^{-4}	1.365^{-5}
0.248	0.710	-1.359^{-2}	1.320^{-4}	2.222^{-5}
0.280	0.709	-1.486^{-2}	1.185^{-4}	7.629^{-6}
0.312	0.712	-1.461^{-2}	1.263^{-4}	9.367^{-6}
0.344	0.710	-1.469^{-2}	1.181^{-4}	1.367^{-5}
0.376	0.711	-1.384^{-2}	1.136^{-4}	6.810^{-6}
0.408	0.712	-1.398^{-2}	1.158^{-4}	8.957^{-6}
0.440	0.710	-1.387^{-2}	1.139^{-4}	5.210^{-6}
0.472	0.714	-1.545^{-2}	1.301^{-4}	1.902^{-5}
0.504	0.711	-1.457^{-2}	1.166^{-4}	6.137^{-6}
0.536	0.710	-1.954^{-2}	1.050^{-4}	1.055^{-5}
0.568	0.710	-2.008^{-2}	7.274^{-5}	2.443^{-6}
0.600	0.707	-1.990^{-2}	7.572^{-5}	4.876^{-6}

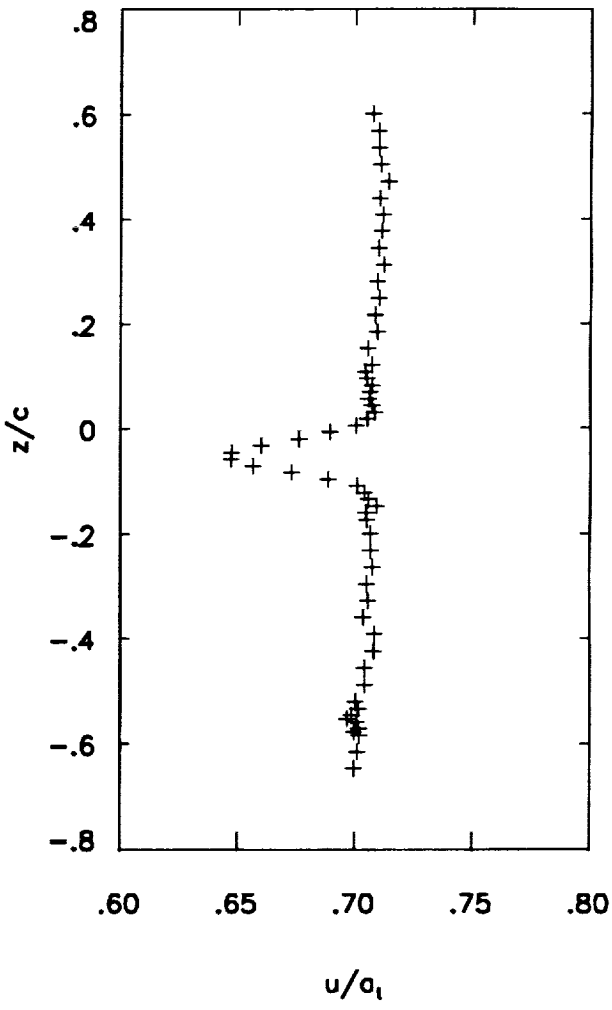

Figure 7. Continued. (d) M_∞=0.750, α=0.5°, Re=6x10^6, x/c=2.5.

$\frac{z}{c}$	$\frac{u}{a_t}$	$\frac{v}{a_t}$	$\frac{\langle u'^2+v'^2\rangle}{2a_t^2}$	$\frac{\langle u'v'\rangle}{a_t^2}$
−0.648	0.708	-3.563^{-3}	1.403^{-4}	3.013^{-5}
−0.616	0.709	-4.325^{-3}	1.315^{-4}	1.825^{-5}
−0.584	0.708	-4.676^{-3}	1.281^{-4}	1.794^{-5}
−0.552	0.708	-5.296^{-3}	1.277^{-4}	1.830^{-5}
−0.520	0.710	-5.814^{-3}	1.232^{-4}	2.236^{-5}
−0.488	0.711	-6.908^{-3}	1.364^{-4}	1.865^{-5}
−0.456	0.711	-5.895^{-3}	1.310^{-4}	1.591^{-5}
−0.424	0.707	-6.027^{-3}	1.289^{-4}	2.346^{-5}
−0.392	0.706	-5.892^{-3}	1.314^{-4}	1.384^{-5}
−0.360	0.708	-6.677^{-3}	1.259^{-4}	1.649^{-5}
−0.328	0.708	-7.364^{-3}	1.317^{-4}	1.666^{-5}
−0.296	0.706	-8.940^{-3}	1.241^{-4}	1.702^{-5}
−0.264	0.710	-1.124^{-2}	1.132^{-4}	7.639^{-6}
−0.232	0.713	-1.160^{-2}	1.128^{-4}	2.998^{-6}
−0.200	0.710	-6.526^{-3}	1.106^{-4}	7.911^{-6}
−0.168	0.710	-7.010^{-3}	1.206^{-4}	7.375^{-6}
−0.136	0.712	-9.202^{-3}	1.758^{-4}	2.231^{-5}
−0.110	0.699	-7.660^{-3}	4.366^{-4}	1.355^{-4}
−0.097	0.688	-4.426^{-3}	5.041^{-4}	1.619^{-4}
−0.084	0.672	-7.669^{-3}	7.465^{-4}	3.007^{-4}
−0.078	0.664	-8.699^{-3}	8.322^{-4}	2.571^{-4}
−0.072	0.655	-9.780^{-3}	7.472^{-4}	2.090^{-4}
−0.067	0.650	-1.216^{-2}	8.156^{-4}	1.836^{-4}
−0.064	0.649	-1.135^{-2}	8.417^{-4}	1.419^{-4}
−0.061	0.651	-1.132^{-2}	8.381^{-4}	9.776^{-5}
−0.059	0.650	-9.834^{-3}	8.465^{-4}	6.672^{-5}
−0.056	0.653	-1.318^{-2}	7.997^{-4}	9.172^{-6}
−0.052	0.652	-1.122^{-2}	8.418^{-4}	1.226^{-5}
−0.046	0.657	-1.469^{-2}	8.396^{-4}	-9.924^{-5}
−0.033	0.672	-1.544^{-2}	7.810^{-4}	-1.958^{-4}
−0.020	0.684	-8.488^{-3}	6.491^{-4}	-1.965^{-4}
−0.008	0.697	-1.410^{-2}	4.200^{-4}	-8.712^{-5}
0.024	0.708	-1.371^{-2}	1.733^{-4}	9.108^{-6}
0.056	0.713	-9.610^{-3}	1.222^{-4}	1.559^{-5}
0.088	0.714	-1.090^{-2}	1.228^{-4}	1.372^{-5}
0.120	0.714	-1.024^{-2}	1.218^{-4}	1.706^{-5}
0.152	0.714	-1.054^{-2}	1.269^{-4}	1.743^{-5}
0.184	0.715	-1.357^{-2}	1.322^{-4}	7.443^{-6}
0.216	0.715	-1.092^{-2}	1.316^{-4}	1.877^{-5}
0.248	0.715	-1.111^{-2}	1.302^{-4}	1.703^{-5}
0.280	0.713	-1.185^{-2}	1.415^{-4}	2.417^{-5}
0.312	0.715	-1.141^{-2}	1.306^{-4}	1.218^{-5}
0.344	0.715	-1.109^{-2}	1.289^{-4}	2.300^{-5}
0.376	0.716	-1.189^{-2}	1.289^{-4}	1.784^{-5}
0.440	0.715	-1.050^{-2}	1.301^{-4}	1.699^{-5}
0.472	0.715	-1.102^{-2}	1.369^{-4}	1.590^{-5}
0.504	0.718	-1.266^{-2}	1.201^{-4}	1.760^{-5}
0.568	0.721	-1.363^{-2}	1.262^{-4}	1.908^{-5}

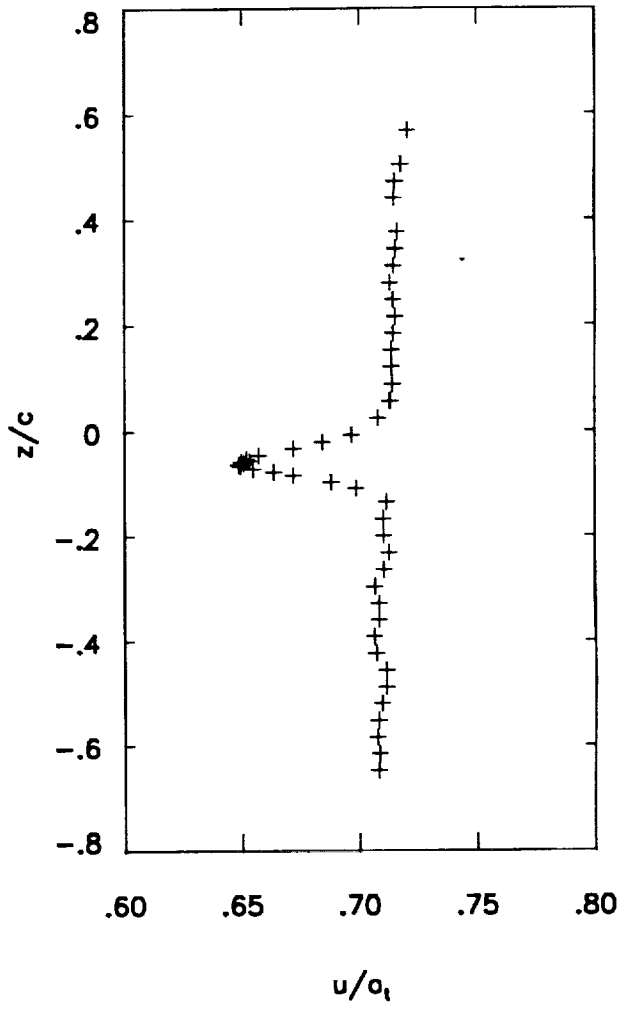

Figure 7. Continued. (e) M_∞=0.750, α=0.9°, Re=6x10^6, x/c=2.5.

$\frac{z}{c}$	$\frac{u}{a_t}$	$\frac{v}{a_t}$	$\frac{\langle u'^2+v'^2\rangle}{2a_t^2}$	$\frac{\langle u'v'\rangle}{a_t^2}$
−0.648	0.707	-5.211^{-3}	1.481^{-4}	2.734^{-5}
−0.616	0.709	-5.691^{-3}	1.503^{-4}	2.551^{-5}
−0.584	0.708	-6.695^{-3}	1.531^{-4}	2.158^{-5}
−0.552	0.709	-6.310^{-3}	1.590^{-4}	2.328^{-5}
−0.520	0.710	-7.978^{-3}	1.576^{-4}	2.277^{-5}
−0.488	0.709	-7.877^{-3}	2.031^{-4}	6.391^{-5}
−0.456	0.711	-7.781^{-3}	1.615^{-4}	5.081^{-5}
−0.424	0.711	-9.053^{-3}	1.623^{-4}	3.022^{-5}
−0.392	0.709	-1.017^{-2}	1.671^{-4}	3.013^{-5}
−0.360	0.711	-8.871^{-3}	1.664^{-4}	3.332^{-5}
−0.328	0.709	-9.348^{-3}	1.801^{-4}	3.614^{-5}
−0.296	0.709	-1.149^{-2}	3.111^{-4}	1.554^{-4}
−0.264	0.713	-1.345^{-2}	2.341^{-4}	1.157^{-4}
−0.232	0.716	-1.338^{-2}	3.567^{-4}	2.265^{-4}
−0.200	0.713	-7.974^{-3}	3.869^{-4}	2.672^{-4}
−0.168	0.710	-1.188^{-2}	4.106^{-4}	2.379^{-4}
−0.136	0.708	-9.615^{-3}	5.587^{-4}	2.590^{-4}
−0.123	0.699	-8.604^{-3}	4.584^{-4}	1.170^{-4}
−0.110	0.690	-7.527^{-3}	1.048^{-3}	5.958^{-4}
−0.097	0.677	-6.270^{-3}	1.396^{-3}	8.112^{-4}
−0.084	0.660	-1.310^{-2}	1.059^{-3}	3.415^{-4}
−0.078	0.653	-1.246^{-2}	8.063^{-4}	1.640^{-4}
−0.072	0.650	-1.409^{-2}	1.180^{-3}	3.513^{-4}
−0.065	0.646	-1.250^{-2}	8.867^{-4}	4.863^{-5}
−0.059	0.651	-1.149^{-2}	1.262^{-3}	3.204^{-4}
−0.046	0.651	-1.339^{-2}	7.770^{-4}	-9.170^{-5}
−0.033	0.660	-1.200^{-2}	8.062^{-4}	-1.726^{-4}
−0.020	0.673	-1.460^{-2}	7.286^{-4}	-1.581^{-4}
−0.008	0.682	-1.346^{-2}	4.913^{-4}	-1.001^{-4}
0.005	0.691	-1.401^{-2}	3.035^{-4}	-5.667^{-5}
0.018	0.696	-1.381^{-2}	2.278^{-4}	-2.800^{-5}
0.031	0.697	-1.283^{-2}	1.530^{-4}	-1.958^{-6}
0.044	0.701	-1.429^{-2}	1.105^{-4}	9.978^{-6}
0.056	0.703	-1.372^{-2}	1.253^{-4}	1.610^{-5}
0.088	0.705	-1.318^{-2}	1.208^{-4}	2.397^{-5}
0.120	0.708	-1.263^{-2}	1.143^{-4}	2.439^{-5}
0.152	0.711	-1.409^{-2}	1.008^{-4}	1.414^{-5}
0.184	0.714	-1.306^{-2}	1.178^{-4}	3.552^{-5}
0.216	0.712	-1.420^{-2}	1.240^{-4}	2.953^{-5}
0.248	0.716	-1.512^{-2}	1.165^{-4}	3.405^{-5}
0.280	0.719	-1.203^{-2}	1.312^{-4}	3.242^{-5}
0.312	0.720	-1.492^{-2}	1.320^{-4}	2.897^{-5}
0.344	0.716	-1.373^{-2}	1.400^{-4}	3.312^{-5}
0.376	0.717	-1.459^{-2}	1.351^{-4}	3.041^{-5}
0.408	0.717	-1.407^{-2}	1.345^{-4}	3.741^{-5}
0.440	0.716	-1.410^{-2}	1.452^{-4}	3.093^{-5}
0.472	0.720	-1.416^{-2}	1.585^{-4}	4.718^{-5}
0.504	0.721	-1.683^{-2}	1.433^{-4}	3.113^{-5}
0.536	0.723	-1.689^{-2}	1.358^{-4}	3.408^{-5}
0.568	0.720	-1.619^{-2}	1.436^{-4}	3.709^{-5}
0.600	0.721	-1.590^{-2}	1.464^{-4}	3.635^{-5}

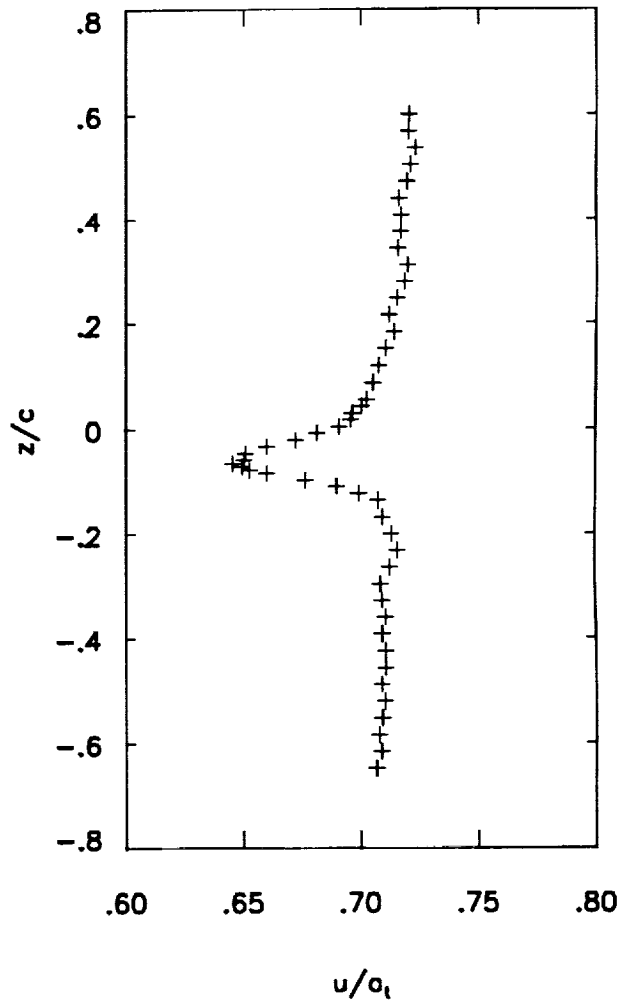

Figure 7. Continued. (f) M_∞=0.749, α=1.5°, Re=6x10^6, x/c=2.5.

$\frac{z}{c}$	$\frac{u}{a_t}$	$\frac{v}{a_t}$	$\frac{\langle u'^2+v'^2\rangle}{2a_t^2}$	$\frac{\langle u'v'\rangle}{a_t^2}$
−0.648	0.731	-5.727^{-3}	1.145^{-4}	6.139^{-6}
−0.616	0.731	-4.233^{-3}	1.141^{-4}	-5.459^{-6}
−0.584	0.735	-1.113^{-2}	9.194^{-5}	1.280^{-6}
−0.552	0.734	-4.635^{-3}	1.049^{-4}	1.340^{-5}
−0.520	0.738	-7.350^{-3}	9.322^{-5}	-1.612^{-6}
−0.488	0.735	-6.789^{-3}	9.593^{-5}	2.279^{-6}
−0.456	0.734	-9.072^{-3}	1.176^{-4}	5.805^{-6}
−0.424	0.734	-7.239^{-3}	1.220^{-4}	-4.957^{-7}
−0.392	0.736	-7.671^{-3}	1.127^{-4}	1.598^{-6}
−0.360	0.730	-8.559^{-3}	1.113^{-4}	6.580^{-6}
−0.328	0.734	-1.092^{-2}	1.084^{-4}	1.602^{-6}
−0.296	0.733	-7.973^{-3}	1.181^{-4}	-1.959^{-6}
−0.264	0.736	-8.796^{-3}	9.640^{-5}	3.398^{-6}
−0.232	0.735	-8.325^{-3}	1.196^{-4}	-3.253^{-6}
−0.200	0.738	-9.568^{-3}	1.259^{-4}	1.767^{-6}
−0.174	0.734	-1.024^{-2}	1.235^{-4}	6.886^{-6}
−0.161	0.732	-8.947^{-3}	1.199^{-4}	8.558^{-6}
−0.148	0.736	-7.545^{-3}	1.495^{-4}	2.711^{-6}
−0.136	0.738	-1.048^{-2}	1.889^{-4}	2.327^{-5}
−0.123	0.733	-9.681^{-3}	3.425^{-4}	5.771^{-5}
−0.110	0.728	-7.381^{-3}	3.999^{-4}	7.956^{-5}
−0.097	0.717	-8.320^{-3}	6.930^{-4}	1.831^{-4}
−0.084	0.707	-7.545^{-3}	7.505^{-4}	1.813^{-4}
−0.072	0.690	-4.687^{-3}	8.691^{-4}	2.329^{-4}
−0.059	0.681	-7.105^{-3}	9.334^{-4}	2.057^{-4}
−0.052	0.676	-1.279^{-2}	9.233^{-4}	1.499^{-4}
−0.046	0.672	-6.991^{-3}	9.272^{-4}	7.287^{-5}
−0.040	0.678	-8.134^{-3}	8.978^{-4}	-2.499^{-6}
−0.033	0.679	-1.168^{-2}	8.263^{-4}	-8.752^{-5}
−0.020	0.688	-1.135^{-2}	8.960^{-4}	-1.977^{-4}
−0.008	0.705	-1.692^{-2}	7.322^{-4}	-2.247^{-4}
0.005	0.708	-1.517^{-2}	6.310^{-4}	-1.769^{-4}
0.018	0.714	-1.384^{-2}	4.750^{-4}	-8.128^{-5}
0.031	0.722	-1.396^{-2}	3.247^{-4}	-4.602^{-5}
0.044	0.723	-1.521^{-2}	2.733^{-4}	-2.948^{-5}
0.056	0.730	-1.165^{-2}	2.033^{-4}	-1.909^{-5}
0.069	0.728	-1.067^{-2}	1.762^{-4}	-2.375^{-6}
0.082	0.734	-1.324^{-2}	1.432^{-4}	2.832^{-6}
0.095	0.734	-1.555^{-2}	1.466^{-4}	5.128^{-7}
0.120	0.736	-1.426^{-2}	1.052^{-4}	3.675^{-6}
0.152	0.738	-1.393^{-2}	1.302^{-4}	1.742^{-5}
0.184	0.736	-1.376^{-2}	1.246^{-4}	1.402^{-5}
0.216	0.739	-1.231^{-2}	1.387^{-4}	1.949^{-5}
0.248	0.741	-1.485^{-2}	1.409^{-4}	2.413^{-5}
0.280	0.738	-1.418^{-2}	1.461^{-4}	1.093^{-5}
0.312	0.739	-1.255^{-2}	1.405^{-4}	2.299^{-5}
0.344	0.738	-1.424^{-2}	1.341^{-4}	1.677^{-5}
0.376	0.740	-1.396^{-2}	1.411^{-4}	9.002^{-6}
0.389	0.742	-1.457^{-2}	1.297^{-4}	2.703^{-5}
0.402	0.741	-1.668^{-2}	1.286^{-4}	1.811^{-5}
0.408	0.746	-1.383^{-2}	1.453^{-4}	2.177^{-5}
0.415	0.742	-1.597^{-2}	1.442^{-4}	2.855^{-5}
0.428	0.741	-1.182^{-2}	1.441^{-4}	2.686^{-5}
0.440	0.739	-1.641^{-2}	1.343^{-4}	1.055^{-5}
0.472	0.740	-1.442^{-2}	1.451^{-4}	1.563^{-5}
0.504	0.741	-1.833^{-2}	1.293^{-4}	1.427^{-5}
0.536	0.742	-1.470^{-2}	1.301^{-4}	2.097^{-5}
0.568	0.745	-1.699^{-2}	1.347^{-4}	2.456^{-5}
0.600	0.742	-1.661^{-2}	1.444^{-4}	1.613^{-5}

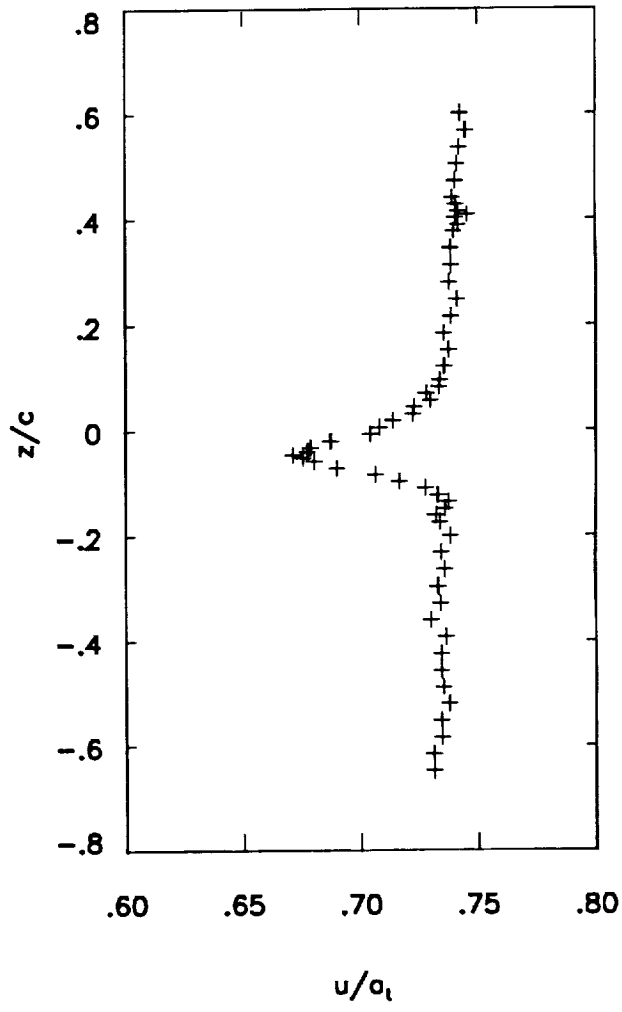

Figure 7. Continued. (g) M_∞=0.784, α=0.5°, Re=6x10^6, x/c=2.5.

$\frac{z}{c}$	$\frac{u}{a_t}$	$\frac{v}{a_t}$	$\frac{\langle u'^2+v'^2\rangle}{2a_t^2}$	$\frac{\langle u'v'\rangle}{a_t^2}$
−0.648	0.743	-1.325^{-3}	1.258^{-4}	2.089^{-7}
−0.616	0.745	-3.159^{-3}	1.354^{-4}	-1.850^{-6}
−0.584	0.740	-3.060^{-3}	1.023^{-4}	8.287^{-6}
−0.552	0.743	-3.481^{-3}	1.054^{-4}	6.501^{-6}
−0.520	0.743	-4.782^{-3}	1.284^{-4}	1.297^{-5}
−0.488	0.742	-5.017^{-3}	1.271^{-4}	1.032^{-5}
−0.468	0.744	-3.551^{-3}	2.022^{-4}	4.368^{-5}
−0.462	0.745	-3.198^{-3}	1.948^{-4}	3.355^{-5}
−0.456	0.745	-4.002^{-3}	1.605^{-4}	2.203^{-5}
−0.449	0.748	-4.679^{-3}	1.818^{-4}	2.508^{-5}
−0.424	0.746	-6.124^{-3}	1.272^{-4}	7.178^{-6}
−0.392	0.743	-6.122^{-3}	1.321^{-4}	8.311^{-6}
−0.360	0.742	-6.599^{-3}	1.142^{-4}	7.196^{-6}
−0.328	0.743	-5.131^{-3}	1.607^{-4}	1.368^{-5}
−0.302	0.744	-7.191^{-3}	1.809^{-4}	3.361^{-5}
−0.296	0.741	-7.303^{-3}	1.546^{-4}	1.348^{-5}
−0.289	0.746	-6.373^{-3}	1.995^{-4}	2.483^{-5}
−0.283	0.747	-7.173^{-3}	1.854^{-4}	2.507^{-5}
−0.276	0.747	-9.658^{-3}	1.707^{-4}	2.230^{-5}
−0.270	0.746	-8.207^{-3}	1.772^{-4}	3.021^{-5}
−0.264	0.746	-8.210^{-3}	1.462^{-4}	8.793^{-6}
−0.232	0.747	-8.161^{-3}	1.476^{-4}	1.252^{-5}
−0.200	0.744	-6.105^{-3}	1.597^{-4}	1.152^{-6}
−0.168	0.742	-7.141^{-3}	2.130^{-4}	1.991^{-5}
−0.136	0.742	-7.130^{-3}	4.481^{-4}	6.006^{-5}
−0.110	0.730	-2.011^{-3}	7.494^{-4}	1.978^{-4}
−0.097	0.717	-2.410^{-3}	9.719^{-4}	2.671^{-4}
−0.084	0.708	-2.780^{-3}	1.025^{-3}	3.142^{-4}
−0.078	0.700	-1.340^{-3}	1.103^{-3}	2.934^{-4}
−0.074	0.701	-2.720^{-3}	1.238^{-3}	3.286^{-4}
−0.072	0.696	-3.911^{-3}	1.075^{-3}	3.036^{-4}
−0.069	0.695	-5.920^{-4}	1.242^{-3}	2.685^{-4}
−0.065	0.691	-1.775^{-3}	1.386^{-3}	3.179^{-4}
−0.059	0.687	-3.267^{-3}	1.269^{-3}	2.675^{-4}
−0.046	0.683	-4.109^{-3}	1.459^{-3}	2.034^{-4}
−0.033	0.679	-4.240^{-3}	1.370^{-3}	-3.654^{-5}
−0.020	0.680	-4.547^{-3}	1.428^{-3}	-1.615^{-4}
−0.008	0.686	-5.162^{-3}	1.396^{-3}	-2.979^{-4}
0.005	0.692	-4.144^{-3}	1.387^{-3}	-3.738^{-4}
0.018	0.699	-6.078^{-3}	1.315^{-3}	-3.742^{-4}
0.024	0.711	-8.150^{-3}	1.038^{-3}	-2.998^{-4}
0.031	0.708	-6.531^{-3}	1.148^{-3}	-3.548^{-4}
0.044	0.717	-5.554^{-3}	1.041^{-3}	-2.677^{-4}
0.056	0.722	-6.892^{-3}	7.681^{-4}	-1.947^{-4}
0.088	0.733	-9.811^{-3}	3.522^{-4}	-1.811^{-5}
0.120	0.739	-9.011^{-3}	2.037^{-4}	5.460^{-6}
0.152	0.743	-9.488^{-3}	1.772^{-4}	2.353^{-5}
0.184	0.744	-9.865^{-3}	1.576^{-4}	2.364^{-5}
0.216	0.745	-9.439^{-3}	1.815^{-4}	3.197^{-5}
0.248	0.745	-9.758^{-3}	1.979^{-4}	3.055^{-5}
0.280	0.749	-1.007^{-2}	1.911^{-4}	3.513^{-5}
0.312	0.753	-9.615^{-3}	1.904^{-4}	3.733^{-5}
0.344	0.750	-9.038^{-3}	1.963^{-4}	4.321^{-5}
0.376	0.751	-1.081^{-2}	2.008^{-4}	4.252^{-5}
0.408	0.753	-1.251^{-2}	1.919^{-4}	3.018^{-5}
0.440	0.753	-1.256^{-2}	1.832^{-4}	3.231^{-5}
0.472	0.753	-1.179^{-2}	1.985^{-4}	4.691^{-5}
0.504	0.755	-1.288^{-2}	1.843^{-4}	3.227^{-5}
0.536	0.756	-1.180^{-2}	1.778^{-4}	3.784^{-5}
0.568	0.753	-1.008^{-2}	1.619^{-4}	3.188^{-5}
0.600	0.754	-1.125^{-2}	1.534^{-4}	3.219^{-5}

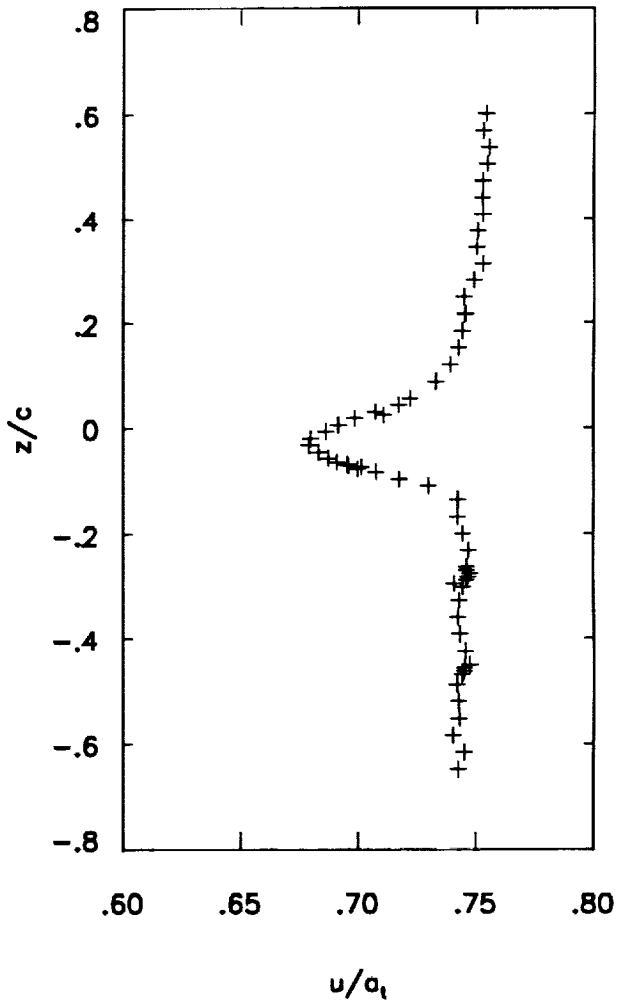

Figure 7. Continued. (h) M_∞=0.781, α=0.9°, Re=6x10^6, x/c=2.5.

$\frac{z}{c}$	$\frac{u}{a_t}$	$\frac{v}{a_t}$	$\frac{\langle u'^2+v'^2\rangle}{2a_t^2}$	$\frac{\langle u'v'\rangle}{a_t^2}$
−0.648	0.738	-4.381^{-3}	1.408^{-4}	1.227^{-5}
−0.616	0.739	-4.614^{-3}	1.307^{-4}	8.201^{-6}
−0.584	0.741	-5.743^{-3}	1.257^{-4}	1.736^{-5}
−0.552	0.741	-3.537^{-3}	1.282^{-4}	2.026^{-5}
−0.520	0.743	-3.998^{-3}	1.306^{-4}	1.858^{-5}
−0.488	0.740	-2.754^{-3}	1.316^{-4}	2.465^{-5}
−0.456	0.743	-5.112^{-3}	1.541^{-4}	1.673^{-5}
−0.424	0.742	-5.725^{-3}	1.218^{-4}	1.540^{-5}
−0.392	0.743	-6.915^{-3}	1.360^{-4}	1.765^{-5}
−0.360	0.742	-5.520^{-3}	1.354^{-4}	1.388^{-5}
−0.328	0.744	-5.809^{-3}	1.305^{-4}	1.040^{-5}
−0.296	0.744	-6.060^{-3}	1.406^{-4}	1.455^{-5}
−0.264	0.746	-3.065^{-3}	1.581^{-4}	1.471^{-5}
−0.232	0.744	-3.300^{-3}	1.592^{-4}	1.449^{-5}
−0.200	0.747	-5.154^{-3}	2.186^{-4}	-3.128^{-7}
−0.168	0.747	-2.799^{-3}	3.839^{-4}	3.772^{-5}
−0.136	0.741	1.166^{-4}	6.949^{-4}	1.093^{-4}
−0.123	0.736	1.094^{-3}	8.761^{-4}	2.209^{-4}
−0.110	0.728	3.461^{-3}	1.147^{-3}	3.036^{-4}
−0.097	0.722	6.919^{-3}	1.412^{-3}	3.990^{-4}
−0.084	0.716	9.245^{-3}	1.779^{-3}	5.816^{-4}
−0.072	0.705	7.123^{-3}	1.954^{-3}	5.941^{-4}
−0.059	0.694	6.603^{-3}	2.103^{-3}	5.501^{-4}
−0.046	0.681	6.035^{-3}	2.317^{-3}	5.525^{-4}
−0.033	0.676	9.102^{-3}	2.550^{-3}	4.828^{-4}
−0.020	0.671	3.743^{-3}	2.469^{-3}	2.712^{-4}
−0.008	0.669	4.000^{-3}	2.602^{-3}	7.655^{-6}
0.005	0.665	7.476^{-3}	2.656^{-3}	-9.619^{-5}
0.012	0.663	6.890^{-3}	2.797^{-3}	-1.564^{-4}
0.018	0.665	3.963^{-3}	2.661^{-3}	-3.292^{-4}
0.031	0.668	2.730^{-3}	2.746^{-3}	-5.368^{-4}
0.044	0.675	4.122^{-3}	2.711^{-3}	-5.738^{-4}
0.056	0.678	1.796^{-3}	2.479^{-3}	-6.273^{-4}
0.069	0.686	1.975^{-4}	2.537^{-3}	-6.926^{-4}
0.082	0.699	-3.141^{-3}	2.226^{-3}	-6.150^{-4}
0.095	0.702	3.702^{-4}	2.005^{-3}	-5.926^{-4}
0.108	0.708	-9.356^{-4}	1.923^{-3}	-5.929^{-4}
0.120	0.716	-3.457^{-3}	1.405^{-3}	-3.789^{-4}
0.133	0.722	-2.903^{-3}	1.215^{-3}	-3.572^{-4}
0.152	0.727	-5.218^{-3}	8.735^{-4}	-2.191^{-4}
0.184	0.729	-7.996^{-4}	6.373^{-4}	-4.269^{-5}
0.216	0.738	-3.338^{-3}	3.904^{-4}	2.242^{-5}
0.248	0.741	-6.712^{-3}	2.135^{-4}	1.498^{-5}
0.274	0.741	-8.265^{-3}	1.380^{-4}	-4.907^{-6}
0.280	0.745	-4.916^{-3}	2.427^{-4}	4.746^{-5}
0.300	0.749	-1.223^{-2}	1.400^{-4}	-9.737^{-6}
0.312	0.743	-5.167^{-3}	2.002^{-4}	4.287^{-5}
0.344	0.744	-6.984^{-3}	2.158^{-4}	4.300^{-5}
0.376	0.746	-8.115^{-3}	2.012^{-4}	3.316^{-5}
0.389	0.753	-1.639^{-2}	1.052^{-4}	-1.082^{-6}
0.402	0.751	-1.672^{-2}	1.370^{-4}	-1.136^{-5}
0.408	0.743	-7.660^{-3}	1.967^{-4}	5.134^{-5}
0.415	0.748	-1.646^{-2}	1.040^{-4}	1.368^{-6}
0.440	0.748	-9.225^{-3}	1.976^{-4}	4.215^{-5}
0.472	0.751	-1.425^{-2}	1.642^{-4}	2.489^{-5}
0.504	0.755	-1.873^{-2}	1.219^{-4}	-5.562^{-6}
0.536	0.749	-2.024^{-2}	1.162^{-4}	2.855^{-6}
0.568	0.753	-2.192^{-2}	1.132^{-4}	6.544^{-6}
0.600	0.753	-1.967^{-2}	1.102^{-4}	4.232^{-6}

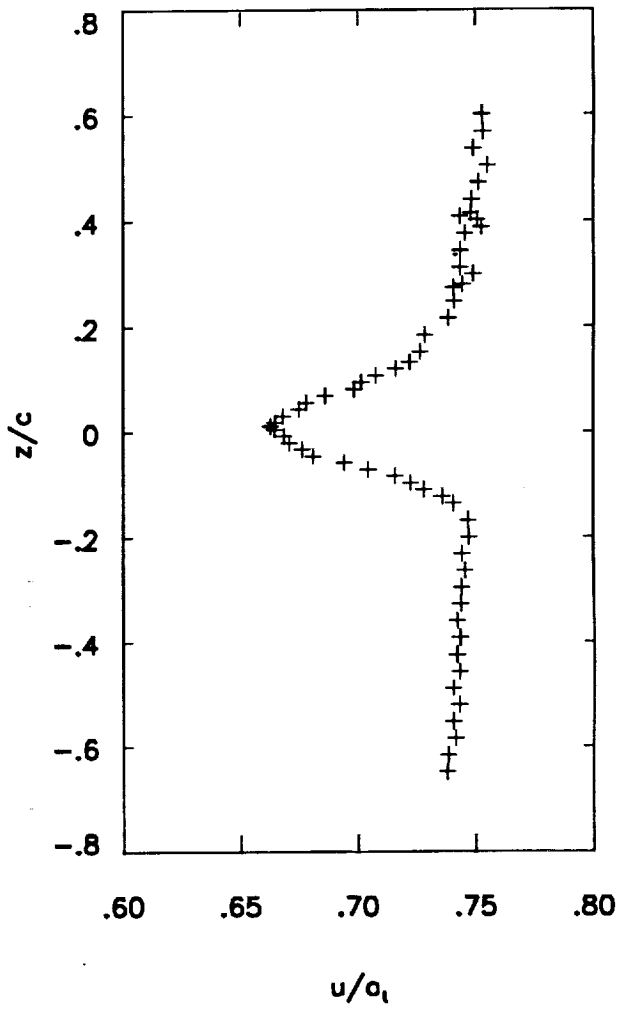

Figure 7. Continued. (i) M_∞=0.781, α=1.5°, Re=6x10^6, x/c=2.5.

$\frac{z}{c}$	$\frac{u}{a_t}$	$\frac{v}{a_t}$	$\frac{\langle u'^2+v'^2\rangle}{2a_t^2}$	$\frac{\langle u'v'\rangle}{a_t^2}$
−0.648	0.762	-3.840^{-3}	1.398^{-4}	1.786^{-5}
−0.616	0.761	-5.859^{-3}	1.406^{-4}	2.263^{-5}
−0.584	0.765	-2.244^{-3}	1.377^{-4}	3.221^{-5}
−0.552	0.764	-5.756^{-3}	1.407^{-4}	2.510^{-5}
−0.520	0.763	-7.748^{-3}	1.351^{-4}	3.081^{-5}
−0.488	0.765	-5.521^{-3}	1.373^{-4}	2.022^{-5}
−0.456	0.763	-7.363^{-3}	1.418^{-4}	2.815^{-5}
−0.424	0.765	-7.238^{-3}	1.413^{-4}	2.795^{-5}
−0.392	0.763	-6.681^{-3}	1.591^{-4}	2.120^{-5}
−0.360	0.760	-6.260^{-3}	1.553^{-4}	3.229^{-5}
−0.328	0.765	-6.672^{-3}	1.481^{-4}	2.903^{-5}
−0.296	0.764	-6.846^{-3}	1.437^{-4}	3.432^{-5}
−0.264	0.766	-6.893^{-3}	1.478^{-4}	3.144^{-5}
−0.232	0.764	-5.974^{-3}	1.507^{-4}	4.002^{-5}
−0.200	0.762	-5.765^{-3}	1.717^{-4}	4.492^{-5}
−0.168	0.759	-7.244^{-3}	2.483^{-4}	5.571^{-5}
−0.136	0.752	-7.001^{-3}	5.100^{-4}	1.218^{-4}
−0.123	0.747	-3.752^{-3}	7.207^{-4}	1.771^{-4}
−0.110	0.739	-3.782^{-3}	9.355^{-4}	2.641^{-4}
−0.097	0.729	-3.699^{-3}	1.177^{-3}	4.242^{-4}
−0.084	0.718	-3.199^{-3}	1.351^{-3}	4.607^{-4}
−0.072	0.707	-2.738^{-3}	1.488^{-3}	4.747^{-4}
−0.059	0.697	5.210^{-4}	1.495^{-3}	4.447^{-4}
−0.046	0.685	-3.749^{-3}	1.515^{-3}	3.999^{-4}
−0.033	0.680	-4.964^{-3}	1.604^{-3}	2.211^{-4}
−0.020	0.682	-4.095^{-3}	1.573^{-3}	3.686^{-5}
−0.008	0.685	-2.598^{-3}	1.790^{-3}	-1.513^{-4}
0.005	0.695	-7.223^{-3}	1.746^{-3}	-3.598^{-4}
0.018	0.701	-4.832^{-3}	1.780^{-3}	-4.389^{-4}
0.031	0.715	-9.456^{-3}	1.440^{-3}	-3.818^{-4}
0.044	0.728	-9.675^{-3}	1.125^{-3}	-2.818^{-4}
0.056	0.732	-9.719^{-3}	1.031^{-3}	-2.288^{-4}
0.069	0.737	-8.658^{-3}	8.624^{-4}	-1.790^{-4}
0.082	0.749	-1.172^{-2}	5.345^{-4}	-8.578^{-5}
0.095	0.747	-1.221^{-2}	4.501^{-4}	-5.477^{-5}
0.108	0.756	-8.594^{-3}	3.308^{-4}	-1.023^{-5}
0.120	0.754	-1.281^{-2}	2.071^{-4}	1.466^{-5}
0.133	0.755	-8.908^{-3}	2.232^{-4}	-1.139^{-8}
0.146	0.755	-8.549^{-3}	1.524^{-4}	2.437^{-5}
0.165	0.757	-8.175^{-3}	1.455^{-4}	2.090^{-5}
0.184	0.760	-1.423^{-2}	1.078^{-4}	6.733^{-6}
0.216	0.761	-1.165^{-2}	1.199^{-4}	2.458^{-5}
0.248	0.761	-1.069^{-2}	1.242^{-4}	3.420^{-5}
0.280	0.765	-9.816^{-3}	1.218^{-4}	2.963^{-5}
0.312	0.766	-1.072^{-2}	1.200^{-4}	3.069^{-5}
0.344	0.766	-1.372^{-2}	1.006^{-4}	2.294^{-5}
0.376	0.767	-1.381^{-2}	1.180^{-4}	3.212^{-5}
0.408	0.769	-1.345^{-2}	1.127^{-4}	1.864^{-5}
0.415	0.769	-1.333^{-2}	1.272^{-4}	3.053^{-5}
0.428	0.767	-1.501^{-2}	1.250^{-4}	2.678^{-5}
0.440	0.769	-1.288^{-2}	1.237^{-4}	2.526^{-5}
0.453	0.765	-1.577^{-2}	1.273^{-4}	3.186^{-5}
0.466	0.769	-1.439^{-2}	1.317^{-4}	3.100^{-5}
0.472	0.766	-1.051^{-2}	1.153^{-4}	1.795^{-5}
0.479	0.769	-1.465^{-2}	1.204^{-4}	2.431^{-5}
0.492	0.767	-1.691^{-2}	1.284^{-4}	3.261^{-5}
0.504	0.766	-1.577^{-2}	1.213^{-4}	2.539^{-5}
0.536	0.768	-1.521^{-2}	1.242^{-4}	3.044^{-5}
0.568	0.769	-1.621^{-2}	1.294^{-4}	1.980^{-5}
0.600	0.765	-2.031^{-2}	1.273^{-4}	3.200^{-5}

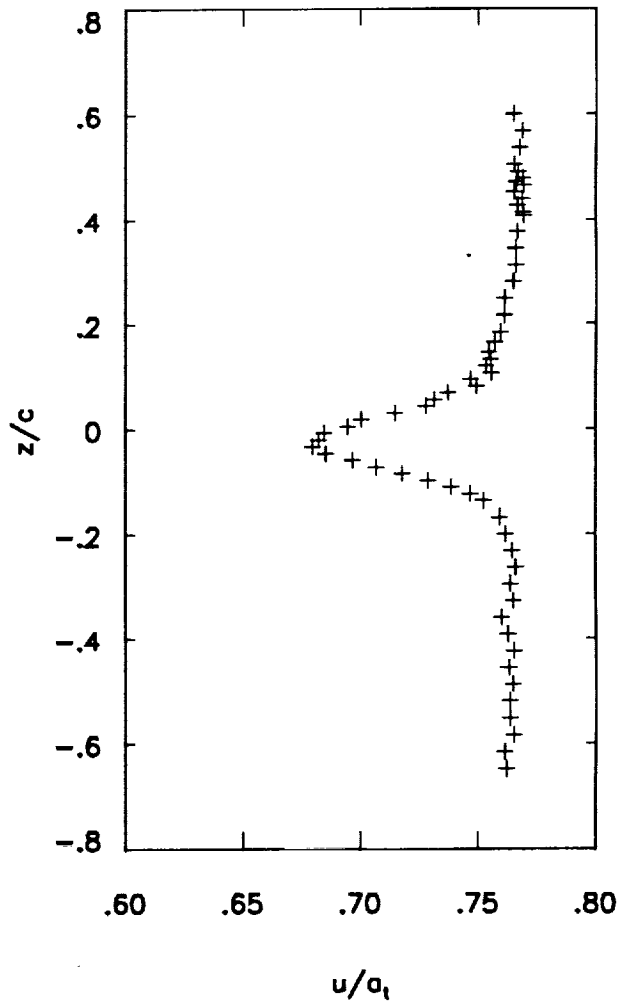

Figure 7. Continued. (j) M_∞=0.802, α=0.5°, Re=6x10^6, x/c=2.5.

$\frac{z}{c}$	$\frac{u}{a_t}$	$\frac{v}{a_t}$	$\frac{\langle u'^2+v'^2\rangle}{2a_t^2}$	$\frac{\langle u'v'\rangle}{a_t^2}$
−0.648	0.773	2.061^{-4}	1.657^{-4}	1.354^{-5}
−0.616	0.774	-2.321^{-5}	1.625^{-4}	2.893^{-5}
−0.584	0.774	-7.213^{-5}	1.492^{-4}	1.363^{-5}
−0.552	0.773	4.698^{-5}	1.504^{-4}	2.758^{-5}
−0.520	0.774	-4.526^{-5}	1.571^{-4}	2.288^{-5}
−0.488	0.774	-2.534^{-4}	1.520^{-4}	2.453^{-5}
−0.456	0.775	2.223^{-4}	1.757^{-4}	2.961^{-5}
−0.424	0.776	-1.763^{-4}	1.680^{-4}	2.452^{-5}
−0.392	0.771	-1.545^{-4}	1.673^{-4}	2.111^{-5}
−0.360	0.774	1.756^{-4}	1.641^{-4}	2.298^{-5}
−0.328	0.773	1.105^{-4}	1.571^{-4}	2.353^{-5}
−0.315	0.776	-3.478^{-4}	1.490^{-4}	3.378^{-5}
−0.302	0.770	-3.735^{-4}	1.630^{-4}	3.065^{-5}
−0.296	0.770	-2.659^{-4}	1.715^{-4}	2.519^{-5}
−0.289	0.775	-3.691^{-4}	1.394^{-4}	2.450^{-5}
−0.276	0.776	-3.480^{-4}	1.441^{-4}	2.467^{-5}
−0.264	0.775	-4.557^{-4}	1.603^{-4}	2.886^{-5}
−0.232	0.775	-5.786^{-4}	1.811^{-4}	3.136^{-5}
−0.200	0.770	1.078^{-3}	2.275^{-4}	4.309^{-5}
−0.168	0.765	1.630^{-3}	3.520^{-4}	6.721^{-5}
−0.136	0.762	1.378^{-3}	7.707^{-4}	1.970^{-4}
−0.110	0.748	3.487^{-3}	1.113^{-3}	3.453^{-4}
−0.097	0.740	4.212^{-3}	1.324^{-3}	4.532^{-4}
−0.091	0.734	3.913^{-3}	1.567^{-3}	5.833^{-4}
−0.084	0.730	3.365^{-3}	1.620^{-3}	4.670^{-4}
−0.078	0.724	-6.607^{-3}	1.762^{-3}	6.319^{-4}
−0.074	0.720	-1.626^{-2}	1.938^{-3}	6.834^{-4}
−0.069	0.718	-2.022^{-2}	1.927^{-3}	6.483^{-4}
−0.064	0.712	-1.919^{-2}	2.131^{-3}	7.659^{-4}
−0.059	0.707	-2.152^{-2}	2.170^{-3}	6.134^{-4}
−0.046	0.699	-1.933^{-2}	2.212^{-3}	5.669^{-4}
−0.033	0.689	-1.785^{-2}	2.298^{-3}	5.530^{-4}
−0.020	0.689	-2.116^{-2}	2.511^{-3}	3.427^{-4}
−0.014	0.683	-1.344^{-3}	2.330^{-3}	2.050^{-4}
−0.008	0.682	-8.697^{-4}	2.504^{-3}	1.605^{-4}
−0.001	0.684	-9.288^{-4}	2.443^{-3}	-2.646^{-5}
0.005	0.686	-1.253^{-4}	2.571^{-3}	-1.612^{-4}
0.012	0.687	-1.082^{-3}	2.448^{-3}	-2.800^{-4}
0.018	0.688	-1.149^{-3}	2.624^{-3}	-3.808^{-4}
0.024	0.690	-1.628^{-2}	2.546^{-3}	-4.045^{-4}
0.056	0.710	-3.721^{-3}	2.448^{-3}	-6.664^{-4}
0.088	0.734	-4.725^{-4}	1.989^{-3}	-4.869^{-4}
0.120	0.751	-6.819^{-4}	1.228^{-3}	-2.664^{-4}
0.152	0.762	-3.231^{-4}	6.732^{-4}	-6.628^{-5}
0.184	0.768	5.278^{-5}	4.302^{-4}	1.854^{-5}
0.216	0.767	9.116^{-4}	2.648^{-4}	2.743^{-5}
0.248	0.770	1.453^{-3}	2.417^{-4}	5.129^{-5}
0.280	0.772	1.249^{-3}	2.172^{-4}	4.997^{-5}
0.312	0.773	1.269^{-3}	2.179^{-4}	5.179^{-5}
0.344	0.773	1.701^{-3}	1.949^{-4}	3.451^{-5}
0.364	0.778	1.478^{-3}	1.863^{-4}	4.336^{-5}
0.376	0.778	1.289^{-3}	2.054^{-4}	5.882^{-5}
0.408	0.781	1.367^{-3}	1.882^{-4}	5.799^{-5}
0.440	0.783	1.695^{-3}	1.690^{-4}	4.778^{-5}
0.472	0.780	2.266^{-4}	1.557^{-4}	3.699^{-5}
0.504	0.781	-1.216^{-3}	1.368^{-4}	2.885^{-5}
0.536	0.781	-1.336^{-3}	1.388^{-4}	3.358^{-5}
0.568	0.782	-1.241^{-3}	1.340^{-4}	2.931^{-5}
0.600	0.782	-1.702^{-3}	1.326^{-4}	2.680^{-5}

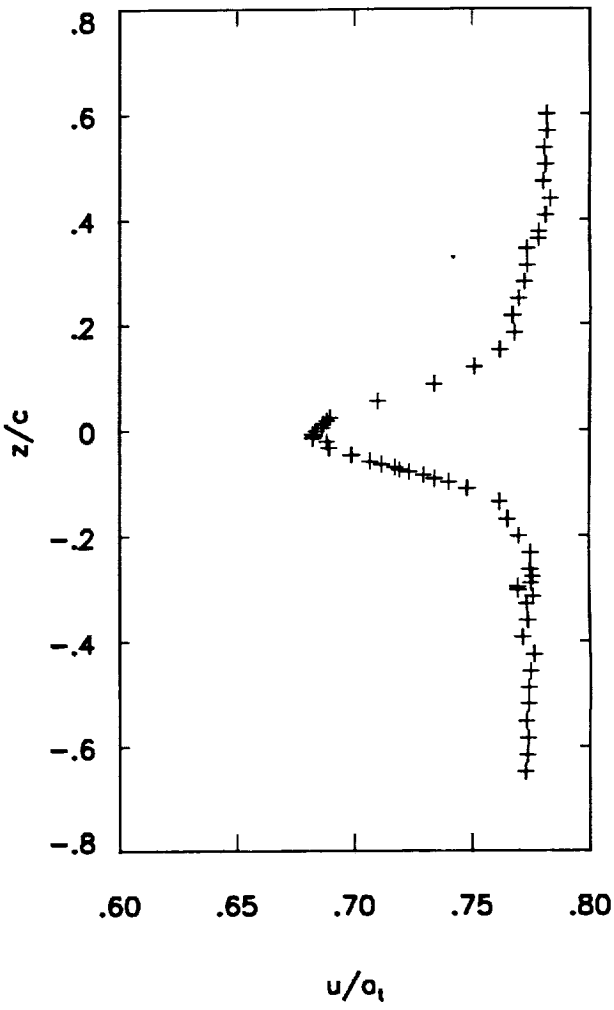

Figure 7. Continued. (k) M_∞=0.803, α=0.9°, Re=6x10^6, x/c=2.5.

$\frac{z}{c}$	$\frac{u}{a_t}$	$\frac{v}{a_t}$	$\frac{\langle u'^2+v'^2\rangle}{2a_t^2}$	$\frac{\langle u'v'\rangle}{a_t^2}$
−0.648	0.767	2.122^{-1}	1.292^{-4}	1.262^{-6}
−0.616	0.772	-2.053^{-1}	1.241^{-4}	-8.629^{-6}
−0.584	0.765	-8.137^{-2}	1.456^{-4}	5.367^{-6}
−0.552	0.769	-1.672^{-1}	1.290^{-4}	3.691^{-6}
−0.520	0.764	-2.243^{-1}	1.506^{-4}	3.467^{-6}
−0.488	0.771	-5.260^{-1}	1.379^{-4}	-1.514^{-6}
−0.456	0.771	-2.661^{-3}	1.775^{-4}	1.826^{-5}
−0.424	0.773	-3.614^{-1}	1.394^{-4}	-3.924^{-6}
−0.392	0.769	-5.271^{-1}	1.570^{-4}	1.163^{-5}
−0.360	0.772	-3.393^{-1}	1.525^{-4}	-1.041^{-5}
−0.328	0.768	-3.145^{-1}	1.520^{-4}	2.076^{-7}
−0.296	0.768	-8.753^{-2}	1.654^{-4}	5.726^{-6}
−0.264	0.771	-1.835^{-1}	1.684^{-4}	-1.714^{-5}
−0.232	0.773	-4.782^{-2}	1.960^{-4}	9.242^{-6}
−0.200	0.769	4.920^{-4}	2.990^{-4}	3.255^{-5}
−0.174	0.765	2.557^{-3}	3.964^{-4}	4.120^{-5}
−0.161	0.767	3.182^{-3}	4.839^{-4}	8.237^{-5}
−0.148	0.766	2.735^{-3}	6.443^{-4}	1.346^{-4}
−0.136	0.763	3.677^{-3}	8.867^{-4}	2.212^{-4}
−0.123	0.753	4.399^{-3}	1.137^{-3}	2.344^{-4}
−0.110	0.746	5.376^{-3}	1.513^{-3}	4.436^{-4}
−0.097	0.742	2.617^{-3}	1.752^{-3}	3.791^{-4}
−0.084	0.741	5.548^{-3}	1.949^{-3}	4.535^{-4}
−0.072	0.724	1.320^{-2}	2.185^{-3}	6.691^{-4}
−0.059	0.710	1.801^{-2}	2.512^{-3}	8.266^{-4}
−0.046	0.703	2.012^{-2}	2.691^{-3}	7.247^{-4}
−0.033	0.693	1.943^{-2}	2.894^{-3}	7.057^{-4}
−0.020	0.683	1.832^{-2}	3.023^{-3}	4.834^{-4}
−0.008	0.676	1.546^{-2}	3.065^{-3}	2.990^{-4}
0.005	0.673	9.271^{-3}	3.190^{-3}	1.885^{-4}
0.018	0.670	1.688^{-2}	3.340^{-3}	-7.027^{-5}
0.031	0.675	6.287^{-3}	3.466^{-3}	-4.365^{-4}
0.044	0.676	1.237^{-2}	3.308^{-3}	-6.035^{-4}
0.056	0.686	3.758^{-3}	3.393^{-3}	-7.978^{-4}
0.069	0.695	3.694^{-3}	3.453^{-3}	-8.296^{-4}
0.082	0.692	6.490^{-3}	3.354^{-3}	-9.167^{-4}
0.095	0.705	1.906^{-3}	3.073^{-3}	-9.886^{-4}
0.108	0.713	4.931^{-3}	3.447^{-3}	-1.096^{-3}
0.120	0.723	2.565^{-3}	2.551^{-3}	-8.160^{-4}
0.146	0.742	-1.478^{-3}	1.712^{-3}	-3.377^{-4}
0.172	0.750	3.736^{-4}	1.491^{-3}	-3.759^{-4}
0.197	0.755	2.068^{-4}	8.395^{-4}	-1.011^{-4}
0.223	0.762	-2.501^{-3}	4.745^{-4}	-5.177^{-5}
0.248	0.761	-1.791^{-3}	5.013^{-4}	8.255^{-7}
0.280	0.765	-7.699^{-4}	3.476^{-4}	2.957^{-5}
0.312	0.766	-2.295^{-3}	2.291^{-4}	-2.101^{-7}
0.344	0.768	-4.205^{-3}	2.104^{-4}	1.720^{-6}
0.376	0.772	-6.803^{-3}	1.776^{-4}	1.755^{-5}
0.408	0.769	-4.590^{-3}	1.705^{-4}	1.559^{-5}
0.440	0.775	-7.044^{-3}	1.778^{-4}	1.534^{-5}
0.472	0.773	-6.597^{-3}	1.658^{-4}	2.182^{-5}
0.504	0.771	-9.682^{-3}	1.491^{-4}	2.275^{-5}
0.536	0.776	-1.074^{-2}	1.369^{-4}	3.068^{-5}
0.568	0.777	-9.091^{-3}	1.496^{-4}	3.204^{-5}

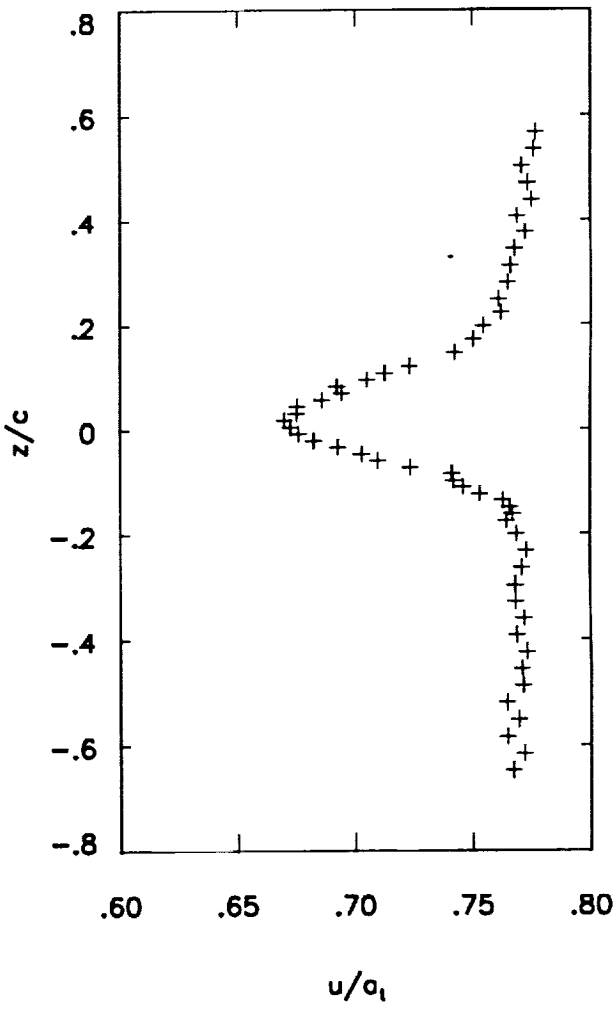

Figure 7. Continued. (l) M_∞=0.803, α=1.5°, Re=6x10^6, x/c=2.5.

$\frac{z}{c}$	$\frac{u}{a_t}$	$\frac{v}{a_t}$	$\frac{\langle u'^2+v'^2\rangle}{2a_t^2}$	$\frac{\langle u'v'\rangle}{a_t^2}$
−0.370	0.643	-8.157^{-3}	1.582^{-4}	3.442^{-5}
−0.338	0.636	-6.273^{-3}	1.419^{-4}	3.766^{-5}
−0.306	0.630	-9.871^{-3}	1.372^{-4}	3.073^{-5}
−0.274	0.632	-1.057^{-2}	1.498^{-4}	2.454^{-5}
−0.242	0.630	-1.357^{-2}	1.239^{-4}	2.518^{-5}
−0.210	0.624	-1.414^{-2}	1.155^{-4}	2.457^{-5}
−0.178	0.621	-1.687^{-2}	1.196^{-4}	1.224^{-5}
−0.146	0.625	-1.922^{-2}	9.830^{-5}	1.750^{-5}
−0.120	0.625	-2.450^{-2}	1.062^{-4}	1.938^{-5}
−0.108	0.622	-2.338^{-2}	1.075^{-4}	6.069^{-6}
−0.095	0.621	-2.500^{-2}	1.145^{-4}	2.109^{-5}
−0.082	0.622	-2.651^{-2}	1.160^{-4}	1.848^{-5}
−0.069	0.623	-2.641^{-2}	1.284^{-4}	2.109^{-5}
−0.056	0.622	-2.727^{-2}	1.339^{-4}	2.251^{-5}
−0.050	0.622	-2.629^{-2}	1.683^{-4}	3.430^{-5}
−0.043	0.618	-2.642^{-2}	2.729^{-4}	4.586^{-5}
−0.037	0.597	-2.252^{-2}	8.119^{-4}	2.082^{-4}
−0.030	0.554	-1.846^{-2}	1.499^{-3}	5.821^{-4}
−0.024	0.501	-1.899^{-2}	2.293^{-3}	7.783^{-4}
−0.021	0.455	5.161^{-4}	3.950^{-3}	1.455^{-3}
−0.018	0.329	1.363^{-2}	5.957^{-3}	3.554^{-3}
−0.015	0.249	1.992^{-3}	4.246^{-3}	1.656^{-3}
−0.013	0.247	-1.176^{-2}	3.584^{-3}	-8.377^{-4}
−0.011	0.258	-2.386^{-2}	3.882^{-3}	-1.874^{-3}
−0.008	0.318	-3.964^{-2}	4.555^{-3}	-2.447^{-3}
−0.005	0.397	-5.908^{-2}	3.649^{-3}	-2.010^{-3}
0.008	0.607	-8.587^{-2}	5.474^{-4}	-9.830^{-5}
0.020	0.630	-8.353^{-2}	1.591^{-4}	2.028^{-5}
0.033	0.639	-8.072^{-2}	1.340^{-4}	1.707^{-5}
0.047	0.642	-8.087^{-2}	1.346^{-4}	1.273^{-5}
0.059	0.645	-8.108^{-2}	1.385^{-4}	1.758^{-5}
0.072	0.648	-7.824^{-2}	1.385^{-4}	2.098^{-5}
0.085	0.654	-7.934^{-2}	1.436^{-4}	1.758^{-5}
0.110	0.659	-7.816^{-2}	1.474^{-4}	2.171^{-5}
0.142	0.668	-7.820^{-2}	1.563^{-4}	2.331^{-5}
0.175	0.674	-7.578^{-2}	1.635^{-4}	2.854^{-5}
0.206	0.678	-7.361^{-2}	1.666^{-4}	2.233^{-5}
0.238	0.686	-7.078^{-2}	1.459^{-4}	2.652^{-6}
0.270	0.689	-7.158^{-2}	1.551^{-4}	1.454^{-5}
0.303	0.693	-6.799^{-2}	1.525^{-4}	1.459^{-5}
0.334	0.694	-6.331^{-2}	1.627^{-4}	5.842^{-6}
0.366	0.702	-6.539^{-2}	1.615^{-4}	7.824^{-6}
0.398	0.698	-5.925^{-2}	1.648^{-4}	-2.898^{-6}
0.431	0.699	-6.061^{-2}	1.591^{-4}	7.985^{-6}
0.462	0.705	-5.527^{-2}	1.690^{-4}	1.350^{-5}

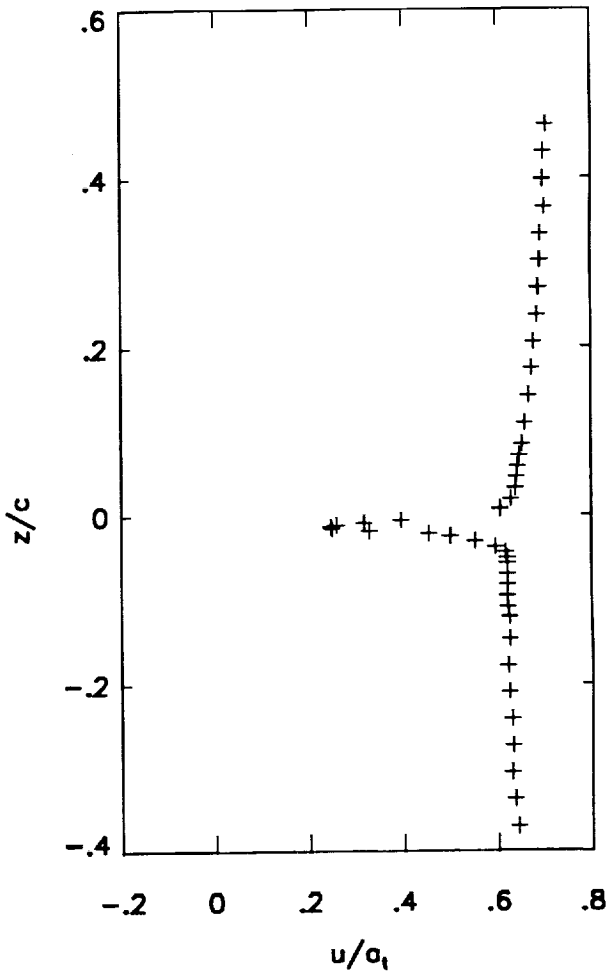

Figure 7. Continued. (m) M_∞=0.728, α=1.0°, Re=6x10^6, x/c=1.04.

$\frac{z}{c}$	$\frac{u}{a_t}$	$\frac{v}{a_t}$	$\frac{\langle u'^2+v'^2\rangle}{2a_t^2}$	$\frac{\langle u'v'\rangle}{a_t^2}$
−0.338	0.697	4.157^{-3}	1.612^{-4}	3.151^{-5}
−0.306	0.691	1.782^{-3}	1.863^{-4}	3.512^{-5}
−0.274	0.691	1.636^{-3}	1.499^{-4}	2.323^{-5}
−0.242	0.691	-2.418^{-3}	1.664^{-4}	2.475^{-5}
−0.210	0.689	-4.839^{-3}	1.930^{-4}	6.380^{-6}
−0.178	0.686	-3.088^{-3}	1.798^{-4}	3.087^{-5}
−0.146	0.688	-4.694^{-3}	1.402^{-4}	1.502^{-5}
−0.114	0.689	-8.771^{-3}	1.552^{-4}	2.456^{-5}
−0.082	0.696	-5.379^{-3}	1.618^{-4}	3.140^{-5}
−0.056	0.700	-6.882^{-4}	2.247^{-4}	4.437^{-5}
−0.043	0.699	-5.561^{-4}	4.174^{-4}	7.086^{-5}
−0.037	0.689	1.398^{-2}	9.915^{-4}	2.878^{-4}
−0.030	0.646	9.618^{-3}	2.172^{-3}	7.285^{-4}
−0.028	0.629	1.200^{-2}	2.748^{-3}	8.965^{-4}
−0.025	0.612	1.010^{-2}	3.014^{-3}	9.833^{-4}
−0.023	0.590	1.863^{-2}	3.494^{-3}	6.931^{-4}
−0.020	0.560	3.777^{-2}	4.860^{-3}	1.367^{-3}
−0.018	0.485	5.217^{-2}	9.280^{-3}	4.227^{-3}
−0.015	0.385	7.019^{-2}	1.207^{-2}	6.419^{-3}
−0.013	0.253	5.834^{-2}	1.548^{-2}	9.996^{-3}
−0.010	0.164	3.052^{-2}	1.359^{-2}	7.015^{-3}
−0.008	0.104	1.085^{-2}	1.230^{-2}	1.806^{-3}
−0.005	0.077	-1.462^{-2}	1.269^{-2}	-1.980^{-3}
−0.003	0.080	-3.625^{-2}	1.374^{-2}	-5.574^{-3}
0.000	0.098	-3.284^{-2}	1.247^{-2}	-3.839^{-3}
0.003	0.134	-4.942^{-2}	1.595^{-2}	-7.279^{-3}
0.005	0.174	-5.804^{-2}	1.765^{-2}	-7.792^{-3}
0.008	0.187	-5.650^{-2}	1.577^{-2}	-7.399^{-3}
0.010	0.195	-6.724^{-2}	1.755^{-2}	-8.843^{-3}
0.013	0.306	-9.379^{-2}	1.859^{-2}	-1.138^{-2}
0.015	0.378	-9.647^{-2}	1.686^{-2}	-8.599^{-3}
0.017	0.346	-9.940^{-2}	1.800^{-2}	-1.069^{-2}
0.018	0.422	-1.095^{-1}	1.438^{-2}	-6.182^{-3}
0.020	0.389	-8.843^{-2}	1.491^{-2}	-6.588^{-3}
0.023	0.426	-1.064^{-1}	1.637^{-2}	-8.297^{-3}
0.025	0.480	-1.220^{-1}	1.319^{-2}	-6.384^{-3}
0.027	0.555	-1.414^{-1}	6.832^{-3}	-1.393^{-3}
0.033	0.577	-1.228^{-1}	8.696^{-3}	-2.799^{-3}
0.047	0.690	-1.124^{-1}	1.898^{-3}	-2.503^{-4}
0.059	0.718	-1.020^{-1}	1.005^{-3}	5.404^{-5}
0.078	0.720	-9.386^{-2}	4.085^{-4}	7.116^{-5}
0.110	0.716	-8.236^{-2}	2.151^{-4}	5.704^{-5}
0.142	0.718	-7.776^{-2}	1.571^{-4}	3.193^{-5}
0.175	0.720	-7.802^{-2}	1.441^{-4}	3.496^{-5}
0.206	0.729	-7.235^{-2}	1.633^{-4}	4.556^{-5}
0.238	0.739	-6.648^{-2}	1.680^{-4}	5.659^{-5}
0.270	0.737	-6.924^{-2}	1.771^{-4}	5.065^{-5}
0.303	0.745	-6.583^{-2}	1.382^{-4}	2.299^{-5}
0.334	0.749	-6.367^{-2}	1.446^{-4}	2.437^{-5}
0.366	0.749	-6.368^{-2}	1.431^{-4}	3.033^{-5}
0.398	0.748	-6.335^{-2}	1.415^{-4}	2.464^{-5}
0.431	0.753	-6.086^{-2}	1.338^{-4}	1.736^{-5}
0.462	0.755	-6.335^{-2}	1.338^{-4}	2.354^{-5}

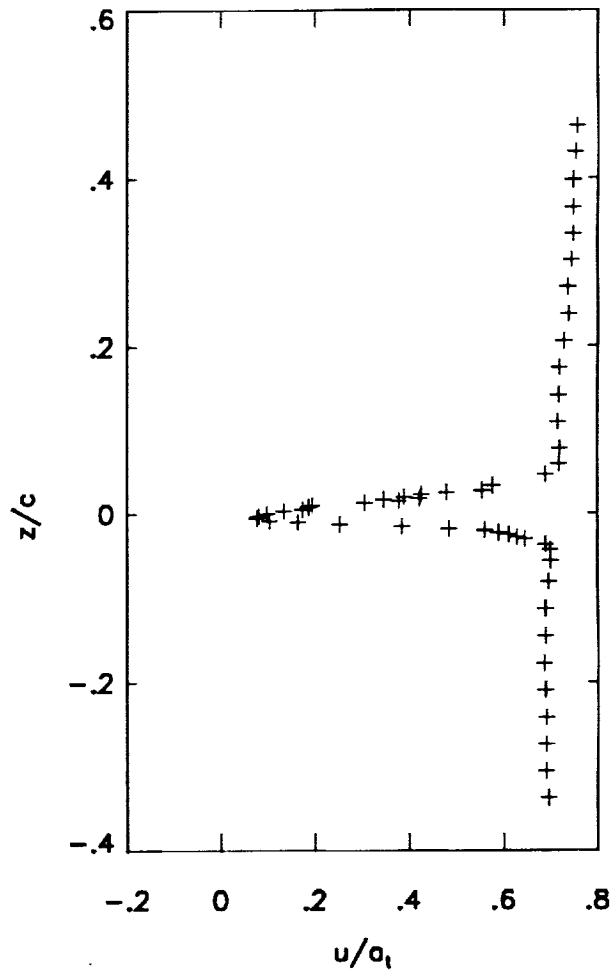

Figure 7. Continued. (n) M_∞=0.781, α=1.0°, Re=6x10^6, x/c=1.04.

$\frac{z}{c}$	$\frac{u}{a_t}$	$\frac{v}{a_t}$	$\frac{\langle u'^2+v'^2\rangle}{2a_t^2}$	$\frac{\langle u'v'\rangle}{a_t^2}$
−0.338	0.733	1.694^{-2}	1.541^{-4}	2.645^{-5}
−0.306	0.726	1.643^{-2}	1.281^{-4}	2.862^{-5}
−0.274	0.728	1.577^{-2}	1.465^{-4}	1.938^{-5}
−0.242	0.729	1.457^{-2}	1.151^{-4}	2.349^{-5}
−0.210	0.721	1.535^{-2}	1.190^{-4}	2.330^{-5}
−0.178	0.722	1.467^{-2}	1.185^{-4}	2.460^{-5}
−0.146	0.725	1.310^{-2}	1.268^{-4}	2.972^{-5}
−0.114	0.727	1.522^{-2}	1.354^{-4}	2.987^{-5}
−0.082	0.737	1.495^{-2}	1.750^{-4}	3.208^{-5}
−0.056	0.746	2.215^{-2}	4.527^{-4}	7.089^{-5}
−0.043	0.734	3.284^{-2}	1.453^{-3}	3.713^{-4}
−0.031	0.678	3.649^{-2}	4.207^{-3}	1.509^{-3}
−0.028	0.662	3.785^{-2}	5.339^{-3}	1.943^{-3}
−0.025	0.650	4.327^{-2}	5.382^{-3}	1.413^{-3}
−0.023	0.654	4.283^{-2}	5.346^{-3}	1.057^{-3}
−0.020	0.619	6.212^{-2}	6.376^{-3}	1.634^{-3}
−0.018	0.585	8.363^{-2}	7.945^{-3}	2.756^{-3}
−0.015	0.493	9.285^{-2}	8.285^{-3}	3.037^{-3}
−0.013	0.360	9.933^{-2}	1.556^{-2}	8.827^{-3}
−0.010	0.222	9.184^{-2}	2.284^{-2}	1.438^{-2}
−0.008	0.084	4.369^{-2}	2.045^{-2}	9.693^{-3}
−0.006	0.054	2.549^{-2}	1.820^{-2}	8.241^{-3}
−0.005	0.050	2.868^{-2}	2.087^{-2}	8.232^{-3}
−0.002	−0.007	-1.237^{-2}	1.640^{-2}	1.633^{-3}
0.000	−0.032	-1.290^{-2}	1.435^{-2}	1.072^{-3}
0.003	−0.025	-1.964^{-2}	1.571^{-2}	-6.509^{-4}
0.005	−0.003	-2.682^{-2}	1.822^{-2}	-2.519^{-3}
0.008	0.013	-3.443^{-2}	1.954^{-2}	-3.934^{-3}
0.010	0.012	-3.418^{-2}	1.765^{-2}	-5.366^{-3}
0.013	0.044	-4.360^{-2}	2.328^{-2}	-5.614^{-3}
0.016	0.062	-4.049^{-2}	2.051^{-2}	-5.462^{-3}
0.017	0.102	-7.536^{-2}	2.281^{-2}	-9.448^{-3}
0.018	0.101	-5.747^{-2}	2.292^{-2}	-7.855^{-3}
0.021	0.147	-7.847^{-2}	2.415^{-2}	-1.088^{-2}
0.027	0.245	-8.207^{-2}	2.517^{-2}	-9.775^{-3}
0.033	0.350	-8.833^{-2}	2.187^{-2}	-8.132^{-3}
0.040	0.494	-1.316^{-1}	1.467^{-2}	-5.066^{-3}
0.046	0.576	-1.494^{-1}	1.181^{-2}	-3.281^{-3}
0.053	0.662	-1.490^{-1}	6.576^{-3}	-1.096^{-3}
0.059	0.709	-1.452^{-1}	3.553^{-3}	1.106^{-4}
0.065	0.739	-1.228^{-1}	2.722^{-3}	-3.521^{-4}
0.072	0.758	-1.089^{-1}	2.115^{-3}	-1.228^{-4}
0.078	0.768	-1.004^{-1}	1.697^{-3}	-2.396^{-5}
0.091	0.774	-8.081^{-2}	7.820^{-4}	2.050^{-5}
0.110	0.774	-7.627^{-2}	4.612^{-4}	3.159^{-5}
0.142	0.772	-6.889^{-2}	2.459^{-4}	6.267^{-6}
0.174	0.766	-6.577^{-2}	1.726^{-4}	2.727^{-5}
0.206	0.764	-6.087^{-2}	1.617^{-4}	1.896^{-5}
0.238	0.766	-5.937^{-2}	1.424^{-4}	1.940^{-5}
0.270	0.770	-6.064^{-2}	1.481^{-4}	1.375^{-5}
0.302	0.770	-6.289^{-2}	1.501^{-4}	1.518^{-5}
0.334	0.768	-5.468^{-2}	1.454^{-4}	2.678^{-5}
0.366	0.771	-5.620^{-2}	1.490^{-4}	3.203^{-5}
0.398	0.777	-5.278^{-2}	1.567^{-4}	1.426^{-5}
0.430	0.775	-5.250^{-2}	1.491^{-4}	2.170^{-5}
0.462	0.777	-5.184^{-2}	1.651^{-4}	2.100^{-5}

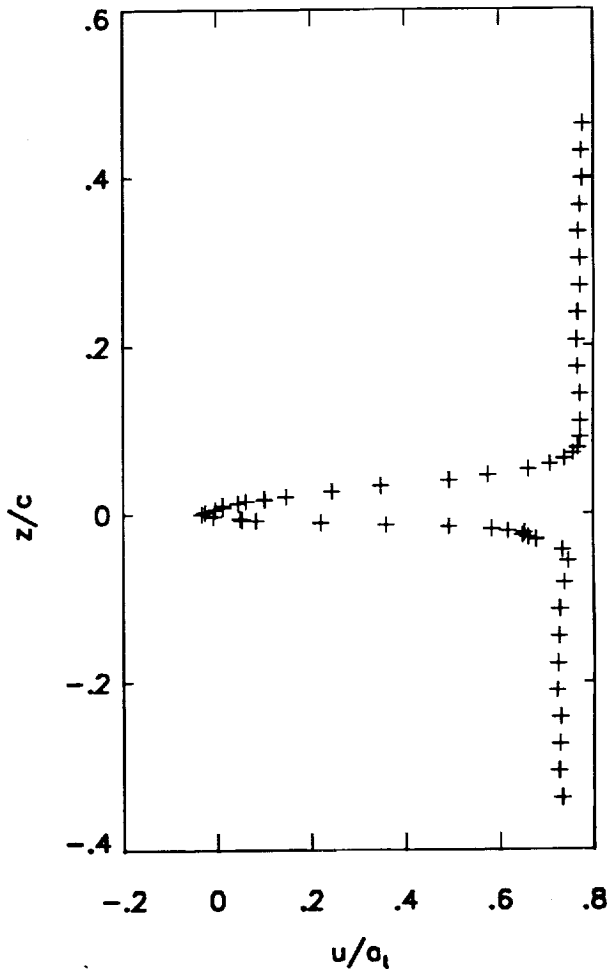

Figure 7. Concluded. (o) M_∞=0.802, α=1.0°, Re=6x10^6, x/c=1.04.

$\frac{z}{c}$ = 0.1204 □			$\frac{z}{c}$ = 0.2484 △			$\frac{z}{c}$ = 0.5044 ◇		
$\frac{x}{c}$	$\frac{u}{a_t}$	$\frac{v}{a_t}$	$\frac{x}{c}$	$\frac{u}{a_t}$	$\frac{v}{a_t}$	$\frac{x}{c}$	$\frac{u}{a_t}$	$\frac{v}{a_t}$
0.0498	0.8702	0.2087	-0.0291	0.7288	0.1363	0.1290	0.8330	0.0690
0.0881	0.9736	0.1625	0.0088	0.7726	0.1417	0.1682	0.8457	0.0573
0.1253	1.0127	0.1249	0.0442	0.8144	0.1390	0.2082	0.8685	0.0448
0.1687	1.0346	0.0841	0.0883	0.8754	0.1226	0.2487	0.8717	0.0301
0.2053	1.0380	0.0635	0.1291	0.9172	0.1011	0.2843	0.8738	0.0174
0.2506	1.0412	0.0412	0.1720	0.9564	0.0765	0.3291	0.8652	0.0016
0.2848	1.0350	0.0273	0.2091	0.9743	0.0560	0.3678	0.8521	-0.0059
0.3030	1.0511	0.0241	0.2519	0.9814	0.0357	0.4120	0.8425	-0.0150
0.3189	1.0447	0.0088	0.2873	0.9875	0.0259	0.4417	0.8339	-0.0179
0.3214	1.0391	0.0150	0.2875	0.9775	0.0188	0.4889	0.8251	-0.0256
0.3252	1.0355	0.0127	0.2997	0.9837	0.0165	0.5295	0.8195	-0.0298
0.3334	1.0395	0.0084	0.3038	0.9849	0.0133	0.5708	0.8106	-0.0356
0.3410	1.0314	0.0035	0.3097	0.9850	0.0118	0.6001	0.8042	-0.0385
0.3507	1.0116	0.0031	0.3177	0.9889	0.0090	0.6375	0.7959	-0.0424
0.3588	0.9373	0.0003	0.3261	0.9878	0.0030			
0.3610	0.9087	-0.0072	0.3348	0.9683	-0.0047			
0.3651	0.9081	-0.0007	0.3398	0.9781	-0.0051			
0.3735	0.8797	-0.0058	0.3434	0.9748	-0.0068			
0.3828	0.8789	-0.0096	0.3501	0.9566	-0.0137			
0.3911	0.8855	-0.0132	0.3578	0.8955	-0.0199			
0.3982	0.8833	-0.0181	0.3679	0.8796	-0.0222			
0.4012	0.8891	-0.0181	0.3697	0.8746	-0.0196			
0.4050	0.8893	-0.0157	0.3752	0.8763	-0.0222			
0.4305	0.8983	-0.0200	0.3813	0.8728	-0.0186			
0.4853	0.9041	-0.0350	0.3915	0.8723	-0.0185			
0.5154	0.9007	-0.0434	0.3984	0.8716	-0.0204			
0.5650	0.8860	-0.0569	0.4074	0.8724	-0.0186			
			0.4077	0.8728	-0.0201			
			0.4142	0.8726	-0.0206			
			0.4419	0.8712	-0.0244			
			0.4802	0.8714	-0.0316			
			0.5179	0.8658	-0.0405			

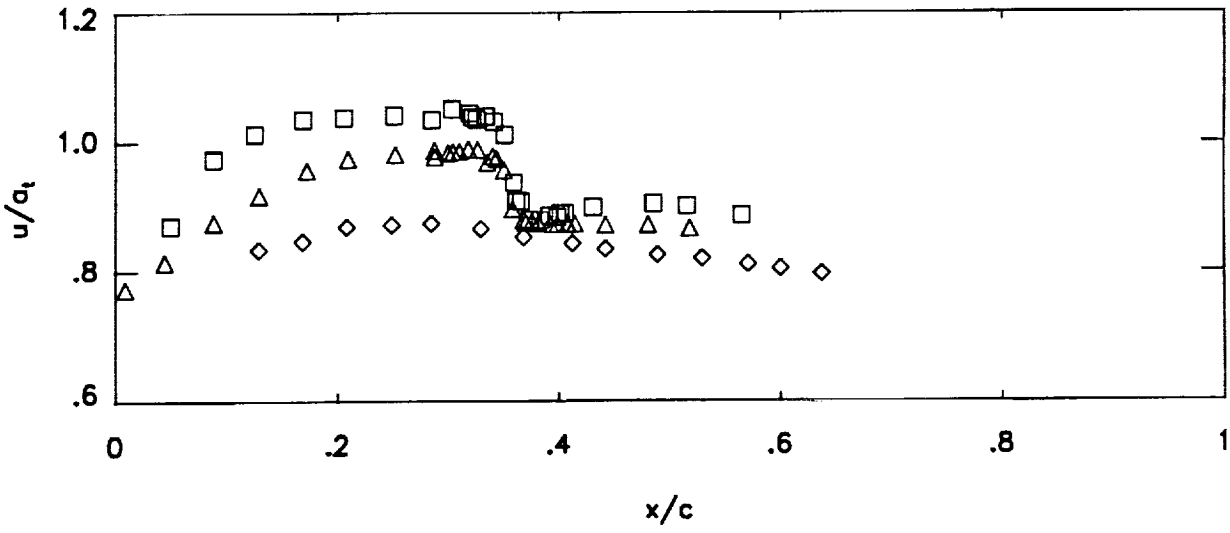

Figure 8. LDV flowfield data above the wing. (a) M_∞=0.730, α=1.0°, Re=2x10^6.

$\frac{z}{c} = 0.1204$ □			$\frac{z}{c} = 0.2484$ △			$\frac{z}{c} = 0.6325$ ◇		
$\frac{x}{c}$	$\frac{u}{a_t}$	$\frac{v}{a_t}$	$\frac{x}{c}$	$\frac{u}{a_t}$	$\frac{v}{a_t}$	$\frac{x}{c}$	$\frac{u}{a_t}$	$\frac{v}{a_t}$
0.3667	1.0765	0.0007	0.4455	1.0467	−0.0159	0.4457	0.9093	−0.0049
0.4090	1.0851	−0.0145	0.4829	1.0442	−0.0324	0.4831	0.9012	−0.0263
0.4462	1.0820	−0.0197	0.5235	1.0407	−0.0426	0.5146	0.8886	−0.0355
0.4905	1.0830	−0.0394	0.5249	1.0422	−0.0323	0.5661	0.8481	−0.0474
0.5089	1.0961	−0.0495	0.5303	1.0363	−0.0425	0.6019	0.8308	−0.0500
0.5228	1.0811	−0.0526	0.5406	1.0324	−0.0485	0.6429	0.8169	−0.0519
0.5257	1.0908	−0.0537	0.5490	1.0264	−0.0494	0.6763	0.8062	−0.0536
0.5331	1.0808	−0.0554	0.5583	1.0470	−0.0508	0.7263	0.7930	−0.0549
0.5406	1.0785	−0.0608	0.5635	1.0555	−0.0568	0.7555	0.7844	−0.0554
0.5477	1.0924	−0.0631	0.5650	0.9854	−0.0647	0.7952	0.7766	−0.0564
0.5577	1.1124	−0.0672	0.5737	0.8771	−0.0805	0.8345	0.7696	−0.0566
0.5640	1.0541	−0.0554	0.5803	0.8326	−0.0827	0.8823	0.7594	−0.0553
0.5648	0.9144	−0.0454	0.5878	0.8247	−0.0819	0.9161	0.7546	−0.0550
0.5713	0.9089	−0.0397	0.5970	0.8216	−0.0804			
0.5795	0.8387	−0.0456	0.6034	0.8223	−0.0778			
0.5878	0.8256	−0.0518	0.6074	0.8213	−0.0842			
0.5976	0.8345	−0.0622	0.6114	0.8232	−0.0768			
0.6028	0.8407	−0.0685	0.6201	0.8240	−0.0761			
0.6049	0.8373	−0.0654	0.6315	0.8246	−0.0760			
0.6107	0.8437	−0.0744	0.6369	0.8238	−0.0765			
0.6196	0.8442	−0.0788	0.6454	0.8229	−0.0766			
0.6270	0.8429	−0.0816	0.6457	0.8206	−0.0822			
0.6502	0.8367	−0.0854	0.6511	0.8241	−0.0764			
0.6879	0.8208	−0.0950	0.6589	0.8217	−0.0777			
0.7236	0.8058	−0.1001	0.6785	0.8157	−0.0839			
0.7626	0.7880	−0.1033	0.7233	0.8041	−0.0874			
0.8058	0.7697	−0.1040	0.7650	0.7895	−0.0902			
0.8391	0.7533	−0.1040	0.8050	0.7755	−0.0903			
0.8830	0.7326	−0.1038	0.8435	0.7635	−0.0891			
0.9254	0.7140	−0.1002	0.8769	0.7523	−0.0883			
0.9633	0.6983	−0.0943	0.9176	0.7388	−0.0853			
0.9971	0.6864	−0.0883	0.9576	0.7278	−0.0800			
			0.9992	0.7158	−0.0766			

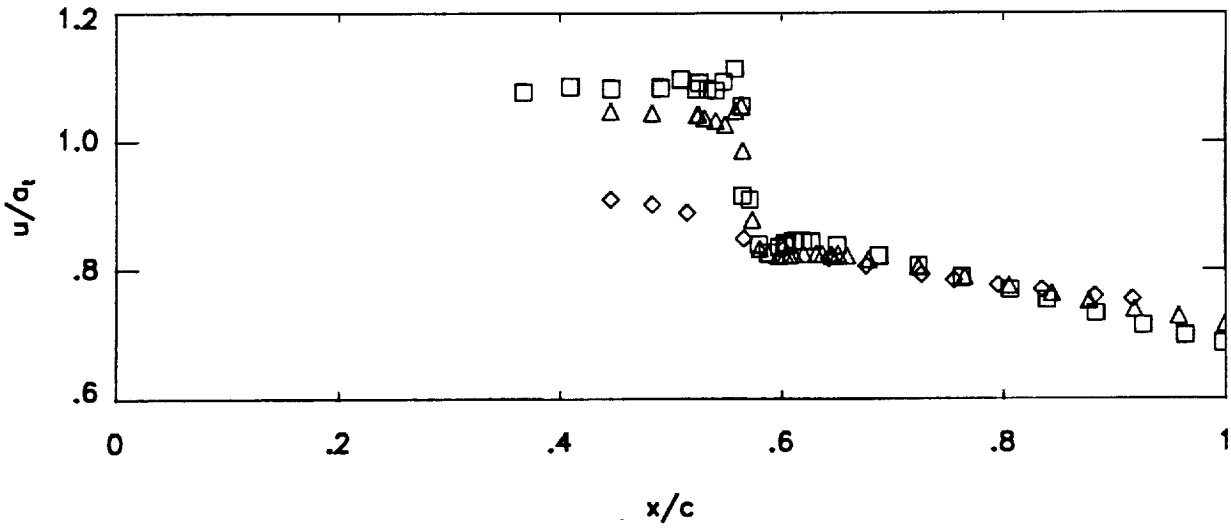

Figure 8. Continued. (b) M_∞=0.750, α=1.0°, Re=2x10^6.

$\frac{z}{c} = 0.1204$ □			$\frac{z}{c} = 0.3764$ △			$\frac{z}{c} = 0.6325$ ◇		
$\frac{x}{c}$	$\frac{u}{a_t}$	$\frac{v}{a_t}$	$\frac{x}{c}$	$\frac{u}{a_t}$	$\frac{v}{a_t}$	$\frac{x}{c}$	$\frac{u}{a_t}$	$\frac{v}{a_t}$
0.3174	1.0702	0.0167	0.4457	1.0162	−0.0056	0.4457	0.9455	−0.0003
0.3524	1.0952	0.0070	0.4824	1.0257	−0.0160	0.4823	0.9580	−0.0059
0.3792	1.0815	−0.0024	0.5206	1.0364	−0.0260	0.5205	0.9602	−0.0165
0.4194	1.0931	−0.0131	0.5700	1.0375	−0.0390	0.5618	0.9634	−0.0306
0.4311	1.1053	−0.0174	0.5878	1.0324	−0.0379	0.6095	0.9536	−0.0472
0.4392	1.0961	−0.0194	0.5971	1.0316	−0.0480	0.6402	0.8858	−0.0632
0.4558	1.0927	−0.0222	0.6041	1.0364	−0.0485	0.6779	0.8486	−0.0631
0.4912	1.1031	−0.0384	0.6072	1.0227	−0.0481	0.7243	0.8285	−0.0603
0.5097	1.1123	−0.0452	0.6117	1.0274	−0.0504	0.7601	0.8198	−0.0609
0.5499	1.1130	−0.0589	0.6199	1.0213	−0.0519	0.7998	0.8084	−0.0596
0.5881	1.1247	−0.0720	0.6269	1.0132	−0.0533	0.8388	0.8017	−0.0595
0.5958	1.1196	−0.0725	0.6370	1.0255	−0.0592			
0.6030	1.1157	−0.0713	0.6424	1.0347	−0.0594			
0.6050	1.1156	−0.0774	0.6457	1.0384	−0.0600			
0.6063	1.1010	−0.0749	0.6510	1.0342	−0.0570			
0.6109	1.1100	−0.0751	0.6605	0.8970	−0.0687			
0.6199	1.0956	−0.0769	0.6692	0.8265	−0.0726			
0.6289	1.0940	−0.0580	0.6752	0.8126	−0.0736			
0.6351	1.0369	−0.0346	0.6807	0.8176	−0.0754			
0.6430	0.9297	−0.0079	0.6823	0.8093	−0.0737			
0.6525	0.8443	−0.0098	0.6901	0.8070	−0.0709			
0.6630	0.8394	−0.0197	0.6978	0.8062	−0.0703			
0.6690	0.8412	−0.0235	0.7061	0.8062	−0.0694			
0.6739	0.8480	−0.0258	0.7145	0.8053	−0.0678			
0.6750	0.8510	−0.0207	0.7276	0.8075	−0.0686			
0.6831	0.8456	−0.0362	0.7585	0.8081	−0.0680			
0.6833	0.8519	−0.0196	0.7981	0.8044	−0.0680			
0.6910	0.8487	−0.0417	0.8423	0.7959	−0.0693			
0.6989	0.8475	−0.0483	0.8858	0.7873	−0.0704			
0.6993	0.8474	−0.0391	0.9257	0.7777	−0.0701			
0.7070	0.8510	−0.0523	0.9596	0.7700	−0.0703			
0.7107	0.8535	−0.0390	0.9975	0.7628	−0.0690			
0.7138	0.8516	−0.0556						
0.7145	0.8487	−0.0503						
0.7312	0.8469	−0.0612						
0.7460	0.8451	−0.0675						
0.7618	0.8410	−0.0704						
0.7788	0.8367	−0.0748						
0.7940	0.8303	−0.0798						
0.8093	0.8206	−0.0835						
0.8275	0.8131	−0.0865						
0.8412	0.8041	−0.0898						
0.8570	0.8084	−0.0831						
0.8589	0.8005	−0.0913						
0.8728	0.7935	−0.0920						

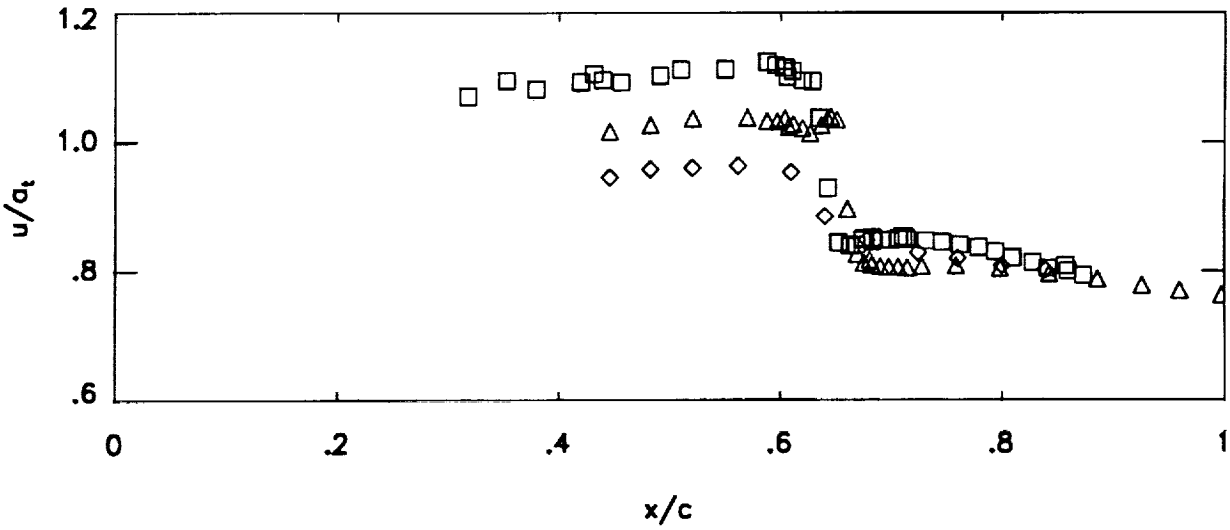

Figure 8. Continued. (c) M_∞=0.780, α=1.0°, Re=2x10^6.

$\frac{z}{c} = 0.2484$ □			$\frac{z}{c} = 0.5044$ △		
$\frac{x}{c}$	$\frac{u}{a_t}$	$\frac{v}{a_t}$	$\frac{x}{c}$	$\frac{u}{a_t}$	$\frac{v}{a_t}$
0.4459	1.0525	−0.0090	0.6199	1.0116	−0.0310
0.4810	1.0655	−0.0230	0.6267	1.0173	−0.0376
0.5233	1.0723	−0.0332	0.6348	1.0225	−0.0366
0.5651	1.0732	−0.0408	0.6430	1.0189	−0.0395
0.5992	1.0840	−0.0561	0.6532	1.0218	−0.0426
0.6199	1.0853	−0.0577	0.6595	1.0162	−0.0448
0.6251	1.0846	−0.0604	0.6666	1.0140	−0.0463
0.6343	1.0865	−0.0622	0.6744	1.0093	−0.0484
0.6427	1.0823	−0.0645	0.6820	0.9972	−0.0498
0.6491	1.0903	−0.0696	0.6902	1.0174	−0.0534
0.6508	1.0842	−0.0644	0.7010	1.0113	−0.0563
0.6617	1.0755	−0.0669	0.7061	0.9707	−0.0557
0.6674	1.0686	−0.0672	0.7170	0.8502	−0.0557
0.6746	1.0905	−0.0688	0.7241	0.8258	−0.0542
0.6817	1.0197	−0.0506	0.7298	0.8158	−0.0541
0.6833	1.0643	−0.0530	0.7374	0.8114	−0.0511
0.6905	0.9738	−0.0288	0.7457	0.8118	−0.0471
0.6985	0.8561	−0.0142			
0.7059	0.8235	−0.0100			
0.7140	0.8149	−0.0110			
0.7229	0.8146	−0.0144			
0.7238	0.8168	−0.0171			
0.7311	0.8170	−0.0170			
0.7382	0.8184	−0.0197			
0.7453	0.8204	−0.0215			
0.7624	0.8258	−0.0284			
0.7992	0.8304	−0.0366			
0.8391	0.8306	−0.0437			
0.8883	0.8276	−0.0499			
0.9232	0.8208	−0.0534			
0.9595	0.8125	−0.0585			

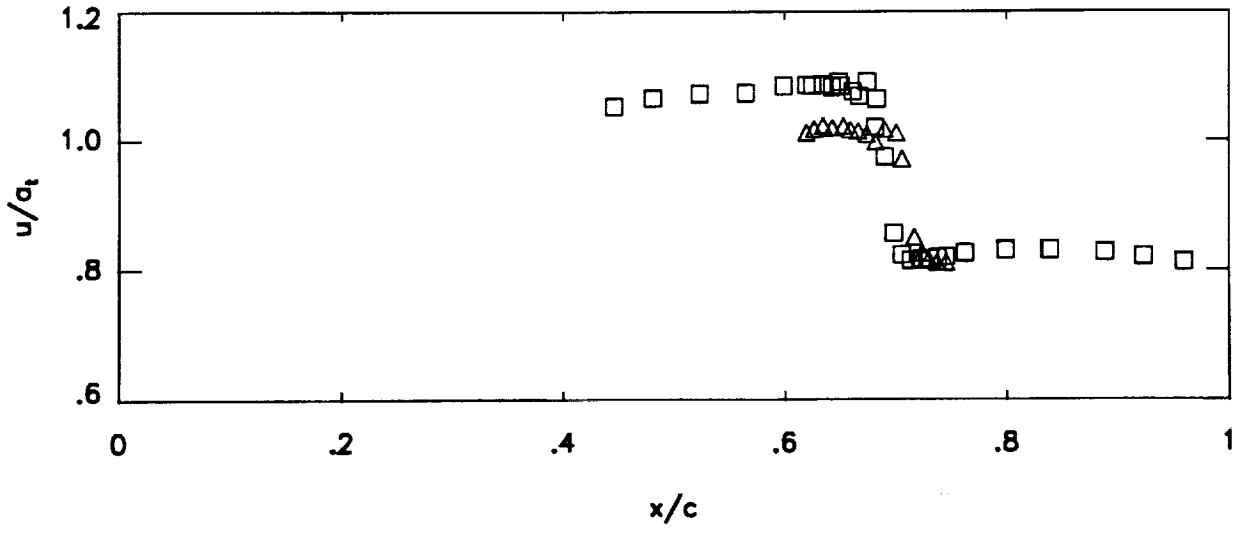

Figure 8. Concluded. (d) M_∞=0.810, α=1.0°, Re=2x10^6.

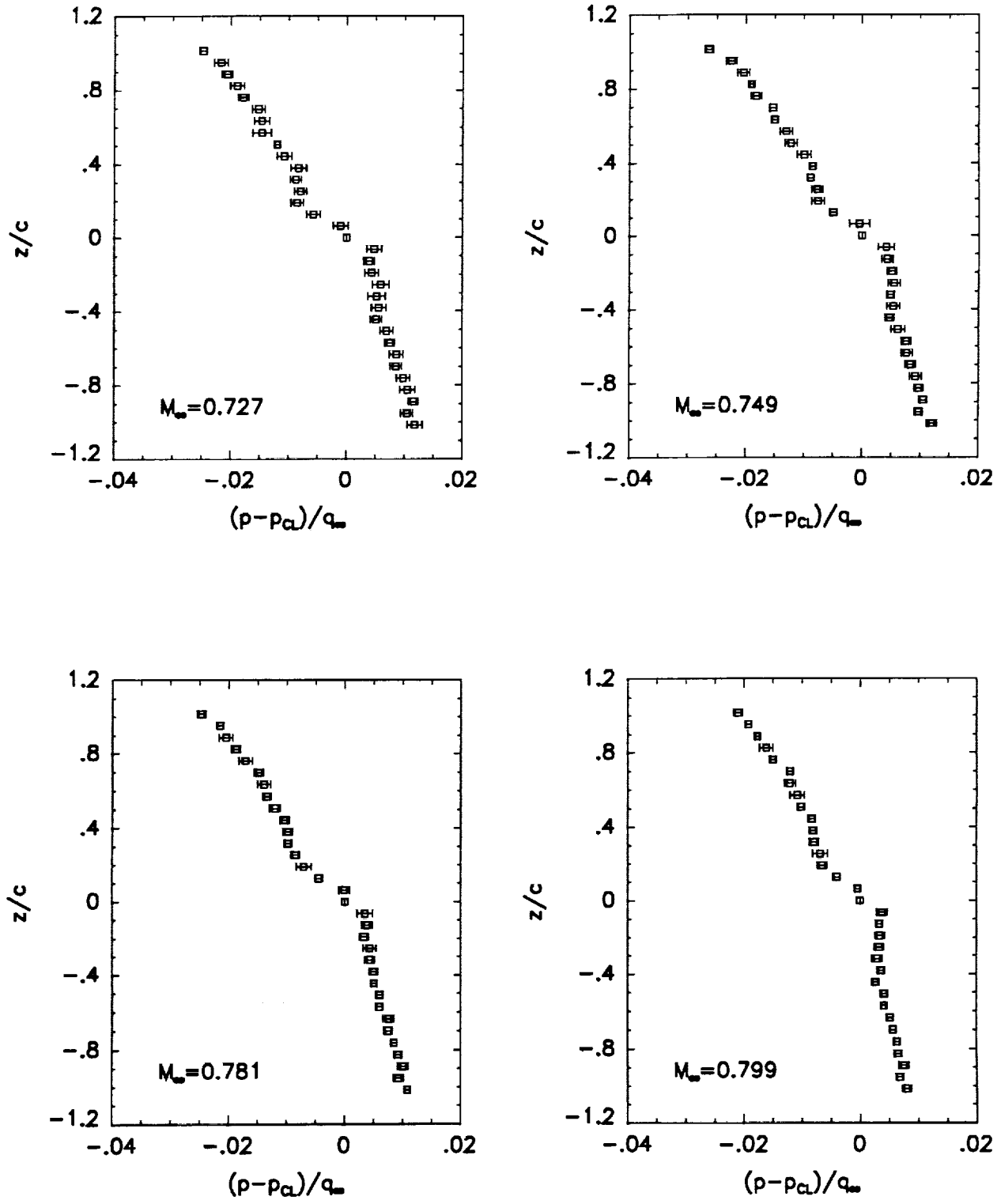

Figure 9. Wake static pressures. (a) α=0.5°, Re=6x10^6, x/c=2.5.

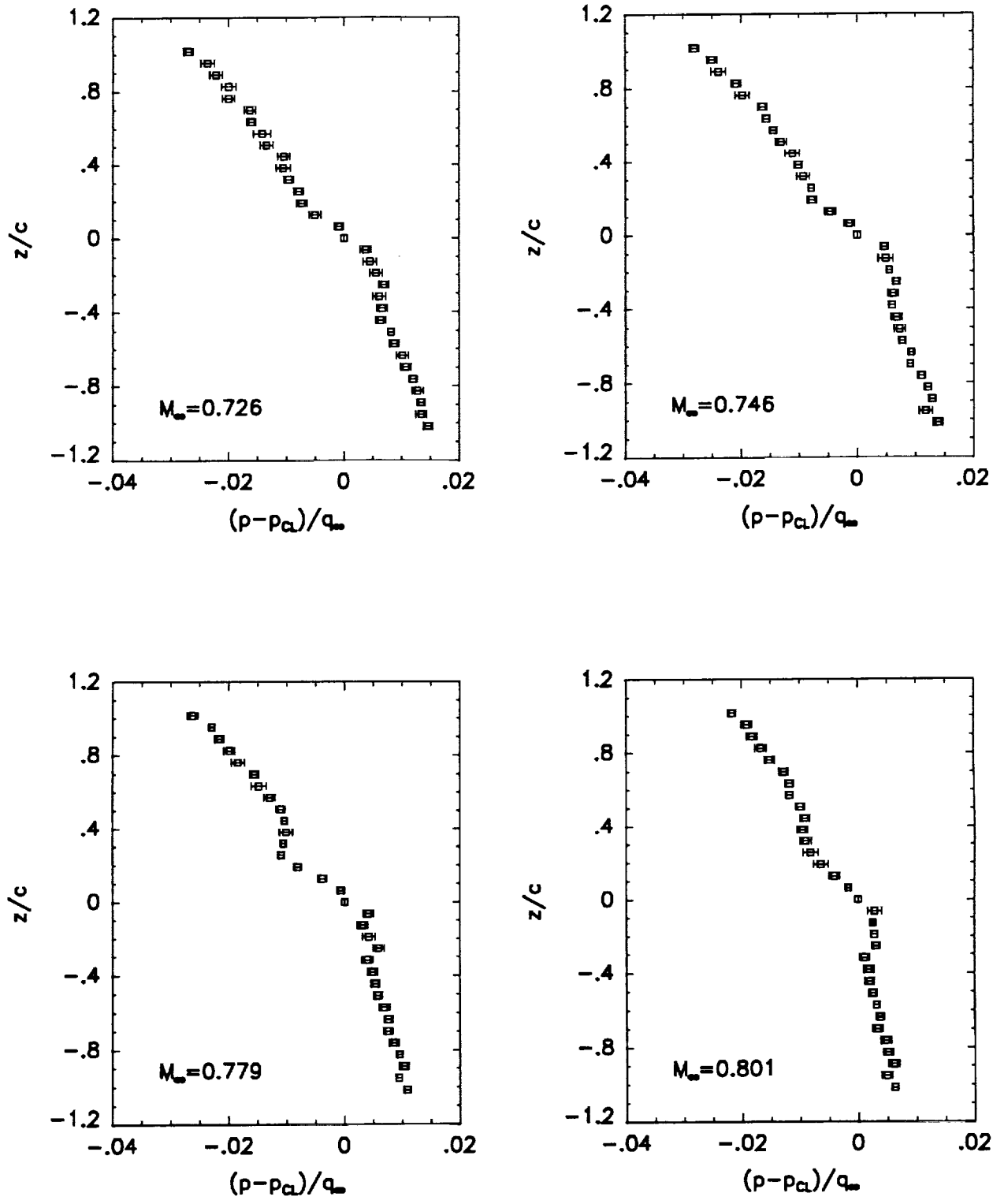

Figure 9. Continued. (b) α=0.9°, Re=6x10^6, x/c=2.5.

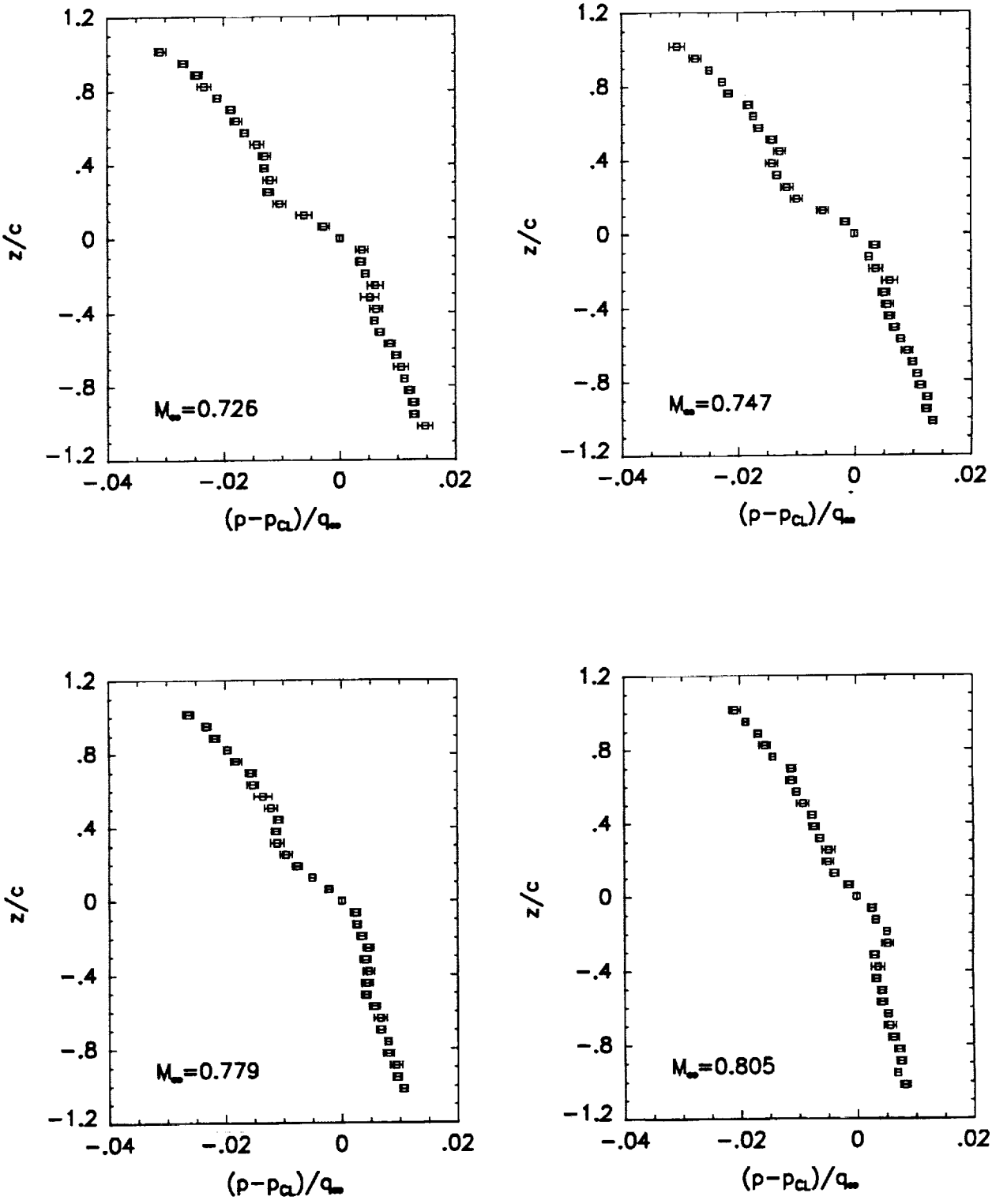

Figure 9. Concluded. (c) α=1.5°, Re=6x10^6, x/c=2.5.

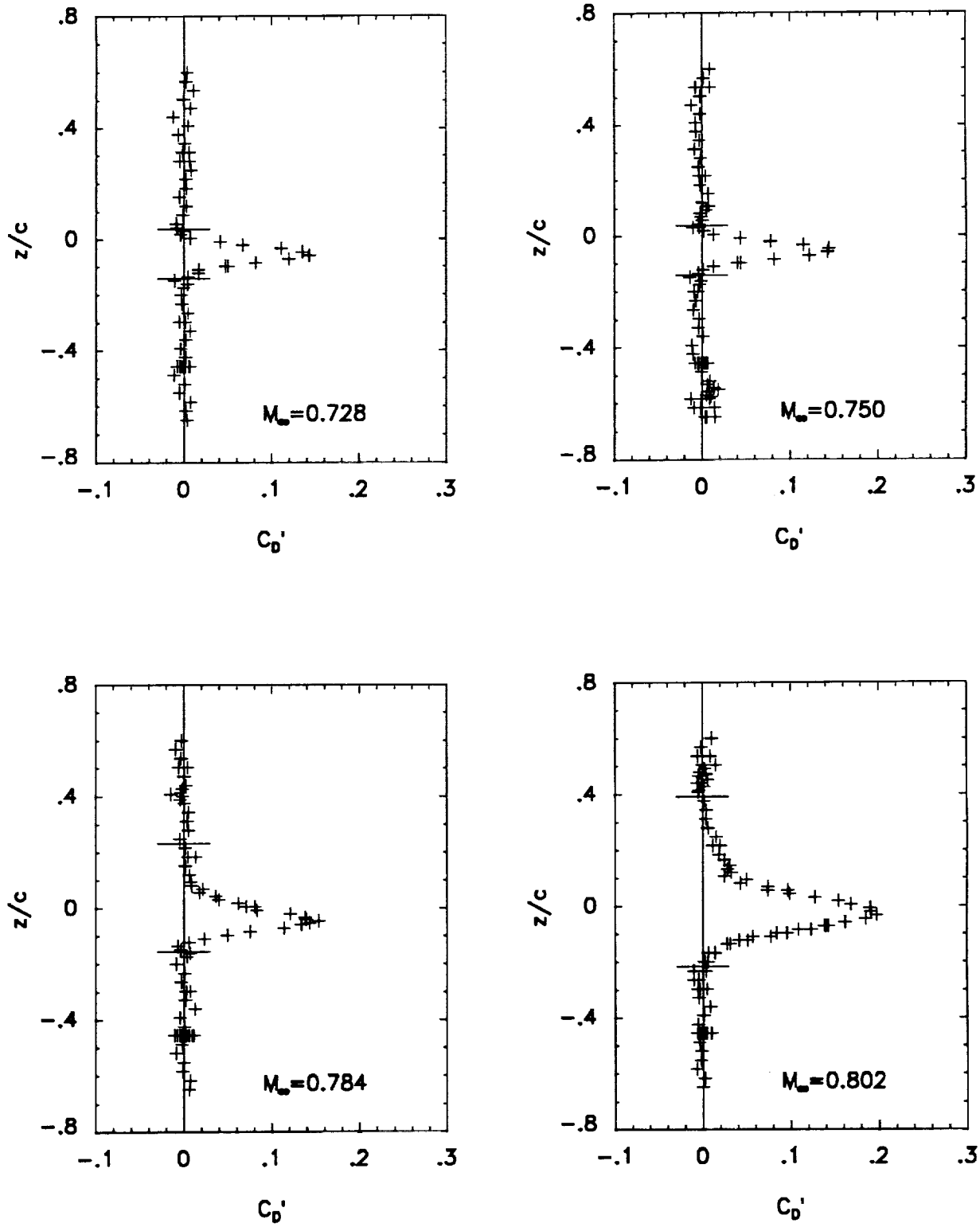

Figure 10. Point drag coefficient. (a) α=0.5°, Re=6x10^6, x/c=2.5.

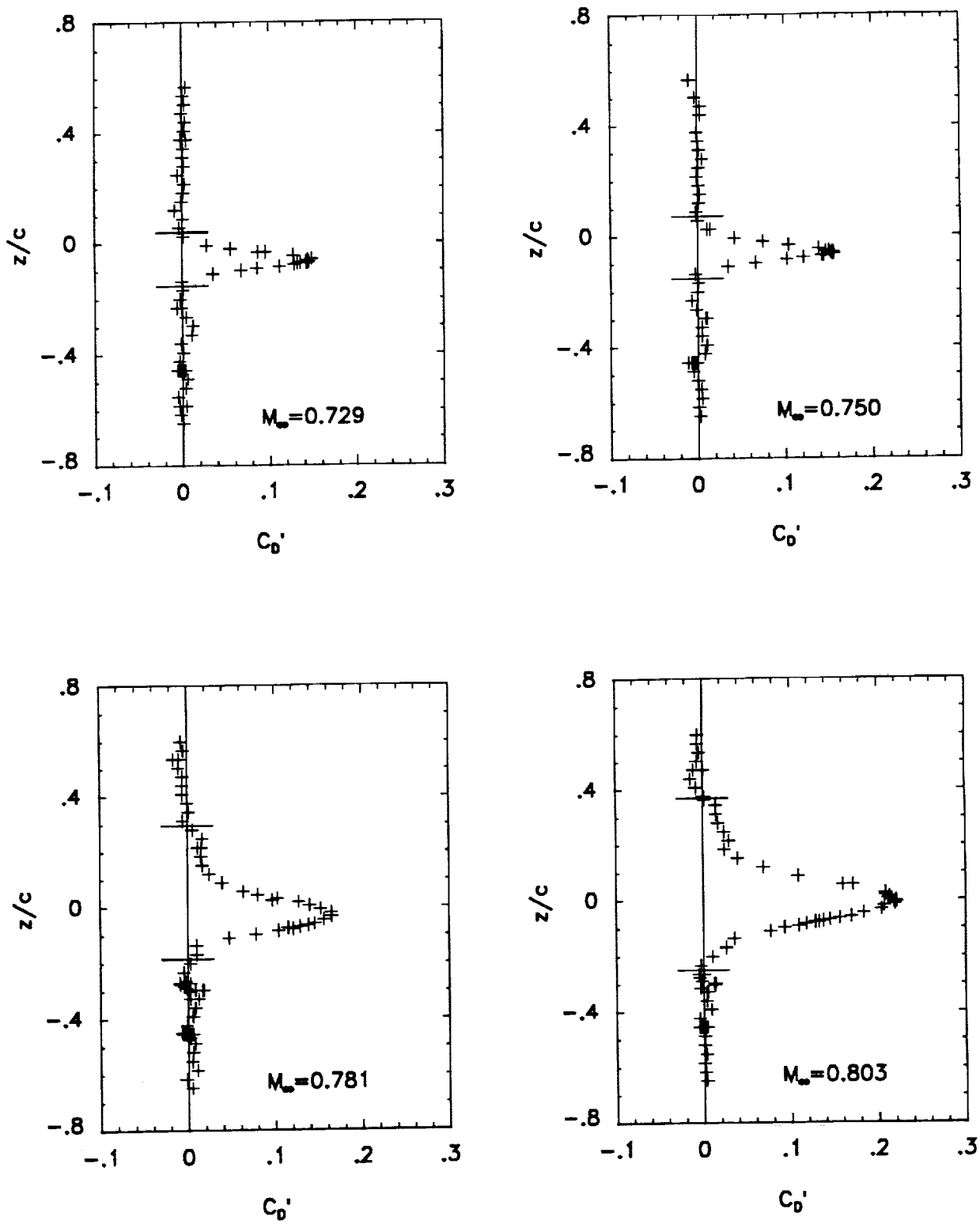

Figure 10. Continued. (b) α=0.9°, Re=6x10^6, x/c=2.5.

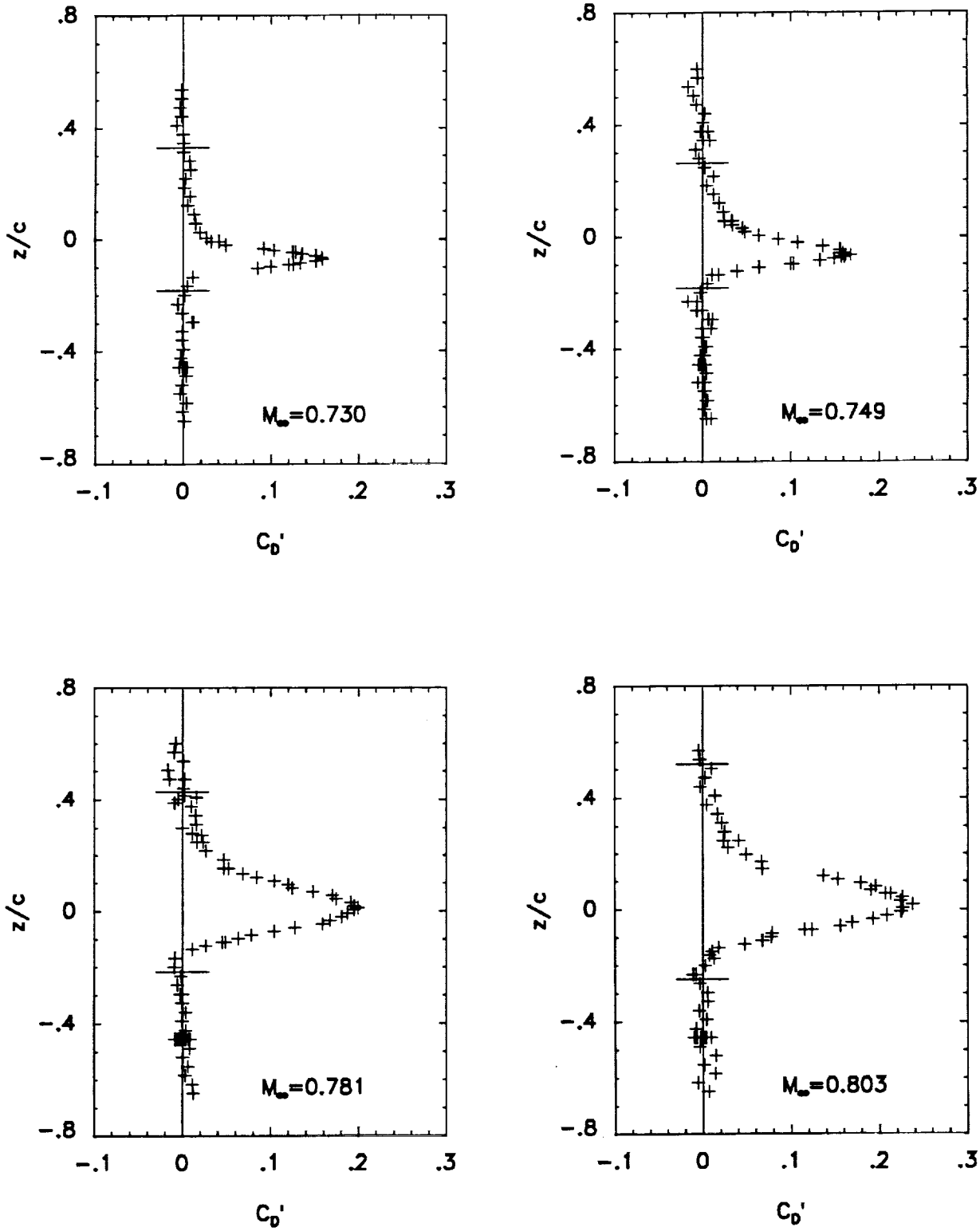

Figure 10. Concluded. (c) α=1.5°, Re=6x10^6, x/c=2.5.

REPORT DOCUMENTATION PAGE

Form Approved
OMB No. 0704-0188

1. AGENCY USE ONLY *(Leave blank)*	2. REPORT DATE	3. REPORT TYPE AND DATES COVERED
	July 1992	Technical Memorandum

4. TITLE AND SUBTITLE

An Experimental Investigation of a Supercritical Airfoil at Transonic Speeds

5. FUNDING NUMBERS

505-59-40

6. AUTHOR(S)

G. G. Mateer, H. L. Seegmiller, L. A. Hand, and J. Szodruch

7. PERFORMING ORGANIZATION NAME(S) AND ADDRESS(ES)

Ames Research Center
Moffett Field, CA 94035-1000

8. PERFORMING ORGANIZATION REPORT NUMBER

A-92089

9. SPONSORING/MONITORING AGENCY NAME(S) AND ADDRESS(ES)

National Aeronautics and Space Administration
Washington, DC 20546-0001

10. SPONSORING/MONITORING AGENCY REPORT NUMBER

NASA TM-103933

11. SUPPLEMENTARY NOTES

Point of Contact: G. G. Mateer, Ames Research Center, MS 229-1, Moffett Field, CA 94035-1000
(415) 604-6255 or FTS 464-6255

12a. DISTRIBUTION/AVAILABILITY STATEMENT

Unclassified — Unlimited
Subject Category 34

12b. DISTRIBUTION CODE

13. ABSTRACT ***(Maximum 200 words)***

Detailed experimental data have been obtained on a supercritical airfoil and in the surrounding flowfield. Surface pressures were measured on both the model and wind-tunnel walls. The velocity field above the airfoil and the field in its wake was documented using a laser Doppler velocimeter. The data illustrate the effect of Mach number and angle of attack on the flow over the airfoil. Angles of attack ranged from 0.5 to 1.5 degrees and the Mach number was varied from 0.73 to 0.8. These variations were sufficient to provide separated and attached flows on the airfoil that were not time dependent. The profile drag was determined via non-intrusive measurements. The data are also on a 3.5-inch diskette included with this document, and are available through E-mail.

14. SUBJECT TERMS

Transonic, Supercritical airfoil, Experimental

15. NUMBER OF PAGES

58

16. PRICE CODE

A04

17. SECURITY CLASSIFICATION OF REPORT	18. SECURITY CLASSIFICATION OF THIS PAGE	19. SECURITY CLASSIFICATION OF ABSTRACT	20. LIMITATION OF ABSTRACT
Unclassified	Unclassified		